Structure of Exotic Nuclei and Superheavy Elements in Meson Field Theory

Dissertation
zur Erlangung des Doktorgrades
der Naturwissenschaften

vorgelegt beim Fachbereich Physik
der Johann Wolfgang Goethe–Universität
in Frankfurt am Main

von
Khin Nyan Linn
aus Myanmar

Frankfurt am Main, July 2008
(D30)

vom Fachbereich Physik
der Johann Wolfgang Goethe–Universität
als Dissertation angenommen.

Dekan: Prof. Dr. Dirk-Hermann Rischke

Gutachter: Prof. Dr. S. Schramm

Datum der Disputation: 7.7.2008

Zusammenfassung

Im Rahmen dieser Arbeit wird die Struktur von exotischen und überschweren Kernen mit Hilfe eines relativistischen Ansatzes untersucht, bei dem die relativistische Mesonen-Feldtheorie eine zentrale Rolle spielt. Bei dem relativistischen mean-field (RMF) Modell wird die Wechselwirkung der Nukleonen miteinander über den Austausch verschiedener effektiver Mesonen (Skalar, Vektor und Isovektor-Vektor) beschrieben. Das exakte Dichtefunktional des stark wechselwirkenden Systems wird angenähert, indem die mesonischen Felder auf ihre gemittelten Feldwerte begrenzt werden. In den meisten RMF Rechnungen wird weiterhin die "no-sea" Näherung verwendet, das heißt, antinukleonische Freiheitsgrade werden nicht berücksichtigt. Es wurde gezeigt, dass das RMF Modell ähnlich flexibel und vielseitig ist wie nicht-relativistische Modelle mit dem Vorteil, dass einige relativistische Effekte, wie zum Beispiel die Spin-Bahn Wechselwirkung, automatisch auftreten und das RMF Modell die Kernsättigung erklären kann [Due56, Mil72, Wal74]. Ein Programm auf der Basis des RMF Modells wurde dahingehend angepaßt, dass die selbstkonsistenten Dirac (für die Nukleonen und Lambda-Teilchen) und Klein-Gordon (für die Mesonen) Gleichungen im Rahmen der sphärischen und axial deformierten Näherung numerisch gelöst werden konnten. Vorher war bereits gezeigt worden, dass das Modell endliche Kerne und Sättigungseigenschaften von Kernmaterie korrekt beschreibt. [Sch02]

Die Elemente mit geraden Ladungszahlen Z (von 8 bis 120) und ihre Eigenschaften für alle möglichen, geraden Neutronenzahlen wurden untersucht und mit drei verschiedenen Sätzen von Parametern (ChiM[Sch02], NLZ-2[Bür02b] und NL3 [Lal97]) berechnet. Die RMF Modelle (NL3 und NL-Z2) sind bei der Beschreibung der Eigenschaften von Kernen über einen großen Bereich von Massenzahlen sehr erfolgreich, das besondere Merkmal von NL-Z2 ist dabei die niedrige Inkompressibilität. Das chirale Modell (ChiM) benutzt eine chirale Symmetrie und wurde entwickelt, um eine gute Beschreibung der Kernsättigung und eine annehmbare Beschreibung von Kernen und Hyperkernen mit einem einzigen Modell und einem Satz von Parametern zu ermöglichen. Die nukleare Asymmetrieenergie in den ChiM Parametern liegt nahe an dem empirischen Wert. Bei

einer Testrechnung ergab sich eine gute Übereinstimmung zwischen dem chiralen Modell (ChiM) und experimentellen Ergebnissen [Fis00] bezüglich des Grundzustandes von ^{68}Se mit starker oblater Deformation ($\beta_2 \sim$ -0.3).

Mit Hilfe der RMF Theorie und drei verschiedenen Parametersätzen haben wir die Eigenschaften und Synthesemöglichkeiten von exotischen und überschweren Kernen im Bereich bis zur Dripline untersucht. Wenn einem Kern an der nuklearen Stabilitätslinie schrittweise mehr Neutronen zugefügt werden, wird die Bindungsenergie des letzten Neutrons immer geringer, bis es nicht mehr gebunden ist und der Kern durch Neutronenemission zerfällt. Ein Kern, der keine weiteren Neutronen binden kann, befindet sich auf der so genannten Neutronen-Dripline, deren Gegenstück die Protonen-Dripline ist. Ein instabiler Atomkern jenseits der Neutronen-Dripline gibt freie Neutronen ab, und die Separationsenergie des Neutrons ist auf der Dripline gleich Null. Die Protonen- und Neutronen-Driplines definieren die Grenzen der Existenz von endlichen Kernen. Die Untersuchung von Kernen nah an der Neutronen-Dripline hilft beim Verständnis von stellarer Nukleosynthese und Neutronensternen in der nuklearen Astrophysik. Der Verlauf der Dripline ist nach wie vor nicht genau bestimmt, und seine experimentelle und theoretische Bestimmung ist ein Problem von großem Interesse in dem Gebiet der Kernstrukturforschung. Die Driplines, unter Berücksichtigung axialer Deformation (mit Hilfe des ChiM Parametersatzes) wurden für Kerne mit $8 \leq Z \leq 120$ berechnet. Für die Ketten von Isotopen mit magischer Protonenzahl sind die stabilsten Kerne in unseren Rechnungen nicht die mit magischer Neutronenzahl, abgesehen von $Z = 20$. Dieses Ergebnis ist im Einklang mit dem einer vorangegangenen Rechnung mit dem Parametersatz NL3. Für größere Kerne können wir die Protonen und Neutronen Driplines klarer festlegen als in Rechnungen mit dem Parametersatz NL3. Bei unseren Rechnungen (wie auch bei Rechnungen mit NL3) mit axialer Deformation finden wir geschlossene Neutronenschalen für die magischen Neutronenzahlen ($N = 82, 126, 184$).

Die Untersuchung von protonen- und neutronenreichen Kernen bis zu den Proton- und Neutron-Driplines ist ein besonderer Schwerpunkt dieser Arbeit. Wir haben eine systematische Untersuchung von 1661 Kernen durchgeführt, um zum ersten Mal überhaupt die Hypothese der axialen Deformation von gerade-gerade-Kernen ($8 \leq Z \leq 100$) mit unterschiedlichen Neutronenzahlen im Rahmen der RMF-Theorie mit dem ChiM Parametersatz zu überprüfen. Die Protonen Quadrupoldeformationsparameter β_{2p} für die Kerne ($8 \leq Z \leq 100$) wurden vorher mit Hilfe des RMF-BCS Modells und der FRDM und HFB-2 Massenformeln berechnet. Aus unserer systematischen Untersuchung lässt sich schliessen:

1) Die meisten sphärischen Kerne (-0.05 $\leq \beta_2 \leq$ 0.05) befinden sich bei oder in der Nähe der magischen Zahlen.

2) Während in den isotonischen Ketten mit den bekannten magischen Neutronenzahlen ($N = 82, 126, 184$) die sphärische Form des Kerns erhalten bleibt, werden die Kerne mit magischen Protonenzahlen deformiert, wenn man sich entlang der isotopischen Ketten von den magischen Neutronenzahlen wegbewegt (Ausnahmen bilden die isotopischen Ketten mit $Z = 8$ und 20). Über die Berechnung der axialen Deformation für $8 \leq Z \leq 100$ lassen sich ausserdem semi-magische Zahlen ($Z = 40, 172, 182, 186$) und die wohlbekannten doppelt-magischen Kerne (^{16}O, ^{40}Ca, ^{48}Ca, ^{132}Sn, ^{208}Pb), abgesehen von der isotonischen Kette mit $Z = 28$, identifizieren. Bei den Blei-Isotopen finden wir zwei neue doppelt-magische Kerne: ^{262}Pb und ^{264}Pb (N = 180, 182).

3) Unter den Pb-Isotopen befinden sich oblat deformierte Kerne ($\beta_2 \sim$ -0.2) in der Nähe der Protonen-Dripline. Einige neutronenreiche Pb Isotope sind axial prolat deformiert ($0.2 \leq \beta_2 \leq 0.3$), alle anderen Pb Isotope haben sphärische Form.

4) Die meisten prolat deformierten Kerne beobachten wir bei Protonenzahlen ab $Z = 50$, isotonisch oder isotopisch von den magischen Zahlen entfernt.

5) Es gibt ausserdem Regionen, in denen starke Deformationen beiden Typs (prolat und oblat) auftreten. Os und Pt Isotope ($Z = 76$ und 78) weisen eine große Anzahl von axial prolaten Deformationen auf, ausser in der Nähe von ($N = 126$).

6) In der Nähe der Neutronen-Dripline von Cf ($Z = 98$) und der Protonen und Neutronen Driplines von Fm ($Z = 100$) haben wir Isotope mit superdeformierten Zuständen ($0.7 \leq \beta_2 \leq 0.8$) gefunden.

7) Relativ stark oblat deformierte Kerne sind selten, aber es gibt einige Bereiche oblater Deformation in der Nuklidkarte, wovon eine nun gekennzeichnet werden soll. Diese oblate Region liegt zwischen den isotonischen Ketten der Zn ($Z = 30$) und Kr ($Z = 34$) Isotope, die Deformation dieser Kerne ist stark ausgeprägt ($0.2 \leq \beta_2 \leq 0.3$)

Axial deformierte Kerne auf der Protonen- und Neutronen-Dripline bei Magnesium wurden im Rahmen der RMF Theorie mit dem ChiM Parametersatz

berechnet. Das Auftreten oblater und prolater Minima für verschiedene Isotope bei diesen Rechnungen stimmt mit den Ergebnissen anderer relativistischer und nicht-relativistischer mean-field Rechnungen überein [Lal98, Bür02a].

Kenntnisse über Kerne weit ausserhalb des Bereichs der exotischen Kerne können nicht nur dabei helfen, die Elementhäufigkeit auf der Erde zu verstehen, sondern auch Aufschluss über die Entwicklung von Materie im Universum geben. Exotische Kerne haben durch ihren hohen Isospin und andere interessante Eigenschaften wie z.B. Halo und Neutronenhaut weltweit Aufmerksamkeit auf sich gezogen. Die RMF Theorie mit dem ChiM Parametersatz kann den Neutronenhalo von ^{34}Ne und die Dicke der Neutronenhaut einer Reihe von Isotopen um $Z = 40$ sowie von Sn und Pb Isotopen vorhersagen. Der Neutronenhalo und die Dicke der Neutronenhaut werden über die Berechnung der Dichteverteilung und der Differenz zwischen den Mittelwerten der Protonen- und Neutronenradien bestimmt. Die berechneten Grundzustandseigenschaften dieser exotischen Kerne, wie z. B. die Bindungsenergie pro Nukleon und die Zwei-Neutronen-Separationsenergie stimmen gut mit den experimentellen Werten [Aud03] und FRDM [Möl95] Rechnungen überein.

Es ist interessant, die Deformation von Blei-Isotopen zu untersuchen. Wir beobachten, dass die niedrigsten drei Zustände im Energiespektrum des neutronenarmen Kerns ^{186}Pb sphärisch, oblat und prolat deformiert sind, siehe Abb. 4.16, und unsere Ergebnisse stimmen mit denen einer anderen dreidimensionalen Rechnung [And00] überein. Potentialkurven für $^{190-204}$Pb weisen bemerkenswert hohe Anregungsenergien relativ zu den niedrigen Superdeformationsbanden (SD Banden) und flache Potentialtöpfe um das SD Minimum auf. Im Vergleich zu benachbarten Kernen zeichnet sich ^{192}Pb dadurch aus, dass es schwierig ist, einen stabilen SD Zustand zu bilden. Die SD Zustände können für diese Kerne aber trotzdem beobachtet werden, wobei es eine vernünftige Übereinstimmung zwischen der RMF Theorie (mit den Parametersätzen NL3, PK1, TM1 und NLSH) [Guo06] und den experimentellen Beobachtungen gibt. Die berechnete Deformation in den SD Minima von $^{190-204}$Pb liegt zwischen 0.6 und 0.7.

Die RMF Theorie mit dem ChiM Parametersatz kann nicht nur für normale Kerne sondern auch für Hyperkerne benutzt werden. Dazu wurden die Rechnungen für exotische Kerne mit hinzugefügten Λ Hyperonen wiederholt. Ein Λ besteht aus jeweils einem u, d und s Quark, und ein Hyperkern entsteht, wenn ein solches Hyperon in einem Kern gebunden wird. Hyperkerne mit einem Hyperon wurden vor 30 Jahren entdeckt und seitdem intensiv experimentell untersucht [Pov76]. Die Lambda-Hyperkerne sind besonders gut dafür geeignet, die Struktur der Kerne zu untersuchen, da das Lambda-Teilchen stark mit dem Kern wechselwirkt und sich von den Nukleonen unterscheiden lässt. Die axiale De-

formation von Ne Isotopen mit und ohne Λ Hyperon wird verglichen. Aus den Rechnungen lässt sich schliessen, dass deformierte Kerne das Ausmaß der Deformation durch den Einschluss eines Λ Hyperons ein wenig vermindern können. Andererseits verändert der Einschluss eines Λ-Hyperons die "bulk Eigenschaften" nicht übermässig, stabilisiert aber neutronenreiche Kerne und verschiebt dadurch die Neutronen-Dripline. Mit Hilfe der RMF Theorie und dem Parametersatz ChiM sagen wir die Existenz von hyperonischen Kohlenstoffisotopen voraus. Das Hinzufügen von zwei Λ-Hyperonen zum ^{12}C Kern ändert die Nukleonendichteverteilung nicht, und die Hyperonendichteverteilung am Rand des Kerns ist mit der der Nukleonen vergleichbar. Bei dem Kohlenstoffisotop, das durch Hinzufügen von drei Λ-Hyperonen zum Kern gebildet wird, sagen wir einen Hyperonhalo vorher, da es Anzeichen dafür gibt, dass der Schwanz der Hyperonendichteverteilung weit aus dem Kern herausreicht.

Die Bestimmung der Protonen und Neutronen Driplines wird in dieser Arbeit ausführlich diskutiert. Dieselbe Rechnung wurde anschliessend mit einem Λ Hyperon im Kern wiederholt. Das Λ Hyperon ist ausgezeichnet dafür geeignet, die Struktur des Kerns zu untersuchen, da es sich im Zentrum des Kerns befindet. Durch die Berechnung der Driplines mit dem RMF Modell lässt sich die Verschiebung der Driplines von normalen Kernen zu Hyperkernen mit einem Lambda untersuchen, was für die geplanten Experimente bei FAIR/GSI in dem Bereich der sehr neutronenreichen Hyperkerne von Interesse sein könnte. Abgeschlossene Schalen zeigen sich unter Einbeziehung eines Λ Hyperons bei den magischen Zahlen 82, 126, 184 so, dass die Hyperkerne mehr Neutronen aufnehmen können und somit eine höhere Bindungsenergien als normale Kerne haben.

Den Abschluss dieser Arbeit bildet die Untersuchung von überschweren Kernen. Die RMF Theorie mit den drei unterschiedlichen Parametersätzen (ChiM, NL3, NL-Z2) wird besprochen. Basierend auf einer detaillierten Analyse der zwei-Nukleonen Separationsenergien S_{2n} und S_{2p} und der zwei-Nukleonen Schalen-Gaps δ_{2p} und δ_{2n} mit den effektiven Wechselwirkungen ChiM, NL3 und NL-Z2 wurden die Protonen und Neutronen Schalenabschlüsse vorhergesagt. Die Protonenzahlen $Z = 114, 120$ und Neutronenzahlen $N = 172, 184, 258$ sind bei allen drei effektiven Wechselwirkungen magisch. Der Grundzustand der überschweren Kerne variiert mit dem Parametersatz, das ergibt eine Berechnung der Potentialhyperflächen. Für diese Kerne ist daher interessant, unser Modell mit axialer Deformation auf eine vollständige dreidimensionale Rechnung auszudehnen, mit deren Hilfe man die Lage des Grundzustandes besser bestimmen könnte.

Contents

List of Figures

List of Tables

–I–

INTRODUCTION

1.1 Objectives

The enlargement of the Nuclear Chart poses a challenge and an opportunity for nuclear physics, offering a better understanding of the isospin dependence of nuclear forces and stellar nucleosynthesis. The objective of this study is to investigate exotic nuclei and the structure of superheavy elements within meson field theory. The GSI is the only accelerator laboratory in the world with the capacity to investigate these nuclei throughout the entire periodic table: from hydrogen, the lightest element, to the superheavy elements. Discovery of new superheavy elements can support long-held nuclear theories regarding the existence of the island of stability and the ultimate limits of the periodic table of the elements. These discoveries also provide scientists a better understanding of how nuclei are held together and how they resist the fission processes and α decay.

The production and investigation of exotic nuclei have become one of the central topics of interest in nuclear physics. By investigating exotic nuclei, we can refine our theoretical nuclear structure models, with the farsightedness beyond the range of isotopes available to us on earth and thereby taking into account the broadest possible spectrum of nuclei. The formation of chemical elements and their abundance are essentially determined by the properties of these exotic nuclei. This research work is dedicated to calculate the structure of exotic nuclei and superheavy elements within meson field theory.

Key for understanding the synthesis of elements in stars is the knowledge of the properties of exotic nuclei up to the proton and neutron driplines. In addition this work focuses on the properties of exotic hypernuclei, neutron rich hypernuclei and proton rich hypernuclei. The results can be used to enhance more comprehensive approach to perceive on the Λ-N interactions and could be very

relevant in the stellar nucleosynthesis. With better knowledge of the structure of possible superheavy elements, one can observe and predict which superheavy elements might be produced experimentally.

1.2   Atomic nuclei

The atomic nucleus represents one of the fundamental building blocks of matter in the universe. It takes its place between the atom and the hadron in a chain of basic constituents which stretches from quarks to galaxies. In common with many of its neighbours in the chain, the basic problem of nuclear structure physics is a quantum many-body one whose unique aspect stems from the number of constituents and the nature of the force. A nucleus consists of a large, but finite number of nucleons: proton and neutron (two types of baryons), interacting via a strong, short-range force. These baryons have a substructure, the sub-atomic fundamental particles known as quarks, bounded by the strong interaction. The mediators for this strong interaction are the gluons. The composition of baryons and antibaryons, the basic building blocks of atomic nuclei, in terms of their quark constituents is shown in Fig (1.1).

Baryons qqq and Antibaryons $\bar{q}\bar{q}\bar{q}$					
Baryons are fermionic hadrons.					
These are a few of the many types of baryons.					
Symbol	Name	Quark content	Electric charge	Mass GeV/c^2	Spin
p	proton	**uud**	1	0.938	1/2
p̄	antiproton	**ūūd̄**	–1	0.938	1/2
n	neutron	**udd**	0	0.940	1/2
Λ	lambda	**uds**	0	1.116	1/2
Ω$^-$	omega	**sss**	–1	1.672	3/2

Figure 1.1: Baryons and Antibaryons: the fundamental building blocks of atomic nuclei and their properties. Source: [con03]

The atomic nucleus is governed by three interactions among the four fundamental interactions in nature, namely; weak interaction, electromagnetic interaction and strong interaction. Weak interaction processes occur in the beta decay of nuclei. The electromagnetic interaction enters through the interaction of protons, the positively charged nucleons. The strong interaction acts between the the hadrons - baryons and mesons. The general properties of the fundamental interactions

are summarised in Fig (1.2). The size of a nucleus, given by the nuclear radius of the order of 10^{-13} cm, is one of the most fundamental bulk properties of an atomic nucleus [Rin80] that needs to be reproduced in theoretical models. Nuclear radii follow approximately the formula $R = r_0 A^{1/3}$ where $r_0 \sim 1.3$fm. The corresponding nuclear charge distribution is positive, representing the charge of the protons contained in the nucleus.

PROPERTIES OF THE INTERACTIONS					
Property / Interaction	Gravitational	Weak (Electroweak)	Electromagnetic	Strong	
				Fundamental	Residual
Acts on:	Mass – Energy	Flavor	Electric Charge	Color Charge	See Residual Strong Interaction Note
Particles experiencing:	All	Quarks, Leptons	Electrically charged	Quarks, Gluons	Hadrons
Particles mediating:	Graviton (not yet observed)	W^+ W^- Z^0	γ	Gluons	Mesons
Strength relative to electromag for **two u quarks at:** 10^{-18} m	10^{-41}	0.8	1	25	Not applicable to quarks
3×10^{-17} m	10^{-41}	10^{-4}	1	60	
for **two protons in nucleus**	10^{-36}	10^{-7}	1	Not applicable to hadrons	20

Figure 1.2: The properties of the fundamental interactions. Source: [con03]

As atomic nuclei get heavier as the number of nucleons they contain increases, they have a tendency to become more unstable against radioactive decay: the nuclei fall apart spontaneously because of the enormous electrical repulsion, induced by the Coulomb interaction of all the positively charged protons. That is why especially superheavy elements are so difficult to produce, and generally so short-lived. So far, researchers have succeeded in making superheavy elements up to number 118 - that is, with 118 protons in the nuclei - by merging big nuclei through atomic collisions. But this instability of superheavy elements does not seem to be inevitable. Calculations have predicted that there should be an 'island of stability', originally assumed to lie around element 114 for nuclei that have the right number of neutrons (in many calculations N=184). The island of stability, however, and its range, or even if it exists at all, depends strongly on the model calculation used.

1.3 Different atomic nuclei towards the driplines

In the area of theoretical and experimental nuclear physics the investigation of exotic nuclei and superheavy elements is of central importance. Especially with the advent of new radioactive beam facilities one can explore a much larger range of isotopes that couldn't be accessed before. Therefore complementary theoretical studies are urgently needed. The boundaries of the nuclear chart define the

so-called driplines. As neutrons are successively added to a nucleus, the binding energy of the least bound neutron decreases steadily until it is no longer bound and the nucleus decays by neutron emission. This defines the neutron dripline, which lies much further away from the valley of stable nuclei than for the corresponding proton dripline, simply because of the lack of Coulomb repulsion. Experimentally, the position of the driplines is still uncertain. In fact, the neutron dripline is only known for nuclei with (roughly) mass 30 or less. Beyond that, its location becomes increasingly uncertain and it is predicted to be further away from the line of stability as the proton number increases.

The interest in the study of nuclei with large neutron excess is not focused on the location of the dripline alone, but is also motivated by the expectation of new features which may appear in these highly exotic nuclei. Exotic nuclei are nuclei in which the ratios of N/Z are very different from those of ordinary nuclei. Exotic nuclei are highly unstable with weak binding of the outer nucleons and after some time they decay into stable nuclei. Beyond the proton dripline, the protons are not emitted instantaneously as they are confined by an additional potential, which originates from the Coulomb barrier for the protons. Nuclear models have to be developed in order to accommodate the fruitful new phenomena that have been unveiled by the continuing experimental work. The study of exotic nuclei [Tan96, Mue99b] with radioactive nuclear beams is one of the most active and important areas in contemporary nuclear physics as it explores strong interaction physics at large isospin and helps to pin down the position of the neutron and proton driplines.

As a consequence of the weak neutron binding the existence of the new effects of nuclear halos and neutron skins among neutron rich nuclei becomes possible. In stable nuclei, due to the Coulomb force the number of neutrons tends to exceed the number of protons. Nuclei with too many neutrons, however, are unstable; beyond the 'neutron drip-line', nuclei become unbound. Nuclei close to the neutron dripline are weakly bound to the core nucleus. The nuclear densities and sizes of the systems approaching the driplines with large N/Z ratios are different from those encountered in nearly stable nuclei. Through quantum-mechanical tunnelling, and because of their lower binding energy , in certain light nuclei close to the neutron dripline, the wave function describing the quantum state of the last neutron (or neutrons), extends to a remarkably large distance out from the centre of the nucleus, so that these last few neutrons spend most of their time far from the normal density core of the nucleus and form a halo. In other words, the nuclear halo has an appreciably larger radius ($\sim 8fm$) than that predicted by the liquid drop model, wherein the nucleus is assumed to be a sphere of constant density. The discovery of this neutron halo is one of the most interesting aspects

in nuclear physics [Tan85a, Han87]. The first observed case of neutron halo, the nucleus ^{11}Li is still a topic of considerable theoretical interest.

In the realm of heavier nuclei, a related phenomena can be predicted in which the steadily increasing neutron excess gives rise to the neutron skin on the outside of the nucleus. In normal nuclear matter, the proton and neutron radii are similar and their distributions overlap. As the other extreme pure neutron matter is only found in neutron stars (with a small fraction of protons present). Analysing the difference in the root mean square (r.m.s) radii of the neutron and proton density distributions can be used to quantitatively describe the existence of halos or skins. Experimental evidence of effects ascribed to a neutron halo or a neutron skin have been observed in several nuclei near the neutron dripline [Han95, Tan96]. The neutron skin of the nucleus has been one of central issues of nuclear structure [Mye85, Kra91]. A thick neutron skin has been observed experimentally only in quite light nuclei ^{6}He and ^{8}He [Tan92]. A neutron skin does not emerge in nuclei near the β stability line, but a neutron skin with more than 10 neutrons can be formed in nuclei far from the stability line [Fuk93]. The formation of a proton skin is quite difficult as the proton dripline is close to the line of equal number of protons and neutrons.

In the region of extremely large atomic number the existence of superheavy elements was predicted about 30 years ago on the basis of the nuclear shell model, which was originally developed in 1949. The model explains why nuclei with certain magic numbers of neutrons and protons are especially stable. These nuclei have closed shells of either protons or neutrons. Magic nuclei are spherical in shape and characterised by exceptionally high nuclear binding energies. The most stable nuclei observed are doubly magic having closed shells of both protons and neutrons. The heaviest known doubly magic nucleus is ^{208}Pb, an isotope of lead consisting of $Z=$ 82 protons and $N=$126 neutrons. In the Gesellschaft für Schwerionenforschung (GSI) in Darmstadt, in Dubna in Russia and in other places, the next "magic" elements, which might occur for an atomic charge of Z=120, appears to be within reach. The additional stability, which arises from the shell closure, results in a greater probability that the nuclei in this region may exist at least sufficiently long for their properties to be measured. This region has thus been called an "Island of Stability" and its discovery would represent a major triumph for nuclear science.

1.4   The Relativistic Meson field theory

A widely and successful approximation method for the ground state properties of the finite nuclei is the microscopic self-consistent mean field theory applying effective interactions. In the present work, we employ the relativistic meson-field (RMF) theory in mean-field approximation. In general the mean field approaches include relativistic meson field theory [Ser86] starting from an effective relativistic meson-baryon Lagrangian density and non-relativistic Hartree-Fock (HF) theory with effective interactions, such as Skyrme or Gogny. In recent years, a number of effective interactions of meson-baryon couplings of RMF theory have been developed, including non linear effective interactions NL1, NL2 [Lee86], NL3[Lal97], NLSH[Sha93], TM1, TM2 [Sug94], PK1, PK1r[Lon04], PL40[Rei88], NL-Z2[Bür02b] and extended versions including chiral symmetry, ChiM [Sch02]. In this thesis, several effective interactions including both nonlinear interactions and the interaction using chiral symmetry are studied and the properties of nuclear matter and of nuclei including deformation are investigated in the whole range between the driplines.

The RMF theory has been used not only for the description of the properties of finite nuclei near the valley of near stability [Vau72, Bei75, Ser86, Rei89, Ser92, Rin96, Rut99, Ben03] but also for the prediction of finite nuclei with large neutron or proton excess. Among the nuclear models, the RMF theory has reached a level of accuracy to present the structure of nuclei. This approach has been a successful tool to microscopically describe bulk nuclear ground-states properties, such as energies, radii and surfaces as well as deformation properties and fission [Rei89, Blu94]. Specifically, the RMF theory explicitly includes the mesonic degrees of freedom and describes the nucleons as Dirac particles.

Nucleons interact in a relativistic covariant manner through the exchange of isoscalar scalar self-coupling σ meson, the isoscalar vector ω meson, the isovector-vector ρ meson, and the photon. The role of relativity in the short-ranged region of the nuclear force and its effect in producing saturation at the correct density and binding energy in nuclear matter is now being recognised. [Rei95]. Another well-known feature in the RMF theory is that the proper spin-orbit interaction and associated nuclear shell structure comes out naturally. The proper spin-orbit coupling arises directly from the relativistic nature of the meson-nucleon interactions. The isospin asymmetry is generated by the isovector ρ meson coupling term in the Lagrangian density so that ρ meson contribution (E_ρ) becomes increasingly important for large isospin asymmetry.

1.5 Outline of Dissertation

Although this work focuses on nuclear structure of exotic nuclei and superheavy nuclei, in fact these are related to enlarge the chart of the nuclei and the boundary of nuclear chart. In addition a study of lambda hypernuclei serves as an extension of the nuclear landscape in the direction of hypercharge or strangeness. Chapter 2 describes the basic concepts used in the study of the structure of atomic nuclei. Chapter 3 introduces basic theoretical modelling methods of nuclei and a brief description of the relativistic mean field theory which is used to investigate the structure of exotic and superheavy nuclei. Nuclear structure of exotic nuclei is discussed in Chapter 4. The modification of nuclear properties by including a Lambda baryon is studied in Chapter 5. The investigation of the driplines, the boundaries of the nuclear chart are presented in Chapter 6. This work is concluded with the results on superheavy nuclei.

–II–

STRUCTURE OF ATOMIC NUCLEI

From a theoretical viewpoint the atomic nucleus can be described as a complex many-body quantum system governed by the interplay of strong and Coulomb interactions. Just as baryons and mesons can be viewed as many-body states of quarks and gluons, the nucleus is composed of the most stable of these baryons— uncharged neutrons and positively charged protons—whose interactions are determined by strong, electromagnetic and - for beta decay - weak forces. The sum of the number Z of protons and the number N of neutrons in a nucleus is called the mass number A=Z+N. The knowledge of how the strong force affects the binding of nucleons inside the nucleus is fundamental to our understanding of the creation of the nuclei in the early universe by extrapolating our knowledge of known nuclei to exotic elements. A few minutes after the Big Bang, the mutual interactions between nucleons led to the formation of light nuclei. During stellar evolution and in violent events like supernovae explosions, the subsequent nuclear processes synthesising heavier nuclei, have been crucial in building the chemical elements found on earth today.

2.1   Nuclear Landscape

The nuclear landscape, shown in Fig (2.1), represents all of the stable and radioactive nuclei with their respective proton number Z and neutron number N. There are 276 known stable nuclei in nature, with 166 even-even, 55 odd N and even Z, 50 even N and odd Z, and 4 odd-odd combinations [Hod00]. The stable nuclei, depicted with black squares, have similar numbers of protons and neutrons and thus extend diagonally across the chart, starting from hydrogen. Heavier nuclei (Z>20) have more neutrons to be stable to overcome the electrostatic repulsion of protons.
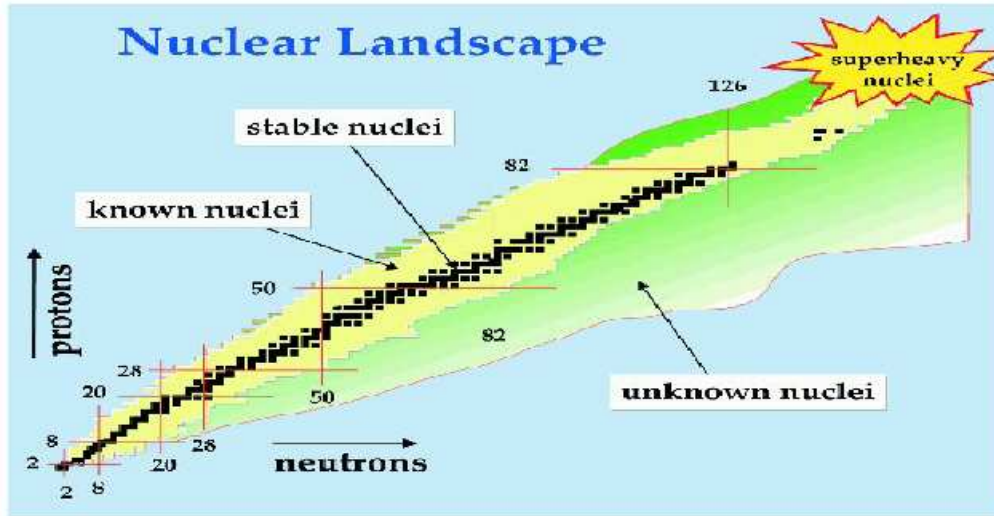
Figure 2.1: Nuclear Landscape illustrates the range of possible atomic nuclei, based on the number of protons and neutrons each contains. Source: [ANL07]

These stable nuclei are surrounded by unstable nuclei, that decay via various channels with a certain half-life. The about 3500 unstable nuclei have, generally, shorter and shorter half-lives as we proceed away from the region of stable of nuclei. Eventually one reaches the driplines at which the nucleus will no longer bind extra neutrons or protons and therefore they drip off without sticking permanently. Many unstable nuclei have been synthesised and studied in nuclear structure laboratories (yellow zone). The limits of bound nuclear systems are uncertain and are known experimentally for only the lightest ($Z \leq 13$) elements. The half-lives vary over an enormous range from 10^{18} years (^{209}Bi) to 10^{-7}s (^{212}Po). Exploring the region between the stability line and driplines (green zone) is of special importance for better understanding the stellar nucleosynthesis.

2.2   Nuclear Deformation

Further away from closed shells, the accumulation of particle-hole strength leads to additional configuration mixing and deviation from spherical symmetry, that is, deformation of the nuclear shape even in the ground state. In a multipole expansion the lowest applicable shape component deviating from sphericity is the quadrapole deformation. Deformed nuclei can also have octupole and hexapole or

higher multipole shape components. The electric nuclear quadrapole moment is a parameter which describes the effective shape of the ellipsoid of the nuclear charge distribution. Nuclear quadrapole moments can be either positive or negative. By convention, the value of Q is taken to be positive if the ellipsoid is prolate (cigar-like shape) and negative if it is oblate (disk-like shape). The latter is the rarer case. The different deformation of nucleus can be seen in Fig. 2.2. The classical definition of a quadrapole moment is

$$Q = \int (3z^2 - x^2)\rho(\mathbf{x})d^3x \tag{2.1}$$

here, $\rho(\mathbf{x})$ = charge density for the corresponding quadrapole moment of the nuclear charge distribution.
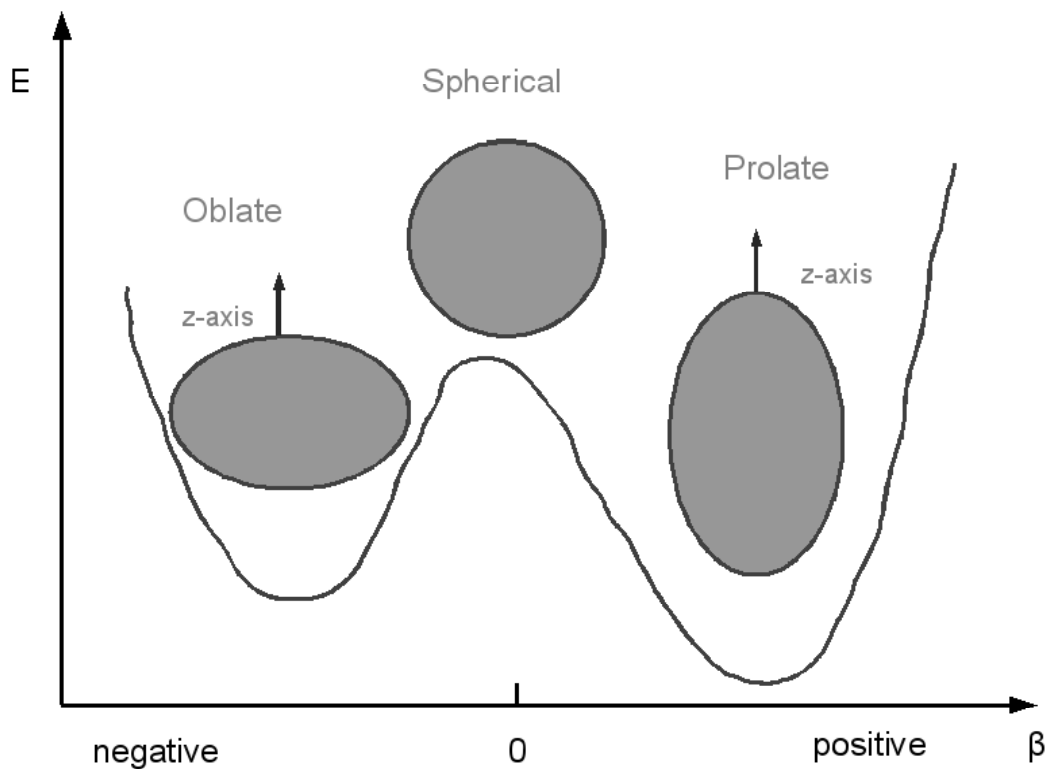
Figure 2.2: Deformation of nucleus

In a mean-field language nuclear deformations result form residual two-body interactions between valence nucleons that favour configurations in which nucleons occupy single-particle orbitals in a deformed mean field. Prolate deformations are preferred at the beginning of large shells (almost empty shells) and oblate

deformations at the end of large shells (almost full shells), although for detailed and realistic situations the prolate ones appear more often in nature.

2.3   Nuclear binding energy

The nuclear binding energy is the basic of the gross properties describing a nucleus. The nuclear binding energy results from the combined effect of the attractive strong interactions between the nucleons and the Coulomb repulsion between the protons. It is defined as the energy required to disassemble a nucleus into free unbound neutrons and protons. As to be expected, an examination of the nuclear mass shows that the mass of a nucleus is always less than the sum of individual masses of protons and neutrons which constitute it. According to the theory of relativity , the nuclear binding energy which holds the nucleus together can be defined as

$$B = (ZM_p + NM_n - M)c^2 \qquad\qquad (2.2)$$

Here a nucleus of mass M contains Z protons and N neutrons.

A key parameter in the study of atomic nuclei is their average binding energy per nucleon, E_B/A. The average binding energy per nucleon varies from one nucleus to another. The characteristic of binding energy per nucleon can be observed in Fig. 2.3. For most nuclei, however, the binding energy per nucleon is about 8 MeV. The fact that there is a peak in the binding energy curve in the region of stability near iron means that either the breakup of heavier nuclei (fission) or the combining of lighter nuclei (fusion) will yield nuclei which are more tightly bound (less mass per nucleon).

The higher the average nuclear binding energy per nucleon, the more energy is required to remove a nucleon from the nucleus and, hence, the more stable the nucleus.

2.4   Nuclear Charge and matter distributions

Nuclear structure determines nuclear charge and matter distributions in the nucleus, and these strongly affect the way the nucleus interacts with other particles. The arrangement of protons is given by the charge distribution and the matter distribution is determined by the densities of neutrons and protons combined. The charge and matter distribution can be measured by analysing the way various particles are scattered by the nucleus. The charge distribution is observed
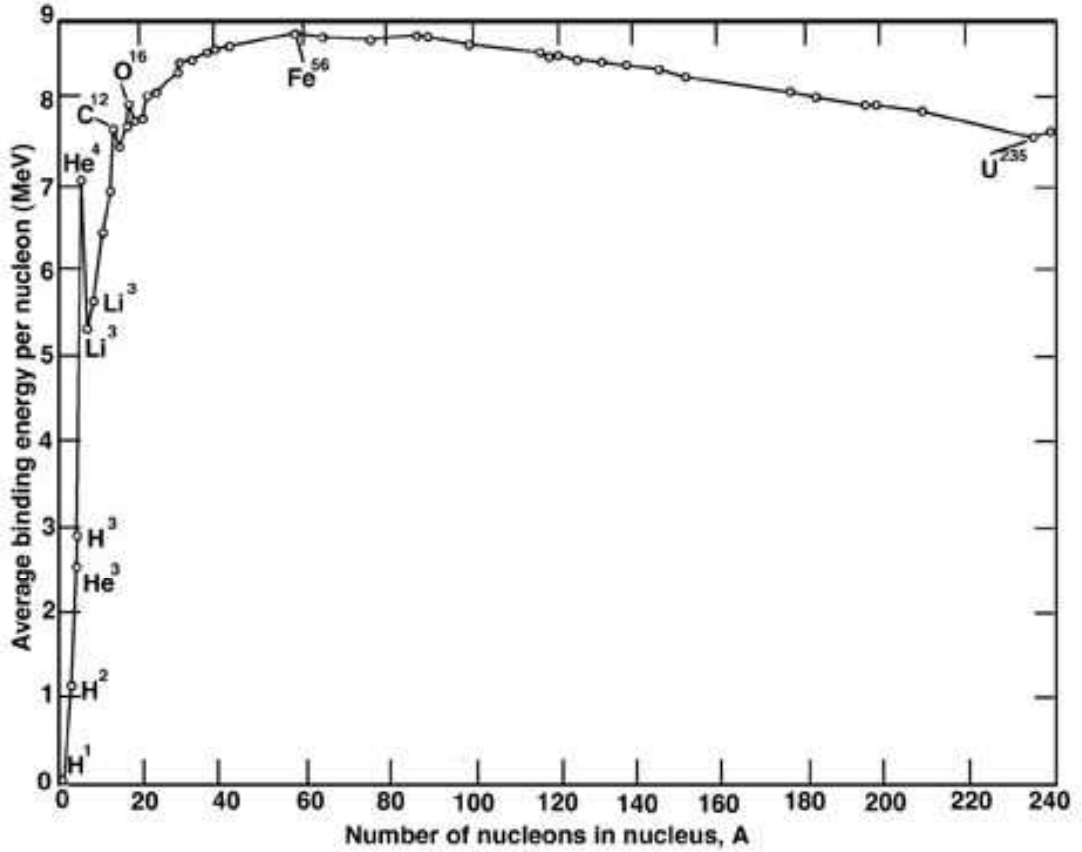
Figure 2.3: Binding energy per nucleon.

by using a probe that interacts only with the charge, and in this study the electron is ideal. Because of the well-understood electromagnetic field, the studies of electron elastic scattering by nuclei have provided accurate charge distributions. In the work of Hofstadter and colleagues at Standford [Hof56] a phaseshift analysis was made of elastic electron scattering from an arbitrary charge distribution through the Coulomb interaction. The best fit to the data, on the average, was found with the following shape, illustrate in Fig. 2.4 .

The distribution of the nuclear charge density is often quite well approximated by means of a Fermi function:

$$\rho(r) = \frac{\rho_0}{1 + e^{(r-R)/a}} \tag{2.3}$$

where ρ_0 is the central density, R= $1.07 \times A^{1/3}$ fm and a = 0.54 fm.
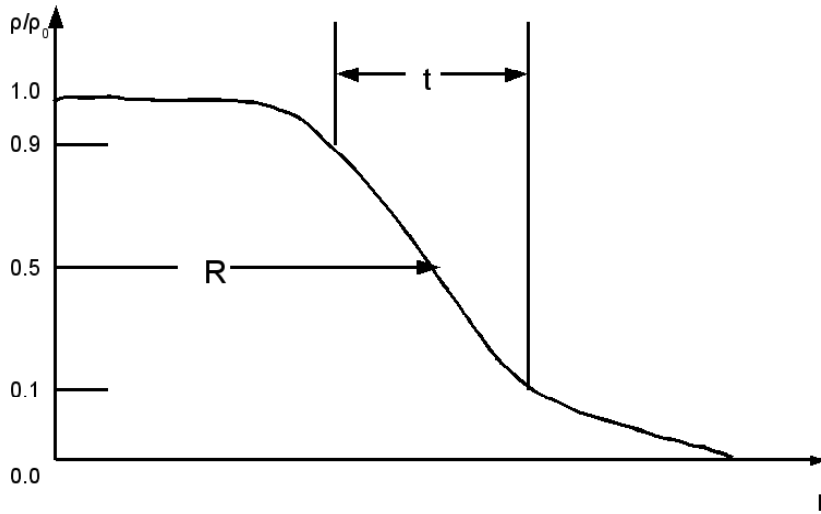
Figure 2.4: Nuclear density

2.5 Thickness of the nuclear surface

The nuclear thickness t is defined as the thickness of the layer where the density drops from 90% to 10% of the central density. This means:

$$t = r_2 - r_1 \quad \text{where} \quad \rho(r_1) = 0.90\rho_0, \quad \rho(r_2) = 0.10\rho_0 \tag{2.4}$$

In accordance with Eq (2.3):

$$1 + \exp(\frac{r_1 - c}{a}) = \frac{1}{0.9} = \frac{10}{9} \rightarrow \exp(\frac{r_1 - c}{a}) = \frac{1}{9} \rightarrow \frac{r_1 - c}{a} = \ln\frac{1}{9} \tag{2.5}$$

and

$$1 + \exp(\frac{r_2 - c}{a}) = \frac{1}{0.1} = 10 \rightarrow \exp(\frac{r_2 - c}{a}) = 9 \rightarrow \frac{r_2 - c}{a} = \ln 9 \tag{2.6}$$

This gives

$$\frac{r_2 - c}{a} - \frac{r_1 - c}{a} = \frac{r_2 - r_1}{a} = \ln 9 - \ln\frac{1}{9} = 2\ln 9 \rightarrow \quad t = r_2 - r_1 = 2a\ln 9 \tag{2.7}$$

With the typical value of $a \sim 0.54$fm, given in the previous section, the thickness of the nuclear surface is about $2 \cdot \ln 9 \cdot 0.54$ fm $= 2.37$ fm.

2.6 Isospin

Isospin was first introduced by Werner Heisenberg in 1932. Isospin is defined as a vector quantity which is conserved in particle reaction caused by strong force. Isospin is a symmetry of the strong interactions as it applies to not only the interaction of the neutron and proton but also in the interaction of baryons and mesons. To be precise, the isospin symmetry is described as the invariance of the Hamiltonian of the strong interactions under the action of the corresponding isospin Lie group SU(2). The isospin properties of a state can generally be described by two numbers T, the total isospin and T_3, the component of to isospin vector in a given (here the 3-) direction. The isospin invariance of strong interaction implies that the proton and the neutron form a symmetry multiplet, in this case an isodoublet with T=1/2 (analogous to the intrinsic spin s). The pions (π^+, π^-, π^0), for instance, are assigned to an isotriplet with T=1. For a combined description of protons and neutrons as nucleons, the nucleon is described by an additional intrinsic degree of freedom representing the isospin. This degree of freedom has two eigenvalues to distinguish protons and neutrons [Wal04] It is similar to ordinary spin 1/2 and can be represented as

$$\eta_p = \begin{pmatrix} 1 \\ 0 \end{pmatrix} \quad \eta_n = \begin{pmatrix} 0 \\ 1 \end{pmatrix} \tag{2.8}$$

The three isospin Pauli matrices can be written as τ_a. If the spin and isospin dependence is included, the single particle wave functions can be presented as

$$\psi_{k,\lambda,\rho} = \phi_k \chi_\lambda \eta_\rho \tag{2.9}$$

here χ_λ is the spin wave function with

$$\chi_\uparrow = \begin{pmatrix} 1 \\ 0 \end{pmatrix}, \quad \chi_\downarrow = \begin{pmatrix} 1 \\ 0 \end{pmatrix}$$
$$\eta_\rho = \text{isospin wave function}$$

The charge of the isospin state is given by

$$q = \frac{1}{2}(1 + \tau_3) \tag{2.10}$$

where τ_3 is the third component of the Pauli matrices. For a general nucleus with N neutrons and Z protons the projection of the isospin can be represented as

$$T_3 = \frac{(N - Z)}{2} \tag{2.11}$$

From the above equation, one can observe that the isospin dependence is a more relevant quantity in neutron rich nuclei than for proton rich nuclei, because of the smaller value of isospin in proton rich nuclei. In contrast, the isospin contribution in neutron rich nuclei is an important feature in nuclear structure research.

2.7   Nuclear Matter Compressibility

The basic gross properties defining symmetric nuclear matter (assuming N=Z and no Coulomb interaction) are its density at saturation point, the energy per baryon at this point and the nuclear matter compressibility. The value of the nuclear matter compressibility is an important ingredient of the equation of state of nuclear matter. The compressibility K_{nm} is generally defined as,

$$K_{nm} = k_f^2 \frac{d^2 E/A}{dk_f^2}\bigg| k_{f0}, \tag{2.12}$$

or, alternatively,

$$K_{nm} = 9\rho^2 \frac{\partial^2 (E/A)}{\partial \rho^2}\bigg|_{\rho=\rho_{nm}}, \tag{2.13}$$

where E/A is the binding energy per nucleon, k_{f} is the Fermi momentum, and k_{f0} is the equilibrium Fermi momentum and $\rho_{\mathrm{nm}} \approx 0.16\mathrm{fm}^{-3}$ is the corresponding saturation density.

The nuclear matter equation of state $E/A = \mathcal{E}/\rho_0$ is a basic physical quantity which is very important for the study of nuclei. It has a minimum $(E/A)_{eq} \approx -16$ MeV at saturation density.

Experimental information on the value of K_{nm} can be derived from the properties of the nuclear giant monopole resonance [Bla76], but the values $K = 210\pm30$ MeV that are derived from these experiments, are on the rather low end for various theoretical estimates of the compression modulus of nuclear matter.[Bla80, Tre81].

2.8   Symmetry Energy

Away from the symmetric case of equal numbers of protons and neutrons a basic quantity for asymmetric matter is given by the symmetry energy. Thus the symmetry energy is one of the most important quantities in the study of nuclear structure especially towards neutron-rich nuclei. The source of the symmetry energy is the imbalance between the number of protons and neutrons. As the Pauli exclusion principle states that no two fermions can occupy the same quantum

state, at a given energy level, there is only a finite number of quantum states available for the nucleons. When protons or neutrons are added to a given nucleus, the filling up of the fermi seas is not done anymore in the energetically most preferred way, thus increasing the total energy of the nucleus and decreasing the binding energy. In terms of a semi-empirical mass formula this effect can be written in terms of a phenomenological term called the symmetry energy. [Rin80],

$$E_{sym} = \frac{1}{2} b_{sym} \frac{(N-Z)^2}{A} = a_{sym} T^2 \qquad (2.14)$$

with $T = |Tz| = |N - Z|/2$, the isospin projection, which originates from the kinetic energy and additional interaction effects, i.e., $a_{sym} = a_{kin} + a_{int}$. The symmetry energy shows the typical quadratic isospin dependence in the semi-empirical mass formula.

The symmetry energy coefficient a_4 from the state of equation for asymmetric nuclear matter can be seen as a kind of incompressibility in the variation of the neutron-proton ratio [Cha97].

$$E_{sym} = \frac{1}{2} \frac{\partial^2 (E/A)}{\partial I^2} \bigg|_{I=0} \quad with \ \ I = (N-Z)/A \qquad (2.15)$$

The symmetry energy used in RMF model is given by (the constants are defined in the following section) ,

$$E_{sym} = \left(\frac{k_F^2}{6\sqrt{k_F^2 + m_N^{*\,2}}} + \frac{1}{2} \frac{g_{N\rho}^2}{m_\rho^{\,2}} \rho - \frac{1}{2} \frac{g_{N\delta}^2}{m_\delta^{\,2}} \frac{\rho^{s2}}{\rho} \right)_{\rho=\rho_{nm}} \qquad (2.16)$$

–III–

Nuclear Models

In the last two decades our knowledge concerning the structure of nuclei has steadily improved through the development of more sophisticated nuclear models. Originally there are two basic types of simple nuclear model approaches:

1. The Liquid drop model - here the nucleus is considered as a collective object with no individual particle states. It can provide a description of the gross properties of nuclei in terms of volume, surface and symmetry energy terms.

2.The phenomenological Shell Model - the nucleons are taken into account as individual particles in discrete energy states in an external potential. The observed magic numbers can be explained theoretically by including a spin-orbit force in the shell model.

In this work I make use of the relativistic meson field theory, which will be explained in detail in section 3 of this chapter. In contrast to the shell model it is based on a relativistic formulation for the nucleon and meson fields, and the mean potential for the nucleons is generated in a self-consistent way through the interaction of the nucleons with the mesonic mean fields. This model is applied to study the ground-state properties of nuclei over the entire range of the periodic table, from light doubly magic nucleus $^{16}_{8}$O, to superheavy nuclei and, furthermore to exotic nuclei up to the proton and neuron driplines. The parameters in this model are adjusted to phenomenological and experimental data of nuclear matter and a few finite nuclei.

3.1   Nuclear Liquid Drop Model

The liquid drop model is one of the first models of nuclear structure, originally proposed by George Gamow. It is a simple model that does not explain all the properties of nuclei, but does explain the spherical shape of most stable

nuclei. It can also be used to predict the binding energy of the nucleus. The nucleus is modeled as a droplet of incompressible nuclear fluid made of neutrons and protons, with an internal repulsive electric force proportional to the number of protons. The shape of the droplet is spherical as it minimises the positive surface tension energy. As the fluid is incompressible, the density of the droplet is constant. The nucleons in the nucleus behave like the molecules in the fluid, that is, there is a short-range attractive force holding the nucleons together. The basic assumption of the liquid drop model is that each nucleon in a nucleus interacts only with its nearest neighbours like a molecule in a liquid. The nuclear saturation property explains qualitatively the features found experimentally, that is a nearly constant interior nucleon density and a surface radius approximately equal to $1.2A^{1/3}$. The analogy of this experimental finding with the properties of a droplet of a incompressible nuclear fluid results in the formulation of the liquid drop model, where the nuclear binding energy consists of a nuclear-matter contribution and various correction for finite nuclei.

3.1.1 Semi-empirical mass formula

The oldest well-known semi-empirical mass formula of Bethe-Weizsäcker reads

$$B(N, Z) = a_v A + a_s A^{2/3} + a_c Z^2 A^{-1/3} + a_I \frac{(N-Z)^2}{A} - \delta(A), \qquad (3.1)$$

where one obtains by a fit [Mye66, Mye69, Mye70]

$$a_v = 15.68 \quad a_s = 18.56 \quad a_c = 0.717 \quad a_I = 28.1 \quad \text{MeV}$$

$$\delta(A) = \left. \begin{cases} 34.A^{-3/4} & \text{for even} - \text{even} \\ 0 & \text{for even} - \text{odd} \\ -34.A^{-3/4} & \text{for odd} - \text{odd} \end{cases} \right\} \text{nuclei} \qquad (3.2)$$

The physical meaning of formula (3.1) is the following [Gre96, Rin80]. The first term is usually called the volume term (it is proportional to $A[\propto R^3]$) which indicates the constant binding energy per nucleon at equal density of protons and neutrons and so provides one of the most important parameters of nuclear matter. The second term is proportional to the square of the nuclear radius, it describes the reduction of the binding energy due to the nucleons on the surface of the nucleus like the analogous mechanism in the case of the surface tension in liquids. Thus the term $a_s A^{2/3}$ is known as the surface term. These first two terms originate from the strong force. The third term takes into account the Coulomb repulsion between protons which can be calculated approximately by assuming

that the charges are homogeneously distributed over a sphere. The Coulomb energy of such a system is proportional to Z^2/R and so to $Z^2/A^{-1/3}$. The fourth term is the so-called symmetry energy showing the decrease in binding for unequal numbers of protons and neutrons. The last term is known as the pairing term. This term captures the effect of correlations of proton and neutron pairs.

3.2 Nuclear Phenomenological Shell Model

The nuclear shell model has shown remarkable success in the single-particle description of nuclei as well as serving as a complete basis to describe more complicated nuclear states and excitations. The nuclear shell model is sometimes referred to as the independent particle model because it assumes that each nucleon moves independently of all the other nucleons and is acted upon by the average field produced from the action of all the other nucleons. Neutrons and protons are arranged into shells within the nucleus like the shells in atoms. Each shell is filled to a certain maximum number of protons and neutrons according to the Pauli exclusion principle where no two identical fermions can occupy the same quantum state. The observation of shell structure and discrete energy levels suggest the picture of the nucleon moving in some effective potential created by the interaction with all the other nucleons. This leads to energy quantisation in a manner similar to states in a given external potential like the simple square well and harmonic oscillator potentials.

The experimental evidence for the shell closure in analogy to the inert gases of atomic structure brought about the phenomenological postulation of mean field potentials [May48, Fee49, Hax99, May49, May50] which could later be demonstrated in terms of self-consistent fields. The most important experimental information on shell structure is the existence of magic numbers. Magic numbers were first discovered by Maria Goeppert-Mayer. At some proton or neutron number (the so-called magic numbers occurring at 2, 8, 20, 28, 50, 82, 126) shell closure occurs analogous to the electron shell closure in atoms. These magic nuclei are much more bound than predicted by the liquid drop model.

In fact, it is known experimentally that the magic numbers are characterised by a special stability, like noble gases in atomic physics. This observation is in agreement with the existence of a shell structure of nucleons (protons and neutrons) within the nucleus like that of electrons within the atoms. Furthermore, these magic nuclei (in comparison with neighbouring nuclei in the table of nuclei), are characterised by larger total binding energies of the nuclei, larger separation energies of single nucleons, higher energy of the lowest excited states, the elec-

tric quadrapole moments are near to zero and the existence of larger number of isotopes (isotones) with the same magic numbers of protons (neutrons). The low magic numbers are the same for the protons and neutrons, namely 2, 8, 20, 28, 50, 82, whereas the next number, 126, is experimentally only established for neutrons. Theoretical predictions suggest new magic numbers at 114 or 120 for protons and 172 or 184 for neutrons, with considerable uncertainties depending on the nuclear model. These new hypothetical magic numbers would constitute long-lived superheavy nuclei [Gru69, Nil69, Fis72, Ran74].

According to the assumption of the phenomenological shell model, the Schrödinger equation for the single-particle levels reads

$$\left(-\frac{\hbar^2}{2m}\nabla^2 + V(\mathbf{r}) \right)\Psi_i(r) = \epsilon_i\Psi_i(\vec{r}), \tag{3.3}$$

with a prescribed potential V(**r**). Before discussing how one can derive the form of the average field from a microscopic two-body force, we will choose to have a one-body potential V(**r**). It should be relatively constant inside heavier nuclei to explain the constant density suggested by the fact that the definition of nuclear radii,

$$R = r_0 A^{1/3} \tag{3.4}$$

yields reasonable phenomenological results, but should tend to zero quite rapidly outside the nuclear radius.

Assuming spherical symmetry, a quite realistic and successful potential is the Wood-Saxson potential [Woo54]

$$V(\mathbf{r}) = -\frac{V_0}{1 + \exp[(r - R)/a]} \tag{3.5}$$

where the parameters are the mean radius $R \simeq 1.1$ fm $A^{1/3}$ and the surface thickness $a \simeq 0.5$ fm. The well depth is adjusted to $V_0 \simeq 50$ MeV. The shape of the Wood-Saxson potential corresponds to the experimentally measured nuclear density distributions. A practical disadvantage of the potential is that one is not able to write down an analytic expression for the wave functions. For this reason, one often finds two simple approximations for qualitative considerations and also as basis states for more extended calculations:

The harmonic-oscillator potential

$$V(\mathbf{r}) = \frac{1}{2}m\omega^2\mathbf{r}^2 \tag{3.6}$$

with $\hbar\omega \simeq 41$ MeV $\times A^{-1/3}$ typically.

The square-well potential

$$V(\mathbf{r}) = \begin{cases} -V_0 & \text{for} \quad r \leq R \\ -\infty & \text{for} \quad r > R \end{cases} \tag{3.7}$$
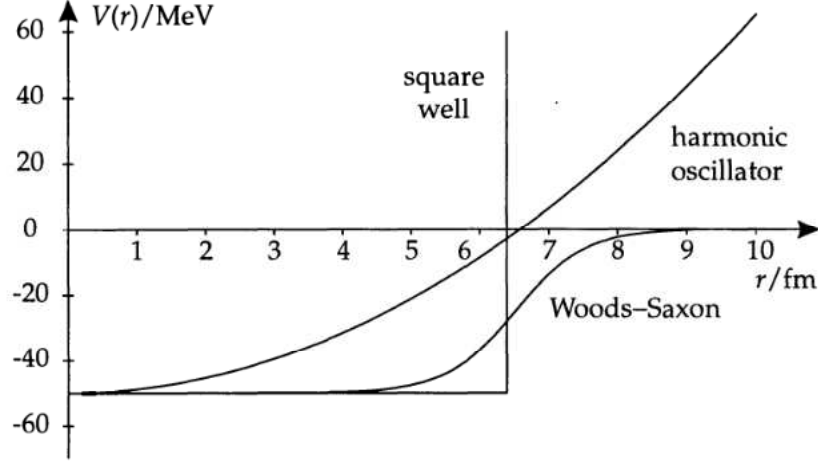
Figure 3.1: Sketch of the functional form of three phenomenological shell-model potentials: Wood-saxson, harmonic oscillator and the square well. Sources: [Gre96]

All three potentials are sketched in Fig (3.1).

The decisive idea that made the single particle shell model an effective tool in nuclear physics was the inclusion of a strong spin-orbit force by Goeppert-Mayear and Jensen. They suggested an additional strong, attractive, single-particle spin-orbit coupling term in the single particle Hamiltonian operator.

$$H' = f(r)\mathbf{l} \cdot s \tag{3.8}$$

Mathematically this leads to a jj-coupling scheme for the nucleons, since $\mathbf{l} \cdot \mathbf{s}$ commutes with $\mathbf{s}^2$, $\mathbf{l}^2$, $\mathbf{j}^2$, j_z but not with l_z and s_z. The single-particle eigenstates are characterised by the eigenvalues $|nlsjm_j\rangle$.

$$\begin{aligned} 2\mathbf{l} \cdot s|nlsjm_j\rangle &= (\mathbf{j}^2 - \mathbf{j}^2 - \mathbf{j}^2)|nlsjm_j\rangle \\ &= [j(j+1) - l(l+1) - s(s+1)]|nlsjm_j\rangle, \end{aligned} \tag{3.9}$$

In the present case, $s = 1/2$, one can state spin-orbit splitting of the doubly degenerate levels $|nlsj = l \pm 1/2\rangle$:

$$\Delta E(l) \sim [l - (l-1)] = 2l + 1. \tag{3.10}$$

The correct magic numbers could be thus predicted when the spin-orbit inter-
action is large enough to push the state of highest l and highest j in a major
oscillator shell down into the next lower shell. Fig (3.2). The success of the
phenomenological shell model justifies the assumption that the nucleons move
independently in an average potential produced by all other nucleons.

Figure 3.2: Single-particle energies for a simple harmonic oscillator(S. H. O) and
modified harmonic oscillator with l^2 term and a realistic shell model potential with l^2
and spin-orbit ($l \cdot s$) terms. Source: [con03]

3.3 The Relativistic Meson Field Theory

The Relativistic Meson Field (RMF) theory has been a significant progress towards relativistic models of the nucleus in recent years. It is an elegant and powerful model to investigate the structure of nuclei, providing a self-consistent relativistic description of nuclei. The RMF theory has achieved remarkable successes in the description and the prediction of the properties of nuclei. [Ser86, Rei89, Ser92, Rin96, Rut99, Ben03]. It describes the nucleus as a system of Dirac nucleons interacting in a relativistic covariant manner via mesonic fields [Ser79, Hor81, Ser86, Ruf88, Rei89, Gam90, Fur97, Lal97, Fur98] usually adopting the mean field approximation for the meson fields [Nik92, Hoc94]. For 30 years before the application of RMF to nuclear structure calculations, models based on single particle degrees of freedom governed by the appropriate Schrödinger equation were central to nuclear structure calculations. In contrast, in the RMF approach the nucleon wave functions are given as solutions of the Dirac equation. In the single-particle non-relativistic approaches many achievements and a large number of sophisticated techniques gave rise to an increased understanding of the nuclear many-body problem.

Disadvantages of these models are the necessary ad-hoc introduction of a large spin-orbit term, the difficulty to describe nuclear saturation, and the lack of a microscopic understanding of the effective interactions in nuclei. One of the most obvious signatures of RMF is the large nuclear spin-orbit force. In the RMF model, the spin orbit interaction emerges naturally from the interplay between two strong and counteracting fields: a long-range attractive scalar field and a short-range repulsive vector field. These fields nearly cancel each other in the calculation of the nuclear potential but add up for the spin orbit interaction. With a few (about eight) free parameters adjusted once, they allow one to describe the nuclear ground-state properties on a quantitative level. In the relativistic framework of the model the interaction is governed by using (effective) mesonic degrees of freedom rather than instantaneous forces. Overall, it was shown that the relativistic mean field model is as flexible and powerful as the non-relativistic models with the additional bonus that some relativistic effects, as the spin-orbit force, come out naturally in the relativistic model and it allows an explanation of the nuclear saturation. [Due56, Mil72, Wal74]

The RMF theory is an effective quantum field theory, starting from an effective Lagrangian density, the protons and neutrons are described as Dirac particles interacting in a covariant manner through the exchange of various mesons including the isoscalar-scalar σ meson, the isoscalar-vector ω meson, the isovector-vector ρ meson and the photon. [Ser86, Rei89] Although the nucleons are somehow
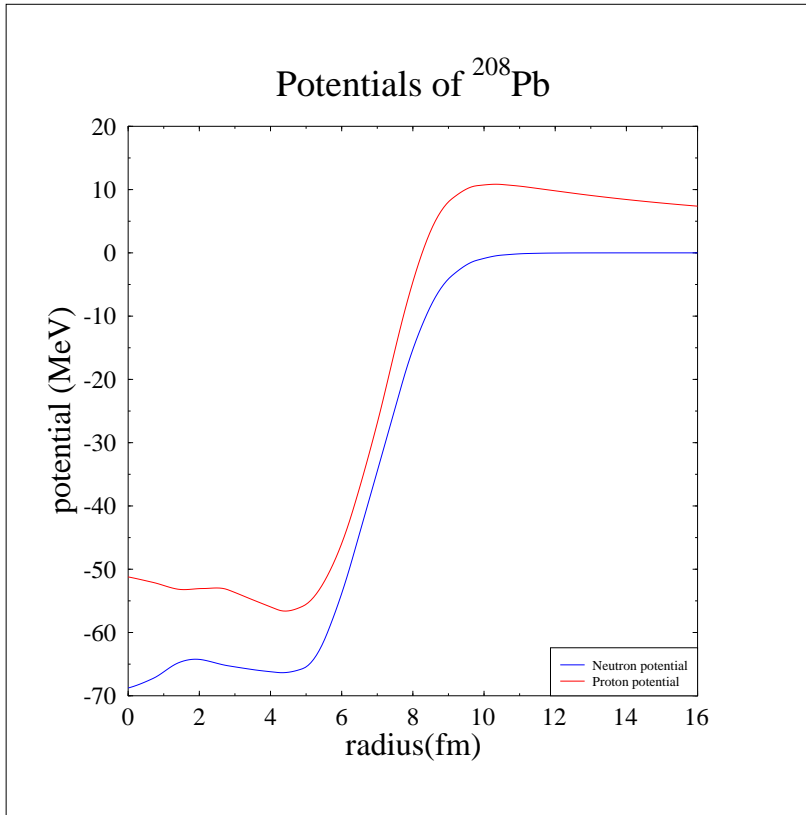
Figure 3.3: Potentials of ^{208}Pb. calculated by the RMF theory with NL3 force

complex QCD objects containing quarks and gluons, they are treated as point particles, it is not possible so far to also include their degrees of freedom to obtain a systematic solution of the nuclear many body problem in finite nuclei on the basis of Quantum Chromodynamics. Most of the applications of the RMF theory in the study of nuclear systems have been performed at the mean-field or Hartree level. In general, RMF theory cannot be treated peturbatively because of its large coupling constants. However, assuming large fields that justify a mean-field approach, using the variational principle, one can obtain the coupled Dirac equations for the nucleons and the Klein-Gordon equations for mesons that have to be solved in a self-consistent way.

In general the equations of the relativistic meson-field theory are very complex and difficult to solve. Two simplifications will be used in this investigation (and in most calculations in this field): the already mentioned mean-field approximation
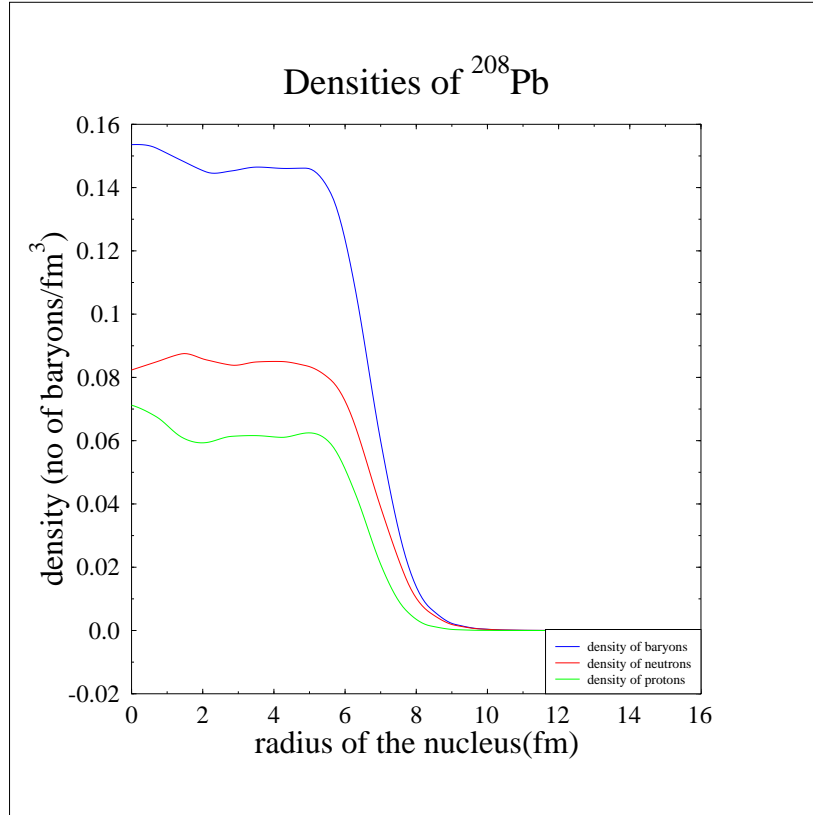
Figure 3.4: Densities of ^{208}Pb. calculated by the RMF theory with NL3 force

and the no-sea approximation. In the mean field approximation the mesons are treated as classical fields. i.e, the meson field operators are replaced by their expectation values, which are classical fields and the no-sea approximation neglects the effect due to negative energy states in the Dirac sea. Moreover, one should note that the pseudoscalar π-meson is not taken into account at the Hartree level since the expectation value of the π-meson is zero in this approximation in nuclear quantum states [Ser86]. However it will appear when more complex exchange diagrams are included. Recent results of one studies with the contribution of π-meson can be found in these references [Ser86, Bro75, Sch02].

The relativistic models based only on a one-meson exchange could not provide essential nuclear properties, that is, they gave too large incompressibility. Boguta and Bodmer introduced the nonlinear self-coupling of the σ meson [Bog77] , which has been widely accepted since then. The meson self-coupling term gives rise to

a new density dependence in the Lagrangian in such a way that the nuclear incompressibility can be lowered to reasonable values. The potential of RMF theory is quite similar to the potential of phenomenological shell model. Neutron and proton potential of Pb isotope which is calculated by RMF theory with the effective interaction NL3 can be seen in Fig. 3.3. From this figure, it can be clearly seen that neutron potential, which is not effected by Coulomb repulsion, is lower than proton potential. Using RMF theory with the parameter set NL3, the density distribution of baryon, neutron and proton for ^{208}Pb can be observed in Fig 3.4.

3.3.1 Relativistic Lagrangian Density

In the relativistic mean- field theory, the dynamics of a nuclear system which contains the corresponding fields $\psi(x)$ for nucleons, $\sigma(x)$, $\omega^\mu(x)$, $\vec{\rho}^\mu(x)$ for mesons and A^μ for photons, is determined through the Lagrangian density $\mathcal{L}$ [Ser86],

$$\mathcal{L} = \mathcal{L}_{\mathcal{N}} + \mathcal{L}_{\mathrm{m}} + \mathcal{L}_{\mathrm{coup}}^{\mathrm{lin}} + \mathcal{L}_{\mathrm{coup}}^{\mathrm{nonlin}} \tag{3.11}$$

where the first term describes the free Lagrangian for nucleons with spin $\frac{1}{2}$ and the mass m,

$$\mathcal{L}_N = \bar{\psi}(i\gamma_\mu \partial^\mu - m)\psi \tag{3.12}$$

Here, we employ the covariant notation of the four matrices $\gamma_\mu = (\gamma^0, -\gamma)$,

$$\gamma^0 = \begin{pmatrix} 1 & 0 \\ 0 & -1 \end{pmatrix} \quad , \quad \gamma = \begin{pmatrix} 0 & \sigma \\ -\sigma & 0 \end{pmatrix} \tag{3.13}$$

where σ corresponds to the three component Pauli spin 1/2 matrices.
The meson term describes free mesons (σ, ω and ρ) and photons,

$$\begin{aligned} \mathcal{L}_{\mathrm{m}} &= \frac{1}{2}(\partial_\mu \hat{\sigma} \partial^\mu \hat{\sigma} - m_\sigma^2 \hat{\sigma}^2) \\ &- \frac{1}{2}(\frac{1}{2}\hat{G}_{\mu\nu}\hat{G}^{\mu\nu} - m_\omega^2 \hat{\omega}_\mu \hat{\omega}^\mu) \\ &- \frac{1}{2}(\frac{1}{2}\hat{\vec{B}}_{\mu\nu} \cdot \hat{\vec{B}}^{\mu\nu} - m_\rho^2 \hat{\vec{\rho}}_\mu \cdot \hat{\vec{\rho}}^\mu) \\ &- \frac{1}{4}\hat{F}_{\mu\nu}\hat{F}^{\mu\nu} \end{aligned} \tag{3.14}$$

The fields $\hat{\sigma}$ and $\hat{\omega}^\mu$ describe the corresponding isoscalar-scalar and isoscalar-vector mesons; $\hat{\vec{B}}_{\mu\nu}$ is the field strength tensor of the isovector-vector ρ meson and $\hat{A}_\mu$ denotes the photon vector field.

The field tensors for the vector mesons (ω, ρ) and photon fields are defined as (since only the neutral ρ meson contributes in the calculation possible nonlinear terms in the field strength tensor do not contribute and are not taken into account)

$$\hat{G}_{\mu\nu} = \partial_\mu \hat{\omega}_\nu - \partial_\nu \hat{\omega}_\mu \tag{3.15}$$

$$\hat{\vec{B}}_{\mu\nu} = \partial_\mu \hat{\vec{\rho}}_\nu - \partial_\nu \hat{\vec{\rho}}_\mu \tag{3.16}$$

$$\hat{F}_{\mu\nu} = \partial_\mu \hat{A}_\nu - \partial_\nu \hat{A}_\mu. \tag{3.17}$$

The nucleon-meson coupling is described by linear coupling terms given as a sum,

$$\mathcal{L}_{\text{coup}}^{\text{lin}} = -g_\sigma \hat{\sigma} \hat{\bar{\psi}} \hat{\psi} - g_\omega \hat{\omega}_\mu \hat{\bar{\psi}} \gamma^\mu \hat{\psi} - g_\rho \hat{\vec{\rho}}_\mu \cdot \hat{\bar{\psi}} \vec{\tau} \gamma^\mu \hat{\psi} - e \hat{A}_\mu \hat{\bar{\psi}} \frac{1 + \tau_3}{2} \gamma^\mu \hat{\psi}. \tag{3.18}$$

with the coupling constants g_σ, g_ω, g_ρ and e. Here, the usual relativistic units of $\hbar = c = 1$ are used for the discussion of this model [Ser86]. M, m_σ, m_ω, m_ρ are the nucleon-, the σ-, ω-, ρ-meson masses respectively, while g_σ, g_ω, g_ρ and $e^2/4\pi = 1/137$ are the corresponding coupling constants for the mesons and photon.

$(J^\pi, T) = (0^+, 0)$ $(J^\pi, T) = (1^-, 0)$ $(J^\pi, T) = (1^-, 1)$
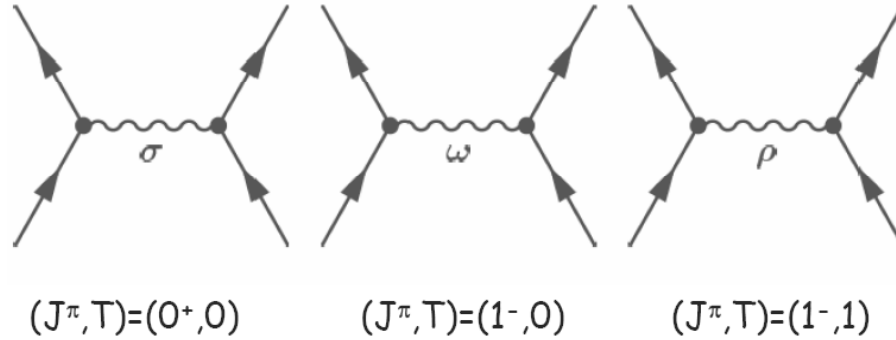
Here the fields have the following meaning:

Fields	T	J^π	Type of fields
$\sigma(\text{x})$	0	0	scalar field (massive)
$V^\nu(\text{x})$	0	1^+	vector field(massive)
A^ν (x)	0	1^+	photon filed (massless)
$\vec{R}^\nu(\text{x})$	1	1^+	isovector-vector field (massive)

Table 3.1: The fields from the relativistic mean field theory
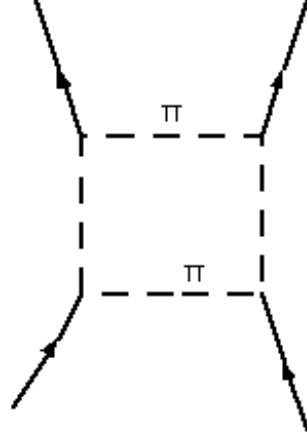
The σ- field can be identified with the 2π- exchange
while $V^\nu(\mathrm{x})$ describes ω- mesons (3π- exchange) and $\vec{R}^\nu(\mathrm{x})$ the ρ-mesons (isotriplet). The σ- field gives rise to the attractive part of the nucleon-nucleon potential, the ω- mesons to the short-range repulsion. The δ-meson with T=1, $J^\pi = 0^+$ is here not taken into account in the study of the properties of finite nuclei.

Possible non-linear terms in the Lagrangian are introduced via

$$\mathcal{L}_{\mathrm{coup}}^{\mathrm{nonlin}} = -U_\sigma[\hat{\sigma}] \tag{3.19}$$

In non-linear versions of the Lagrangian, the coupling is supplemented by a non-linear self coupling of the σ meson,

$$U[\hat{\sigma}] = \frac{1}{2}m_\sigma^2\hat{\sigma}^2 + \frac{1}{3}b_2\hat{\sigma}^3 + \frac{1}{4}b_3\hat{\sigma}^4, \tag{3.20}$$

first introduced by Boguta and Bodmer [Bog77] to improve the compressibility of nuclear matter and to obtain a quantitative description of nuclei.

3.3.2 Equations of Motion

The classical variational principle gives the equations of motion for the nucleon and meson fields,

$$\delta \int \mathcal{L}(\mathrm{q_i}, \partial_\mu \mathrm{q_i})\mathrm{d}^4\mathrm{x} = 0 \tag{3.21}$$

by solving the Euler-Lagrange equations for the Lagrangian density (3.11)

$$\partial_\mu(\frac{\partial \mathcal{L}}{\partial(\partial_\mu q_i)}) - \frac{\partial \mathcal{L}}{\partial q_i} = 0, \tag{3.22}$$

where q_i is one of the generalised coordinates; $q_i=\psi$ corresponds to the nucleon, and $q_i=\sigma$, ω_μ, $\vec{\rho}_\mu$ and A_μ are meson and photon fields respectively. The Dirac equation with the scalar and vector fields describes the nucleon,

$$\{\gamma^\mu(i\partial_\mu + g_\omega\omega_\mu + g_\rho\vec{\tau}\vec{\rho}_\mu + e\frac{1+\tau_3}{2}A_\mu) + (M + g_\sigma\sigma)\}\psi_i = 0 \tag{3.23}$$

from the above Dirac equation, the vector potential $V(\mathbf{r})$ can be represented by:

$$V(\mathbf{r}) = g_\omega\omega_\mu(\mathbf{r}) + \mathbf{g}_\rho\vec{\tau}\vec{\rho}_\mu(\mathbf{r}) + \mathbf{e}\frac{\mathbf{1}+\tau_\mathbf{3}}{\mathbf{2}}\mathbf{A}_\mu)(\mathbf{r}) \tag{3.24}$$

and the scalar potential $S(\mathbf{r})$:

$$S(\mathbf{r}) = \mathbf{g}_\sigma\sigma(\mathbf{r}) \tag{3.25}$$

the latter contributes to the effective mass by:

$$M^*(\mathbf{r}) = \mathbf{M} + \mathbf{S}(\mathbf{r}) \tag{3.26}$$

The conservation of the baryon current is established by:

$$\partial_\mu B^\mu = 0 \tag{3.27}$$

with the conserved baryon current

$$B^\mu = \hat{\psi}\gamma^\mu\psi \tag{3.28}$$

Eq. (3.22) yields the Klein-Gordon equations for the meson and photon fields that read:

$$\begin{aligned}
(-\Delta + m_\sigma^2)\sigma(\mathbf{r}) &= -g_\sigma\rho_s(\mathbf{r}) - b_2\sigma^2(\mathbf{r}) - b_3\sigma^3(\mathbf{r}), \\
(-\Delta + m_\omega^2)\omega^\mu(\mathbf{r}) &= g_\omega j^\mu(\mathbf{r}) + b_4\omega_\mu^2(\mathbf{r})\omega^\mu(\mathbf{r}), \\
(-\Delta + m_\rho^2)\rho^{a\mu}(\mathbf{r}) &= g_\rho j^{a\mu}(\mathbf{r}), \\
-\Delta A^\mu(\mathbf{r}) &= e j_p^\mu
\end{aligned} \tag{3.29}$$

These Dirac and Klein-Gordon equations are difficult to solve so that some approximation are needed. This relativistic mean-field model of the nucleus is formulated on the basic of two approximations, the mean field and no-sea approximation.

1. Mean Field Approximation

The mean field approximation is a treatment for mesonic and baryonic degrees of freedom. The mean field approximation ignores all quantum fluctuations of the meson fields and utilises their expectation values. It means that all meson field operators are replaced by their expectation values, which are classical fields. It can formally be symbolised by [Ser86]

$$\phi \to <\phi> \quad \equiv \quad \phi_0 \tag{3.30}$$

$$V_\mu \to <V_\mu> \quad \equiv \quad \delta_{\mu 0} V_0 \tag{3.31}$$

In this approximation the nucleons interact only via the mean fields. The mean field treatment also simplifies the handling of the nucleons. Nucleons move as independent particles in the mean fields in such a way that the nucleon field operator ψ can be expressed at all times in terms of a single-particle state α as [Rei89]

$$\psi = \sum_\alpha \varphi_\alpha(x^\mu) \hat{a}_\alpha \tag{3.32}$$

here, $\hat{a}_\alpha$ is the annihilation operator for a nucleon in the state α and $\varphi_\alpha(x^\mu)$ is the appropriate single-particle wave function. The scalar density is the summation over the bi-linear expressions of φ_α,

$$<\Psi : \bar{\psi}\psi : \Psi> = \sum_{\alpha < F} \bar{\varphi}_\alpha \varphi_\alpha - \sum_{\alpha < F_0} \bar{\varphi}_\alpha{}^{free} \varphi_\alpha{}^{free} \tag{3.33}$$

where F_0 is the Fermi level with respect to the nucleon number zero and F is the Fermi level with respect to a given nucleus. To ignore the quantum field effects, we rewrite the summation in equation (3.33) as

$$<\Psi : \bar{\psi}\psi : \Psi> = (\sum_{\alpha < F} \bar{\varphi}_\alpha \varphi_\alpha - \sum_{\alpha < F_0} \bar{\varphi}_\alpha{}^{free} \varphi_\alpha{}^{free}) + \sum_{\alpha=1}^{A} \bar{\varphi}_\alpha \varphi_\alpha \tag{3.34}$$

here, A is a nucleon number between F_0 and F (see Fig. 3.5).

2. No-sea approximation

The no-sea approximation is an approximation for the treatment of the nucleons. The RMF approach is considered as an effective Lagrangian for nuclear mean-field calculations at the Hartree level without the negative energy states of nucleons. Neglecting the vacuum contributions reduces the summation to the occupied particle states only, $\alpha = 1, \cdots, A$. This is the so called no-sea approach and the scalar density becomes

$$< \Psi : \bar{\psi}\psi : \Psi > \sim \sum_{\alpha=1}^{F} \bar{\varphi}_\alpha \varphi_\alpha \qquad (3.35)$$

In a complete Hartree calculation, we would also have to include the negative energy states from the Dirac sea. However, this could lead to divergent terms, which can be removed by a proper renormalization in a very complicated way, since the corresponding equations can be solved only numerically [Rin96]. An analytical solution for infinite nuclear matter has already been presented in [Chi74]. If the vacuum polarisation is taken into account, the parameter set of the effective Lagrangian has to be re-adjusted to the experimental data, giving a new force with approximately the same results as in the case when the vacuum polarisation is switched off [Hor84, Was88, Zhu91]. Therefore the no-sea approximation is used in most of the RMF applications in nuclear matter and finite nuclei.

In order to describe the ground-state properties of nuclei, the stationary limit of the time-independent relativistic mean-field equations of motion is taken into account by adopting the mean-field and no sea approximations. Since the ground-state of even-even nuclei is even under the time-reversal and has good parity, the space-like components of the vector fields and the currents vanish. Moreover, only the third (neutral) component of the rho-meson field remains because the single-particle states do not mix isospin. The stationary RMF equations for the meson fields are described as the time-independent inhomogeneous equations with the nucleon densities as source terms:

$$
\begin{aligned}
(-\Delta + m_\sigma^2)\Phi + \frac{\partial U_\sigma[\Phi]}{\partial \Phi} &= -g_{N\sigma}\rho^{\mathrm{s}}, \\
(-\Delta + m_\omega^2)\omega_0 + \frac{\partial U_\omega[\omega_\mu]}{\partial \omega_0} &= g_{N\omega}\rho - \frac{f_{N\omega}}{2m_N}\rho^{\mathrm{t}}, \\
(-\boldsymbol{\Delta} + m_\omega^2)\boldsymbol{\omega} + \frac{\partial U_\omega[\omega_\mu]}{\partial \boldsymbol{\omega}} &= g_{N\omega}\mathbf{j} - \frac{f_{N\omega}}{2m_N}\mathbf{j}^{\mathrm{t}},
\end{aligned}
$$

$$
\begin{aligned}
(-\Delta + m_\delta^2)\delta^0 &= g_{N\delta}\rho^{\mathrm{s}}_{T=1}, \\
(-\Delta + m_\delta^2)\rho_0^0 &= g_{N\rho}\rho_{T=1} - \frac{f_{N\rho}}{2m_N}\rho^{\mathrm{t}}_{T=1}, \\
(-\boldsymbol{\Delta} + m_\rho^2)\boldsymbol{\rho}^0 &= g_{N\rho}\mathbf{j}_{T=1} - \frac{f_{N\rho}}{2m_N}\mathbf{j}^{\mathrm{t}}_{T=1} \\
-\Delta A_0 &= e\rho_p, \\
-\boldsymbol{\Delta}\mathbf{A} &= e\mathbf{j}_p.
\end{aligned}
\tag{3.36}
$$

The corresponding source terms are

$$
\begin{aligned}
\rho^{\mathrm{s}} &= \sum_{\alpha\in\Omega} v_\alpha^2 \bar{\psi}_\alpha \psi_\alpha, \\
\rho &= \sum_{\alpha\in\Omega} v_\alpha^2 \bar{\psi}_\alpha \gamma_0 \psi_\alpha, & \mathbf{j} &= \sum_{\alpha\in\Omega} v_\alpha^2 \bar{\psi}_\alpha \gamma \psi_\alpha, \\
\rho^{\mathrm{t}} &= \nabla\cdot\sum_{\alpha\in\Omega} v_\alpha^2 \bar{\psi}_\alpha \psi_\alpha i\gamma_0\gamma \psi_\alpha, & \mathbf{j}^{\mathrm{t}} &= \nabla\times\sum_{\alpha\in\Omega} v_\alpha^2 \bar{\psi}_\alpha \boldsymbol{\Sigma} \psi_\alpha,
\end{aligned}
\tag{3.37}
$$

here, the index "s" stands for scalar density and "t" represents tensor densities. The isovector densities and electric field can be expressed in terms of "T=1" and for the proton, it is described with the index "p".

$$
\begin{aligned}
\rho^{\mathrm{s}}_{\mathrm{T=1}} &= \sum_{\alpha\in\Omega} v_\alpha^2 \tau_\alpha \bar{\psi}_\alpha \psi_\alpha, \\
\rho_{\mathrm{T=1}} &= \sum_{\alpha\in\Omega} v_\alpha^2 \tau_\alpha \bar{\psi}_\alpha \gamma_0 \psi_\alpha, & \mathbf{j}_{\mathrm{T=1}} &= \sum_{\alpha\in\Omega} v_\alpha^2 \tau_\alpha \bar{\psi}_\alpha \gamma \psi_\alpha, \\
\rho^{\mathrm{t}}_{\mathrm{T=1}} &= \nabla\cdot\sum_{\alpha\in\Omega} v_\alpha^2 \tau_\alpha \bar{\psi}_\alpha \psi_\alpha i\gamma_0\gamma \psi_\alpha, & \mathbf{j}^{\mathrm{t}} &= \nabla\times\sum_{\alpha\in\Omega} v_\alpha^2 \tau_\alpha \bar{\psi}_\alpha \boldsymbol{\Sigma} \psi_\alpha, \\
\rho_{\mathrm{p}} &= \sum_{\alpha\in\Omega} v_\alpha^2 \frac{1}{2}(1+\tau_\alpha)\bar{\psi}_\alpha \gamma_0 \psi_\alpha, & \mathbf{j}_{\mathrm{p}} &= \sum_{\alpha\in\Omega} v_\alpha^2 \frac{1}{2}(1+\tau_\alpha)\bar{\psi}_\alpha \gamma \psi_\alpha.
\end{aligned}
\tag{3.38}
$$

The Relativistic Hartree equation for the time independent basic wave function ψ_α can be written as follows:

$$
\begin{aligned}
\epsilon_\alpha \psi_\alpha = \hat{h}_\alpha \psi_\alpha &= (-i\gamma_0 \gamma\cdot\nabla + m_{\mathrm{N}}\gamma_0 \\
&\quad + \gamma_0 U_\alpha^s + U_\alpha^0 - \gamma_0\gamma\cdot\mathbf{U}_\alpha + i\gamma\cdot\tilde{\mathbf{U}}_\alpha^t + \gamma_0\boldsymbol{\Sigma}\cdot\mathbf{U}_\alpha^t)\psi_\alpha
\end{aligned}
\tag{3.39}
$$

where $\hat{h}_\alpha$ is the single particle Hamiltonian operator. The single particle potentials with the various coupling can be summarised as:

$$
\begin{aligned}
U_\alpha^s &= g_{N\sigma}\Phi + g_{N\delta}\tau_\alpha\delta^0, \\
U_\alpha^0 &= g_{N\omega}\omega_0 + g_{N\rho}\tau_\alpha\rho_0^0 + e\tfrac{1}{2}(1+\tau_\alpha)A_0, & \mathbf{U}_\alpha &= gN_\omega\omega + g_{N\rho}\tau_\alpha\rho_0 + e\tfrac{1}{2}(1+\tau_\alpha)\mathbf{A}, \\
\tilde{\mathbf{U}}_\alpha^t &= \frac{f_{N\omega}}{2m_{\mathrm{N}}}\nabla\omega_0 + \frac{f_{N\rho}}{2m_{\mathrm{N}}}\tau_\alpha\nabla\rho_0^0, & \mathbf{U}_\alpha^t &= \frac{f_{N\omega}}{2m_{\mathrm{N}}}\nabla\times\omega + \frac{f_{N\rho}}{2m_{\mathrm{N}}}\tau_\alpha\nabla\times\rho_0
\end{aligned}
\tag{3.40}
$$

3.3.3 Effective Interactions

In the above Lagrangian density (3.11), there are 10 parameters for nonlinear effective interactions, which are adjusted by fitting the bulk nuclear properties. The mass of the ρ meson is fixed to the experimental value ($m_\rho = 763.0\text{MeV}$), the value is slightly tuned in the chiral model (parameter set ChiM). The parameters are fitted to measured ground state properties, mainly to the charge and neutron radii and the binding energies of several spherical nuclei.

	NL3	NL-Z2	ChiM	PL40
m_N (MeV)	939.0	938.9	939.2	938.9
m_σ(MeV)	508.194	493.150	466.5	547.570
m_ω(MeV)	782.501	780.0	780.6	780.0
m_ρ(MeV)	763.0	763.0	761.1	763.0
gN_σ	10.2170	10.1369	-10.569	10.0514
gN_ω	12.8680	12.9084	13.3265	12.8861
gN_ρ	4.47400	4.55627	5.48851	4.81014
b_2 (fm^{-1})	-10.4310	13.7561	-	-
b_3	-28.8850	-41.4013	-	-

Table 3.2: Effective Interactions in RMF theory: NL3, NL-Z2, ChiM and PL40

In our present work, we use four effective interactions; NL3 [Lal97] NL-Z2, [Bür02b], ChiM [Sch02] and PL40 [Rei88], which are described in Table 3.2. The RMF model descriptions (NL3 and NL-Z2) are quite successful in describing the properties of nuclear properties over a wide range of mass numbers. The prominent feature of NL-Z2 is its low incompressibility.

The chiral model (ChiM), using a chiral symmetry has been developed for a good description of nuclear saturation and a reasonable description of nuclei and hypernuclei with a single model and a single set of parameters. In the chiral model (ChiM), a hadronic model based on a chiral SU(3) ansatz in a nonlinear realization of chiral symmetry is used (for a comprehensive reviews in Ref. [Sch02]). The degrees of freedom in chiral model (parameter set ChiM) are seen in table 3.3.

The nuclear asymmetry energy in ChiM parameter set is quite close to the empirical value. The lowering of the asymmetry energy in the chiral model is obtained due to the influence of the isospin triplet δ meson and the non-linear terms in the vector self-interaction [Bec02]. In a test case the chiral model (ChiM) shows fair agreement with the experimental result in the prediction of ^{68}Se for the

Baryons	n (ddu) p (uud)	
Baryons	Σ^- (sdd) Σ^0 Λ (sdu) Σ^+ (suu)	hyperons
Baryons	Ξ^- (ssd) Ξ^0(ssu)	hyperons
Scalar Mesons	κ^0 ($\bar{s}$ d) κ^+ ($\bar{s}$ u)	
Scalar Mesons	δ^- ($\bar{u}$ d)δ^0, σ, ζ δ^+ ($\bar{d}$u)	
Scalar Mesons	κ^- (u $\bar{s}$) $\kappa^{\bar{0}}$(d $\bar{s}$)	
$\sigma \sim \langle \bar{u}$ u $+ \bar{d}d\rangle$	$\zeta \sim \langle \bar{s}s\rangle$	$\delta^0 \sim \langle \bar{u}$ u $- \bar{d}d\rangle$
Vector Mesons	K^{*0} ($\bar{s}$ d)K^{*+}($\bar{s}$ u)	plus pseudoscalars,
Vector Mesons	ρ^- ($\bar{u}$ d) ρ^0, ω, ϕ ρ^+ ($\bar{d}$ u)	axial vectors and
Vector Mesons	K^{*-} (u $\bar{s}$) $K^{*\bar{0}}$(d $\bar{s}$)	gluonic field χ.

**Table 3.3:** Degrees of freedom in chiral model (parameter set ChiM)

nuclear ground states with substantial oblate ($\beta_2 \sim$ -0.3) deformation. The comprehensive view of experimental results can be seen in Ref.[Fis00]. Our model calculation for ^{68}Se displays oblate ground state ($\beta_2 \sim$ -0.3) and excited prolate state as shown in Fig 3.6.

	NL3	NL-Z2	ChiM	PL40
$\rho_0(fm^{-3})$	0.148	0.151	0.153	0.152
E/A (MeV)	-16.299	-16.07	-15.2	-16.18
m*/m	0.595	0.583	0.6	0.581
K (MeV)	271.76	172	215.33	165
E_{sym} (MeV)	37.4	39.0	31.9	41.7

Table 3.4: Bulk properties of nuclear matter for the forces under consideration: K corresponds to the incompressibility of the nuclear matter for each set of parameters
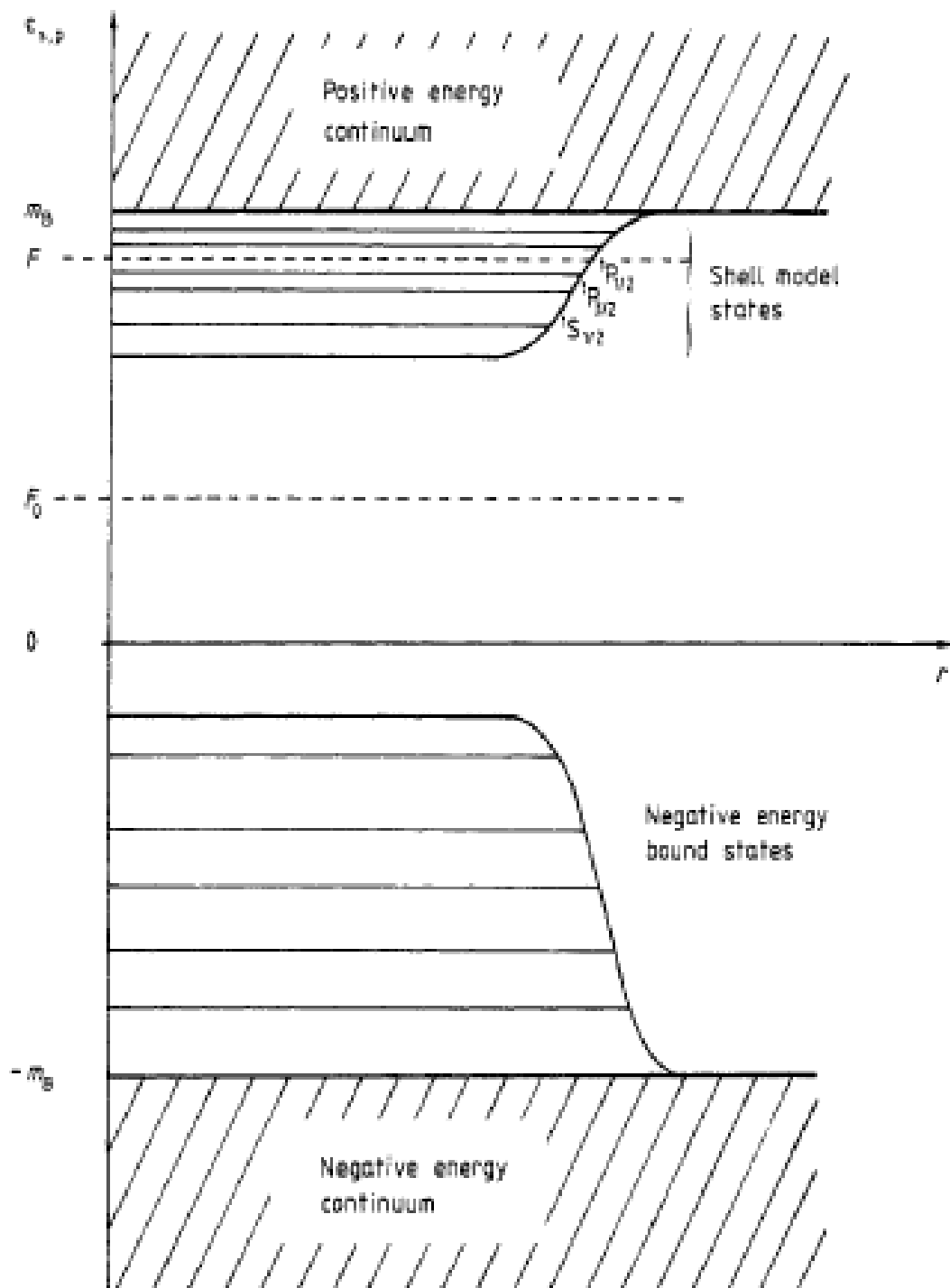
Figure 3.5: Schematic spectrum of the Dirac equation with external r-dependent fileds. The F_0 is the Fermi surface for the total number 0. F is the Fermi surface for a nuclei; here it represents ^{16}O if both proton and neutrons are filled up to F. Sources: [Rei89]
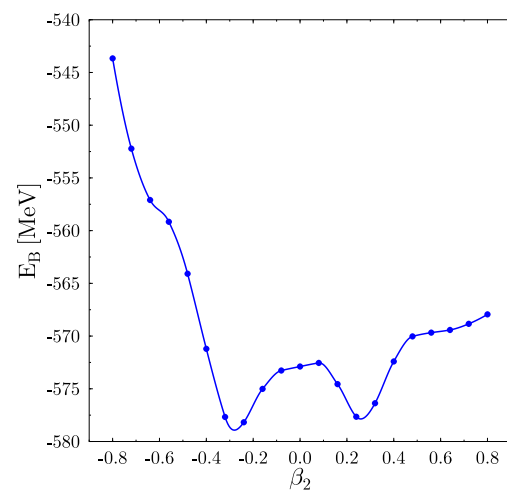
Figure 3.6: Deformation β_2 of ^{68}Se:oblate ground state ($\beta_2 \sim$ -0.3) and excited prolate state.

–IV–

Nature of Exotic Nuclei

In general, the study of the structure of the atomic nucleus provides us with fascinating insights into systems made of many strongly interacting particles. The nuclei far from the β-stability line which are referred to as exotic nuclei have attracted considerable interest in recent years. Nuclei far from stability play an important role in the way the elements are synthesised in the universe. Exotic nuclei are nuclei lying away from the line of β stability with a proton-to-neutron ratio that is very different from the proton-to-neutron ratio in stable nuclei and therefore have a relatively short half-life. The study of exotic nuclei is one of the main frontiers of nuclear structure research [Mue99a, Tan99]. Experimental production and the theoretical investigation of exotic nuclei is of particular interest in understanding the stellar nucleosynthesis, the creation of the heavy elements as they are observed now, and the role of isospin in determining the structure and properties of nuclei. It is therefore a challenge for theoretical investigations to provide models with a high predictive power. Achievements in the description of nuclei near and far away from the β-stability line in the framework of the relativistic mean field (RMF) approach can be found in a series of review articles [Ser86, Rei89, Rin96, Vre05, Men06, Sha93].

4.1 Nucleosynthesis

Nucleosynthesis is the process of creating new atomic nuclei from preexisting nucleons. Explosive nucleosynthesis, including supernova nucleosynthesis, produces most of the heavy elements present in the universe. In explosive environments such as supernovae further nucleosyntesis processes can occur, such as the r-process (in which heavier elements than iron and nickel are produced by rapid absorption of free neutrons) and the rp process (which involves the rapid absorp-

tion of free protons).

Figure 4.1: Kepler's Supernova from pictures by the Spitzer space Telescope, Hubble Space Telescope and Chandra X-ray Observatory.
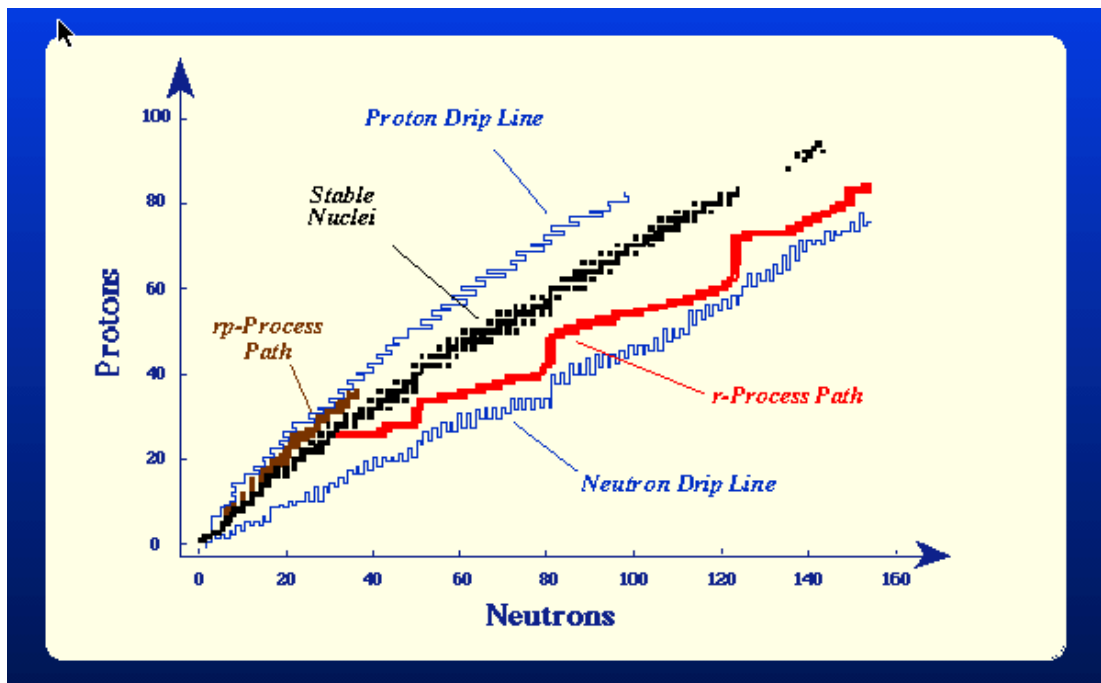
4.2   r-process

The r-process (r- represents rapid) is a neutron capture process for radioactive elements that occurs in high neutron density and high temperature regimes. In the r-process, nuclei are bombarded with a large neutron flux ($\sim 10^{22}$ nucleons/cm^2s^{-1}) to form highly unstable neutron rich nuclei, which very rapidly decay (relatively to normal β decay) to stable neutron rich nuclei. The site of the r-process is believed to be the supernova environment. The r-process is responsible for the synthesis of half of the heavier nuclei beyond the iron group [Cow91, Qia03]. The nuclei in the r-process path are extremely neutron rich and short lived.

4.3   rp-process

The rp-process (rapid proton capture process) consists of consecutive proton captures onto seed nuclei to produce heavier elements. It is also a nucleosynthesis process and occurs with the s process and r process. The process has to occur in very high temperature environments (above 1 x 10^9 K) so that the protons can

overcome the large Coulomb barrier for charged particle reactions. The proton-rich nuclei below a nucleon number of about 80-100 are thought to be produced in a series of rapid proton captures taking place in astrophysical environments characterised by explosive hydrogen burning. This sequence of reactions is termed the rapid proton capture or rp process. A group of nuclei that play an important role in the rp-process are the so called waiting point nuclei. These nuclei have particularly long lifetimes under rp-process conditions owing to long β decay half-lives and low proton capture Q-values. There is a very remarkable difference to the neutron-induced r process: the rp path runs much closer to the stability valley (see in Fig 4.2). This will have significant implications for the properties of the rp process.

Figure 4.2: The comparison of r-process path and rp-process path Sources: [Gui94]

4.4   Neutron Halo in Light Nuclei

Exotic nuclei have casted new light on nuclear structure entirely new feature appeared: eg the neutron halo in ^{11}Li [Tan85b] and neutron skin [Tan92] as the rapid increase in the measured interaction cross section in the neutron-rich light nuclei. The nucleus ^{11}Li showed a remarkably large radius suggesting a
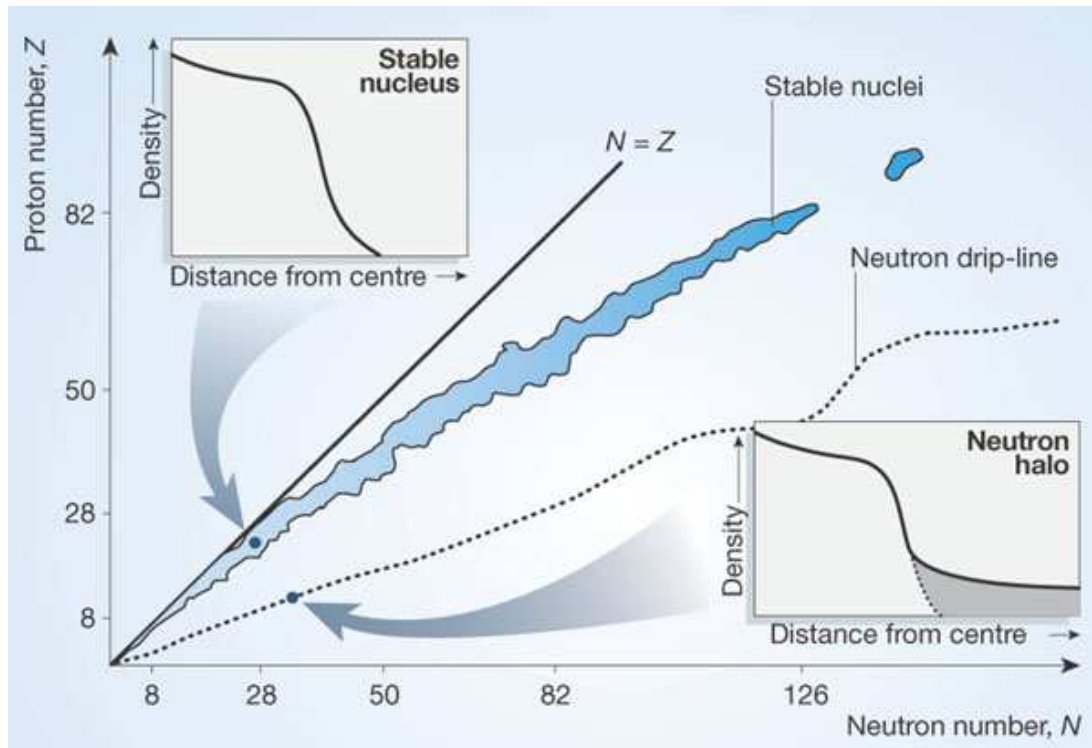
**Figure 4.3:** Nuclear stability and neutron halos. Source: [Hin04]

large deformation or a long tail in the matter distribution. The nuclear densities and sizes of the systems approaching the driplines with exotic N/Z ratios are different from those encountered in near stable nuclei. In certain light nuclei at the neutron dripline, the wave function describing the quantum state of the last neutron or neutrons, extends to a remarkably large distance out from the centre of the nucleus, so that these last few neutrons spend most of their time far from the normal density core of the nucleus and form a halo, in particular near the neutron dripline (see in Fig 4.3).

The structure of exotic nuclei with large isospin values gives rise to many interesting phenomena originating from the extremely weak binding of the outermost nucleons, regions of neutron halos and the existence of neutron skins. The separation energy of the last nucleons become extremely small at the driplines. The Fermi level close to the particle continuum and the lowest particle-hole is often embedded in the continuum. In such a loosely bound system, the neutron density distribution shows an extremely long tail, the neutron halo. The formation of neutron halo in Ne isotopes is presented in Fig. 4.4 and Fig. 4.5. The neutron rms radius display abrupt change from between ^{30}Ne and ^{32}Ne as shown in Fig.

4.4. This is an evidence of existence of neutron halo in ^{32}Ne with remarkably larger radius of neutron. From Fig. 4.5, one can observe that the proton density profiles do not display a distinctive change with the number of neutrons, while the neutron density distribution show an abrupt change between ^{30}Ne and ^{32}Ne. The nucleus ^{32}Ne display a remarkably large radius suggesting a long tail in the neutron density distribution.
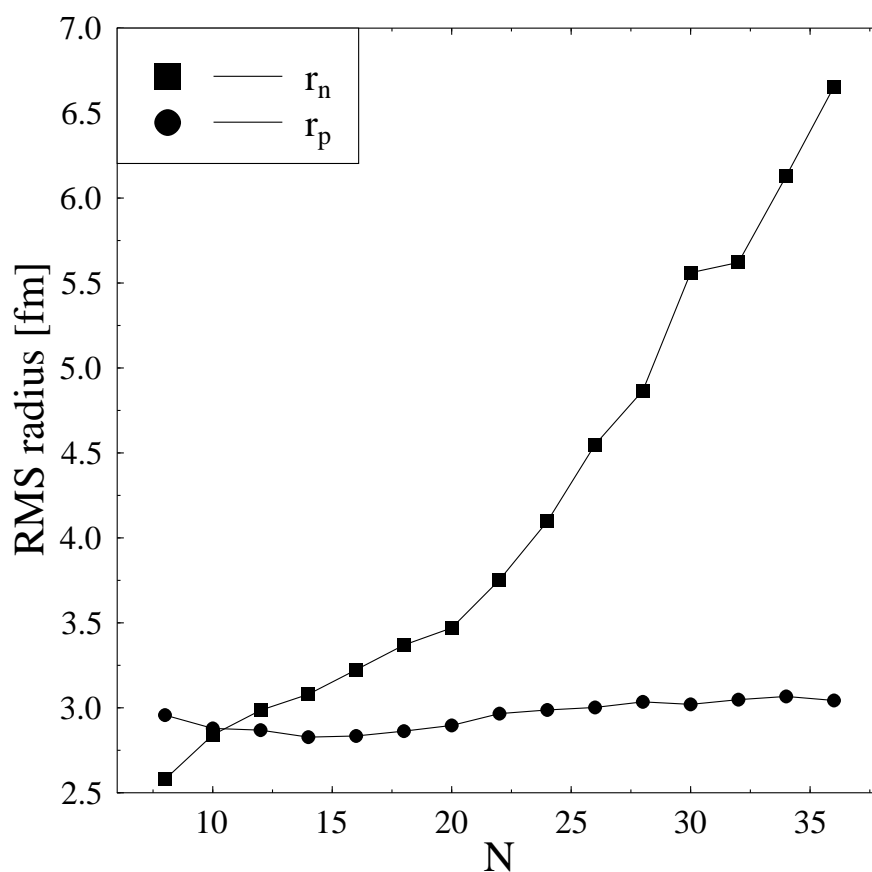
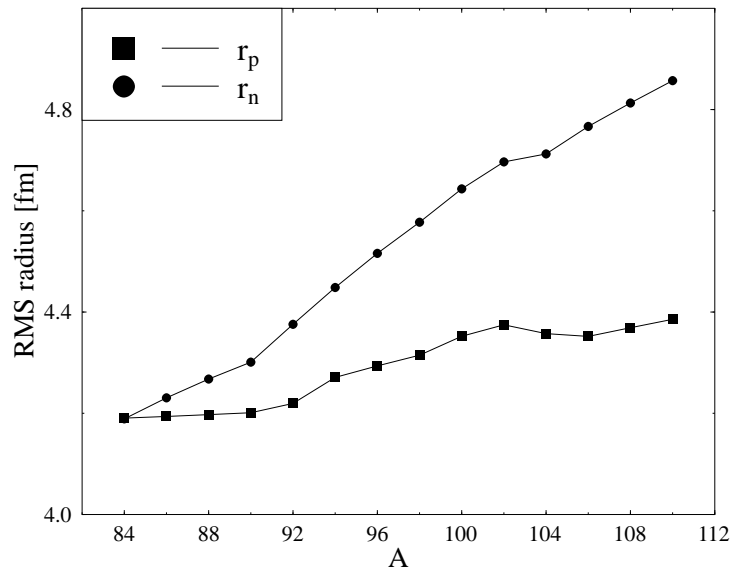**Figure 4.4:** Calculated proton and neutron rms radii for Ne isotopes (with the parameter set ChiM).
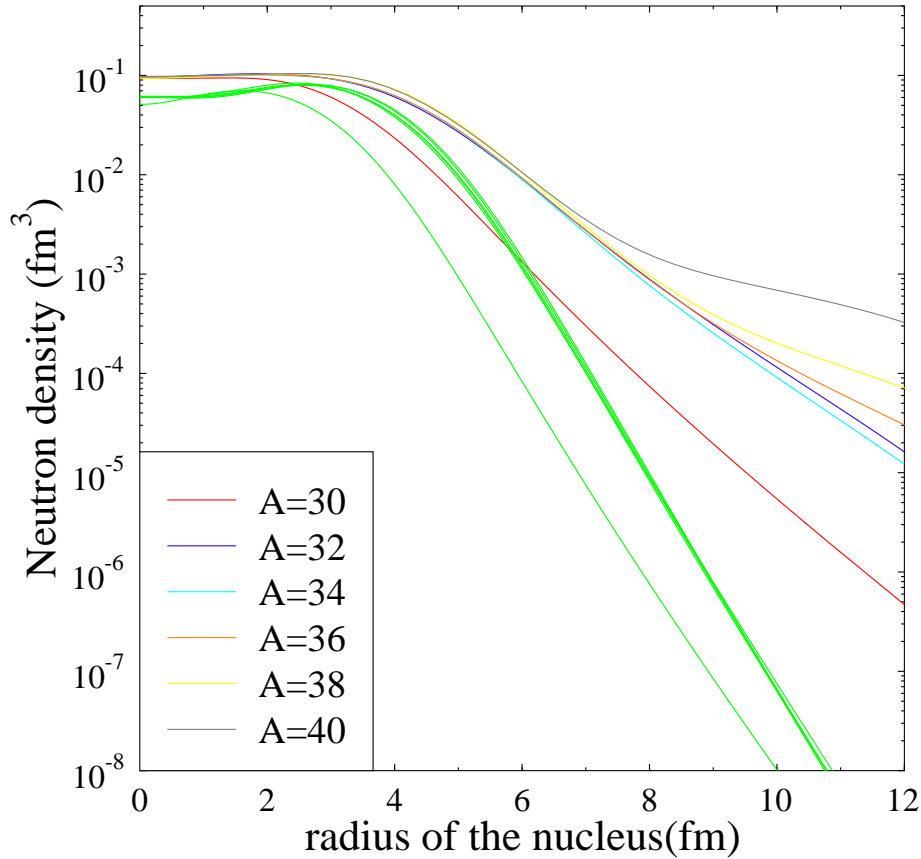
Figure 4.5: Proton and neutron density distributions of Ne isotopes (with the parameter set ChiM).

4.5   Neutron Skin Thickness

The large difference between the proton and neutron density distributions in unstable nuclei is the question of interest among new phenomena concerning exotic nuclei. The presence of a neutron skin in stable nuclei has been discussed since the mid 1950s [Mye69]. No evidence of a thick neutron skin in stable nuclei has been observed, even if many of them have a large neutron excess (N-Z). Thick neutron skins (~ 0.9fm) have been reported by Tanihata et al. in the He isotopes [Tan92]. Another formation of the neutron skin in unstable neutron-rich

nuclei has been observed in Na isotopes [Suz95]. The observation of nucleon density distribution provides basic and important information in nuclear structure. The proton distribution of stable nuclei can be determined accurately by elastic electron or muon scattering. There is, however, no comparable measurement of the neutron density distribution so far. Although it is difficult to obtain the nuclear density distribution, the difference in radii of neutron and proton density distribution can be estimated by comparing radii deduced from electromagnetic scattering to radii derived from nuclear reaction cross sections that are governed by proton and neutron densities.

Figure 4.6: Proton and neutron rms radii for Zr isotopes (with the parameter set ChiM).

The neutron and proton rms radii for the example of Zirconium isotopes (Zr, Z=40) are plotted in Fig. 4.6. The proton rms radius r_p is constant until A = 92. It slightly increases between A = 94 and A =96. The prominent increase of the proton rms radius takes place between A = 98 and 100 and it remains almost constant beyond this point. The prominent increase of r_p around A = 98 is obviously due to the transition from spherical to a quite deformed shape where two protons jump from the N = 3 to N = 4 shell, which has a large radius. The rms neutron radius display a smilar step at the transition point although it

increases steadily with the mass number in neutron excess region. It exhibits the fact that the more and more neutrons are built into the shell with N = 4 and N = 5. Like in proton rms radius, one pair is moved from the N = 3 to N = 4 shell at the shape transition step. One can define as the reinforcing effect of deformation and neutron excess. The calculated rms values (with the parameter set ChiM) are in agreement with the experimental results in Table within error bars.
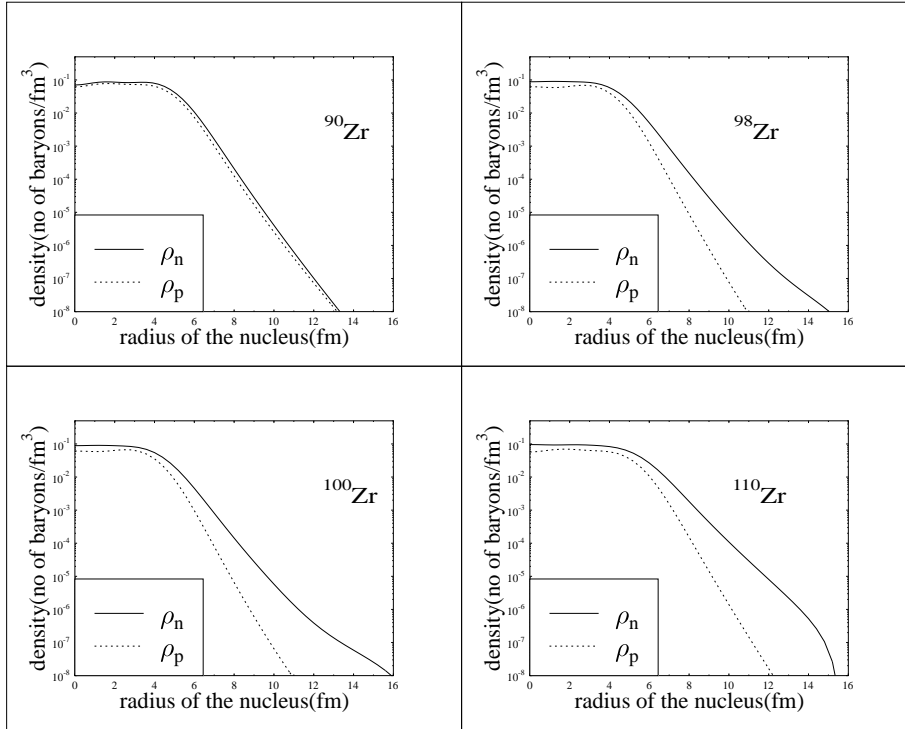
Figure 4.7: Proton and neutron density distributions of Zr isotopes: A very large neutron skin thickness for ^{110}Zr obtained.(with the parameter set ChiM)

In Fig 4.7, we shows the density distribution of neutron and proton for the nuclei ^{90}Zr, ^{98}Zr ^{100}Zr and ^{110}Zr. For ^{90}Zr isotope, the density distribution of neutron ρ_n and the density distribution of proton ρ_p exhibits minor deviation in the nuclear interior and at the surface two distribution are very similar. In the region of nuclei between ^{90}Zr and ^{98}Zr, the change of proton density distribution are not taken into account in comparison with the change of neutron density distribution. The neutron density distribution increases in the interior and considerably at the

surface. The shape transition from nuclei ^{98}Zr to nuclei ^{100}Zr reflects the movement of particles from N = 3 to N = 4 shell. From nuclei ^{102}Zr, proton density distribution changes very little. In the neutron excess (above A = 100)region, the neutron density distribution changes very rapidly and finally a quite large neutron skin thickness is obtained for ^{110}Zr nuclei near the neutron dripline.

A		E/A	r_n	r_p	r_c
84	ChiM	-8.60	4.19	4.19	4.19
	NL1	-8.58	4.23	4.22	4.23
	Expt.	-8.55			
90	ChiM	-8.73	4.30	4.20	4.26
	NL1	-8.73	4.36	4.21	4.29
	Expt.	-8.72			
94	ChiM	-8.66	4.45	4.27	4.37
	NL1	-8.64	4.47	4.23	4.32
	Expt.	-8.67			
96	ChiM	-8.63	4.52	4.29	4.42
	NL1	-8.59	4.53	4.24	4.32
	Expt.	-8.57			
98	ChiM	-8.59	4.58	4.31	4.47
	NL1	-8.53	4.60	4.27	4.34
	Expt.	-8.58			
100	ChiM	-8.55	4.64	4.35	4.53
	NL1	-8.48	4.75	4.44	4.63
	Expt.	-8.52			

Table 4.1: Results of the chiral model calculations of Zr isotopes: binding energy per particle E/A (MeV), root mean square radii (rms) for neutrons (protons) r_n (r_p), charge (r_c) radii (fm). The experimental data are taken from Ref. [Aud03]

4.6 Exotic Nuclei in the Region of Large Atomic Number

In this section we present exotic nuclei in the heavy region, such as Sn and Pb isotopes. The Sn isotopes are of particular interest for nuclear structure and also astrophysical questions because of the closure of the Z=50 proton shell. Relativistic mean field calculations employing the ChiM force, NL3 force and

experimental binding energies are compared in Fig. 4.8 Fig. 4.9 for Pb and Sn isotope. The ChiM force gives a reliable description of the binding energies per nucleon for both Sn and Pb isotopes and it is an agreement with experimental values. The strongest binding is obtained from the case of Pb istopes, at ^{116}Sn, consistent with experimental value. The experimental minimum of ^{208}Pb isotope is also reproduced by using the RMF theory with parameter sets NL3 and ChiM, as shown in Fig.4.8.
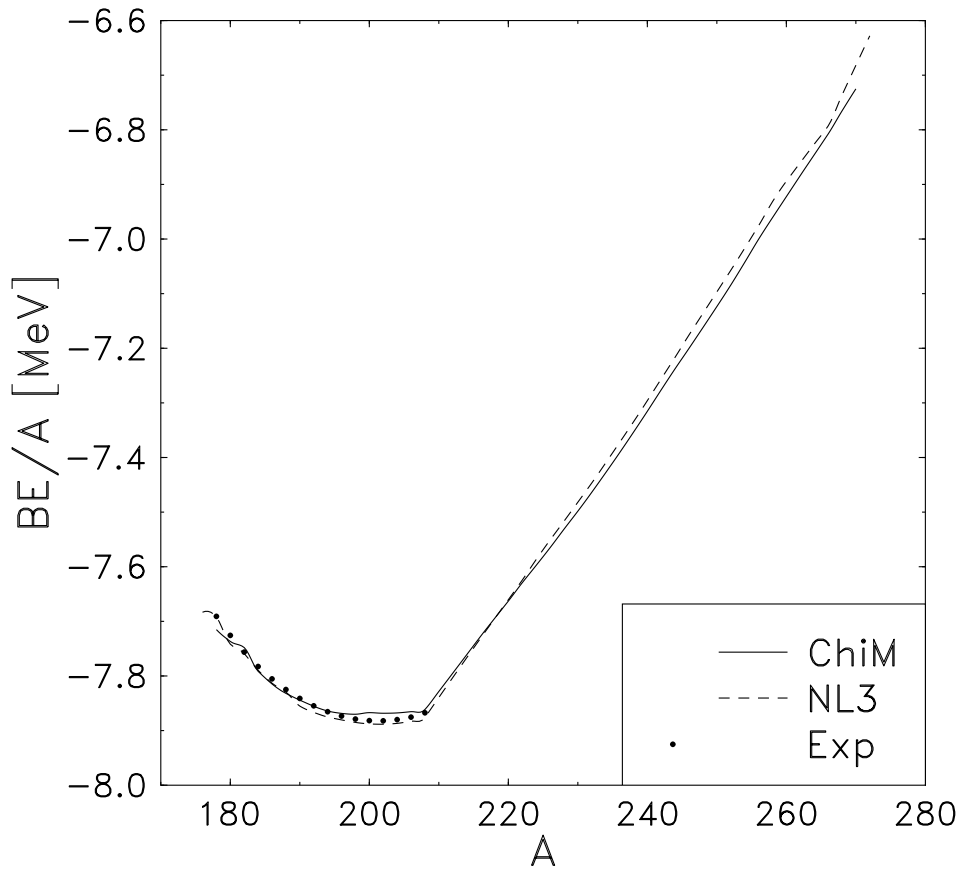
Figure 4.8: The binding energy per particle for Pb isotopes, E/A, against mass number A, calculated by ChiM and NL3 forces and experimental value

At the magic shells a strong sudden decrease is observed in the two neutron
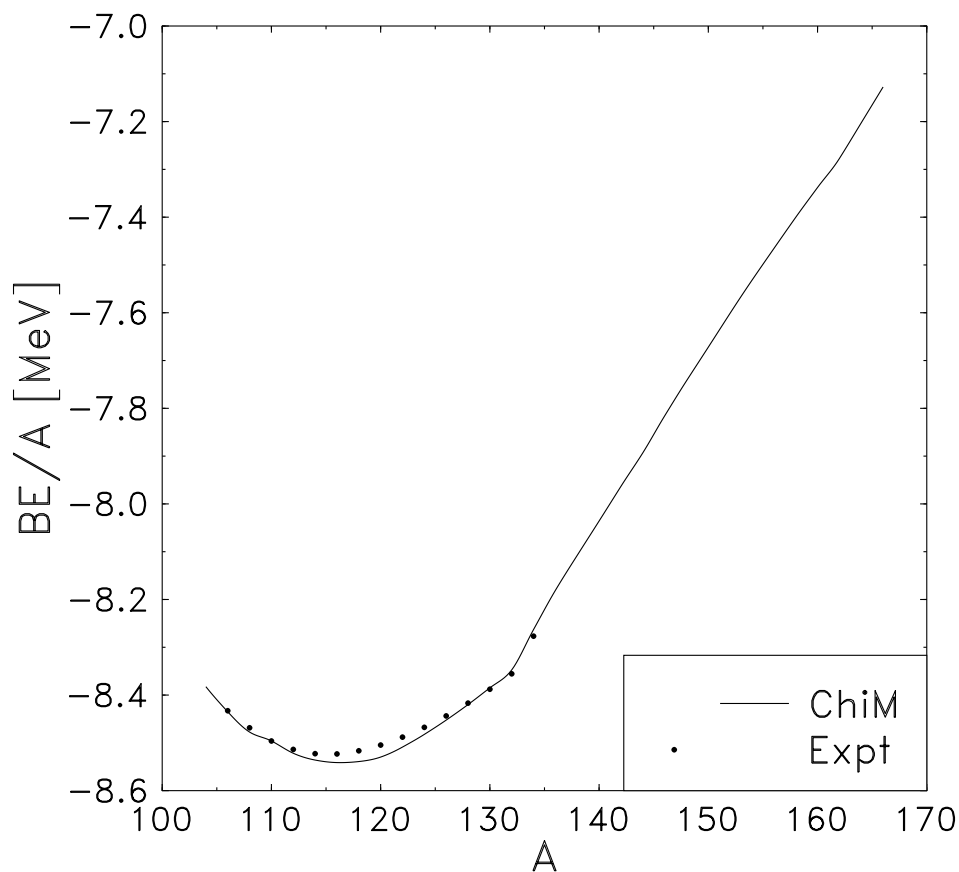
Figure 4.9: The binding energy per particle for Sn isotopes, E/A, against mass number A calculated by ChiM and experimental value

separation energy, as expected (see Fig.4.10). The magic jump in the two-nucleon separation energy

$$S_{2n}(N, Z) = E(N - 2, Z) - E(N, Z)$$
$$S_{2p}(N, Z) = E(N, Z - 2) - E(N, Z) \tag{4.1}$$

is of also quite important observable since it can be used for determining shell closures in the super heavy elements, as will be discussed in the last chapter.

The separation energies for Sn isotopes are shown in Fig 4.10. As shown from this figure the ChiM paramether gives a fair descrption of two neutron separation energies for Sn isotopes and it gives a good agreement with experimental values and FRDM [Möl95].
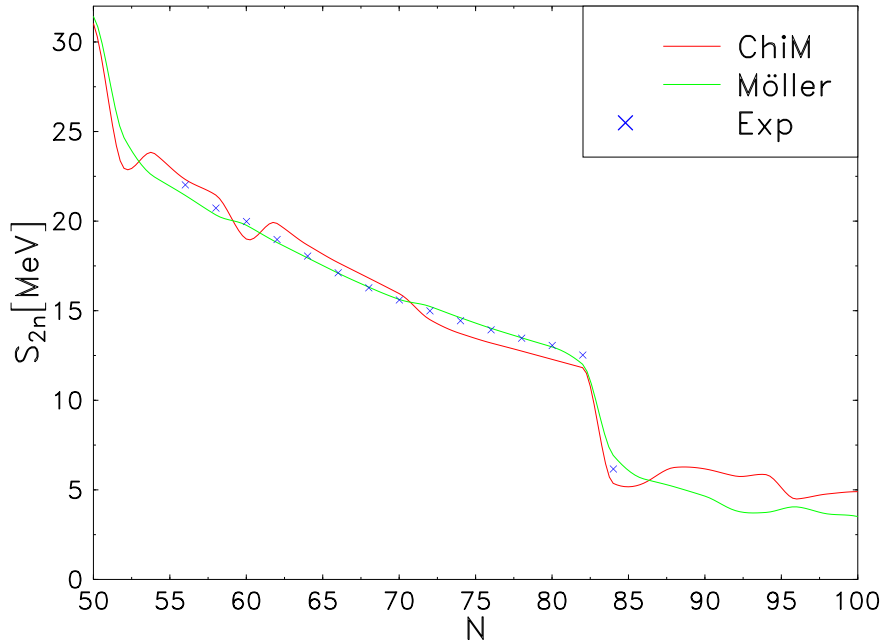
**Figure 4.10:** Two neutron separation energies of Sn isotopes

Neutron density distributions for several Sn and Pb isotopes are displayed in Fig. 4.11 and Fig. 4.12 calculated by ChiM parameter set. In the case of Sn isotopes, an extremely thick neutron skin builds up at ^{102}Sn, the nuclei next to the doubly magic nuclei ^{100}Sn. It leads to a sudden jump in the neutron rms radii. The rms proton and neutron radius for Sn isotopes can be observed in Fig. 4.14. And a quite large neutron skin thickness can also be found beyond ^{132}Sn, another doubly magic nuclei leading a sudden jump in the neutron rms radii. At A = 132 of Sn isotope, the $1h_{11/2}$ shell is filled and pairing does not contribute. The neutron 3p subshells become populated at larger masses of Sn isotopes. Weak binding allow a large extension of valence wave functions into the exterior, thus producing this extremely thick neutron skin. According to Fig.

4.14,the rms neutron radius of Sn isotope increases suddenly at A = 132 while the rms proton radius increases steadily. The neutron skin thickness is cleary visible in Fig. 4.15 for Sn isotopes where the difference of the proton and neutron radii is shown. The neutron density distribution Pb isotopes exhibits an extremely thick neutron skin is building up for isotopes beyond doubly magic nuclei ^{208}Pb. From ^{200}Pb nucleus to ^{216}Pb nucleus are in spherical shape and ^{220}Pb is in prolate shape ($\beta_2 \sim 0.2$). Because of the shape transistion, Pb isotopes beyond ^{208}Pb have large neutron distributions leading to an extremely thick neutron skin. And ^{240}Pb forms quite prolate shape ($\beta_2 \sim 0.32$) and ^{260}Pb, which closes to neutron dripline, is in spherical shape in such a way that the large neutron skin thickness reflects the shape transistion of these elements.

Pb isotopes close to ^{260}Pb and neutron driplines are in spherical shape, Pb isotopes close to the proton dripline and some isotopes near N=164 are in oblate deformed shape, and the rest are in the form prolate shape. It is interesting to investigate the deformation of Pb isotopes. We have carried out the calculated energy surface for ^{186}Pb. We observe that the lowest three states in the energy spectrum of the neutron deficient nucleus ^{186}Pb are spherical, oblate and prolate as shown in Fig. 4.16. Our calculation is in agreement with other three dimensional calculation [And00]

4.7   Superdeformation of Pb isotopes

Superdeformation (SD) of atomic nuclei is one of the most attractive topics in nuclear structure studies. Shape coexistence in Pb isotopes on the proton rich side has been observed experimentally, as for instance in Ref. [And00]. It is also been studied theoretically within the relativistic mean field model [Vre05]. In this work, superdeformation of Pb isotopes is investigated in RMF theory with the parameter set ChiM. Potential energy curves for $^{190-204}$Pb are exhibited in Fig. 4.18. For ^{190}Pb, the RMF theory (with the parameter set ChiM) can produce a considerable high excitation energy relative to the ground SD bands and shallow well in the SD minimum in comparison with its neighbouring nucleus ^{192}Pb signifies it is difficult form the stable SD state. Although the excitation energy of ^{192}Pb isotope is relatively lower, it is relatively easy to form SD state as observed in experiment. As the number of neutron increase, the excitation energy increases with the increasing of depth of well from the ^{194}Pb isotopes. The SD states can still be observed in these nuclei and it is reasonable agreement with the RMF theory (with the parameter set ChiM) and experimental observations. For nuclei (N > 118), however, it is difficult to excite the SD states because the
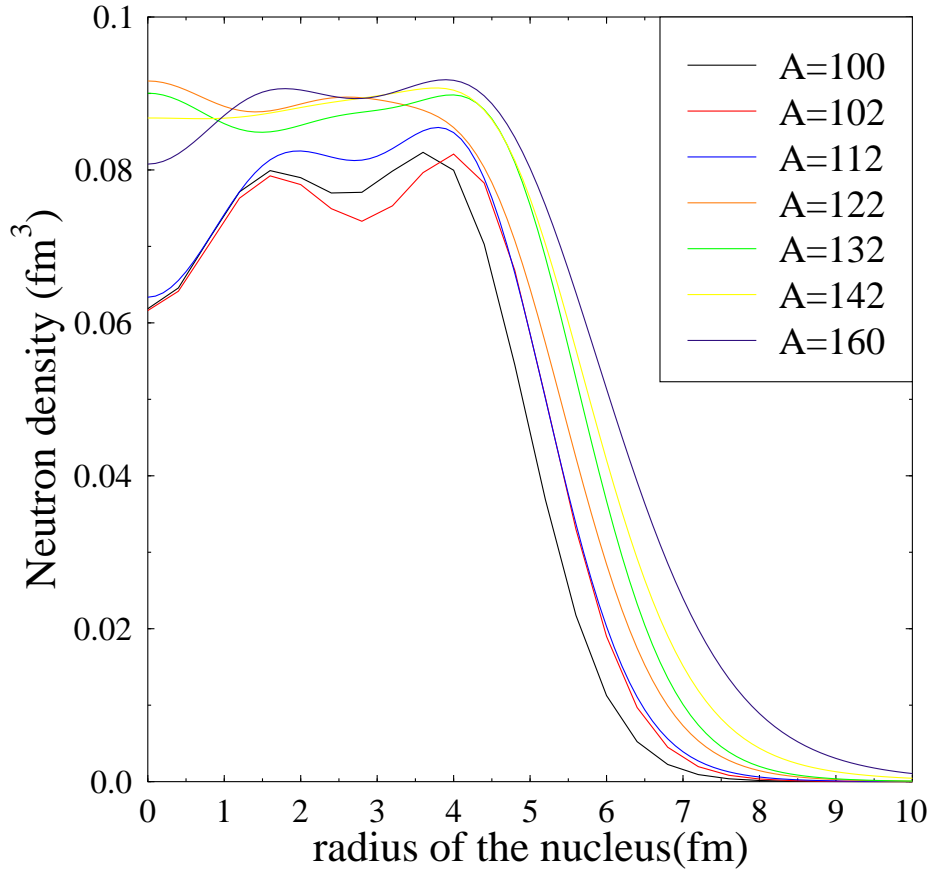
Figure 4.11: Neutron density distributions of Sn isotopes ranging from A = 100 to 160, calculated by ChiM parameter set.

excitation energy is too high as the number of neutrons increase. On the other hand, the SD nuclear states between N = 110 and N = 116 can be observed in the Pb isotope chain. Furthermore, the RMF theory predicts an interesting feature in the ground state. The evolution of shape from the prolate to oblate, and finally to the spherical shapes are found in the Pb isotope chain. From Fig. 4.18, one can clearly observe that the coexistence of the prolate and oblate states for the ground state of ^{190}Pb isotope. Starting from ^{190}Pb, the ground state gradually decreases deformation and moves towards the oblate side as the
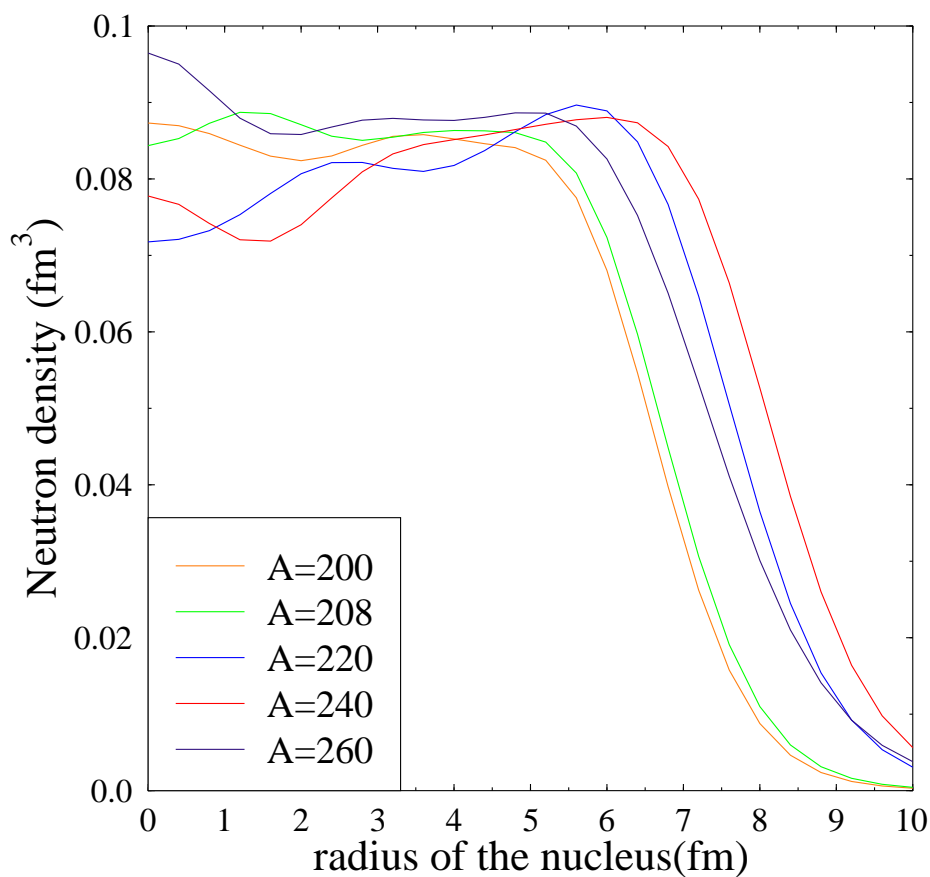
Figure 4.12: Neutron density distributions of Pb isotopes ranging from A = 200 to 260, calculated by ChiM parameter set.

number of neutron increase. Finally, ^{204}Pb has a pronounced spherical shape. Our present work provides a clear SD minimum at nearly all the potential energy curves for the Pb isotopes. The deformation β_2 in SD minima lies systematically between 0.5 and 0.7, our result is consistent with experimental observation.
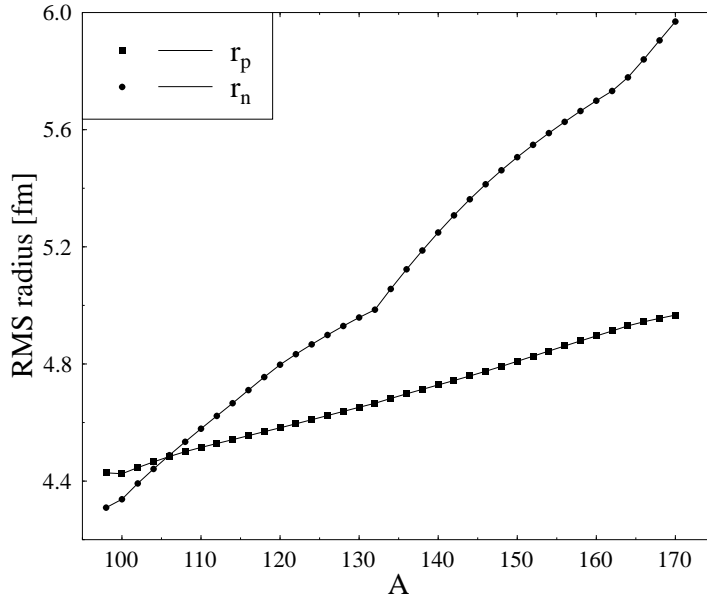
Figure 4.13: The rms proton and neutron radii for Sn obtained in the RMF theory using ChiM parameter set.

4.8   Ground state properties of exotic nuclei near Z =40

The ground state properties of Krypton (Kr, Z=36), Strontium (Sr, Z=38), and Zirconium (Zr, Z=40) nuclei is discussed in the relativistic meson field framework using different parameter sets: ChiM, NL3 and NL4. It is shown that the RMF theory provides a good description of the binding energies and deformation properties of nuclei over a wide range of isospin in the Z = 40 region.
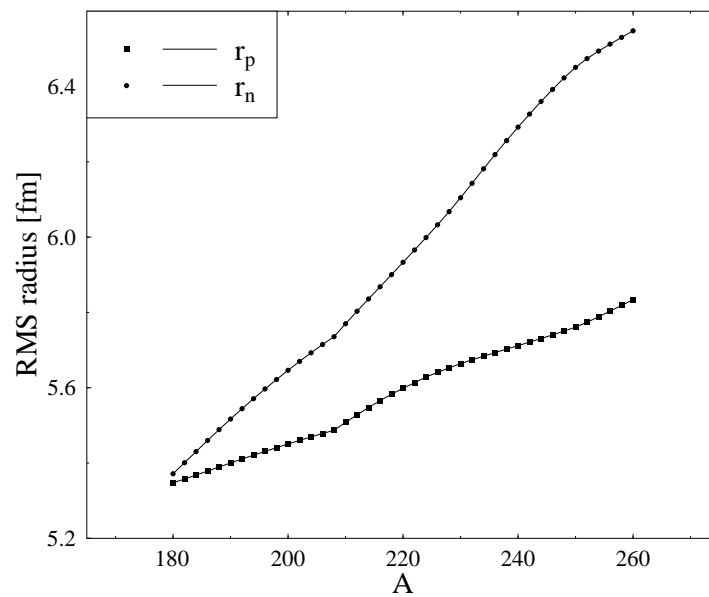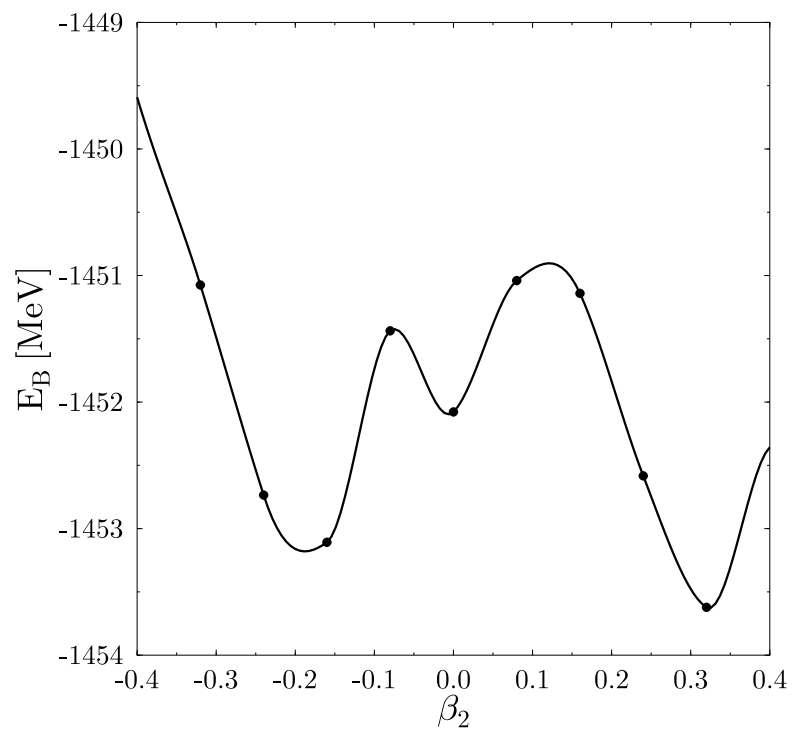
Figure 4.14: The rms proton and neutron radii for Pb obtained in the RMF theory using ChiM parameter set.
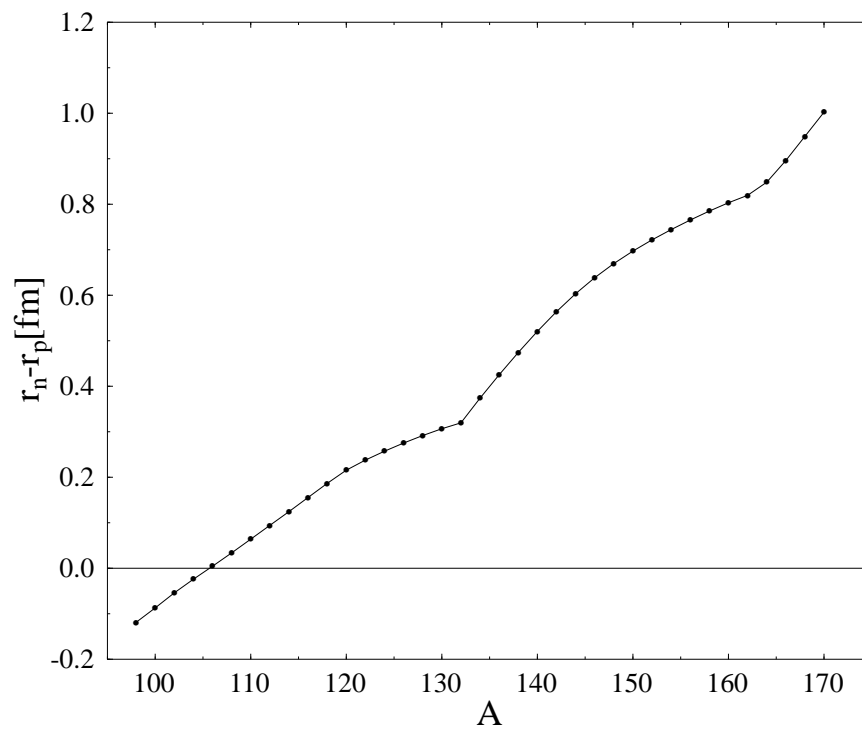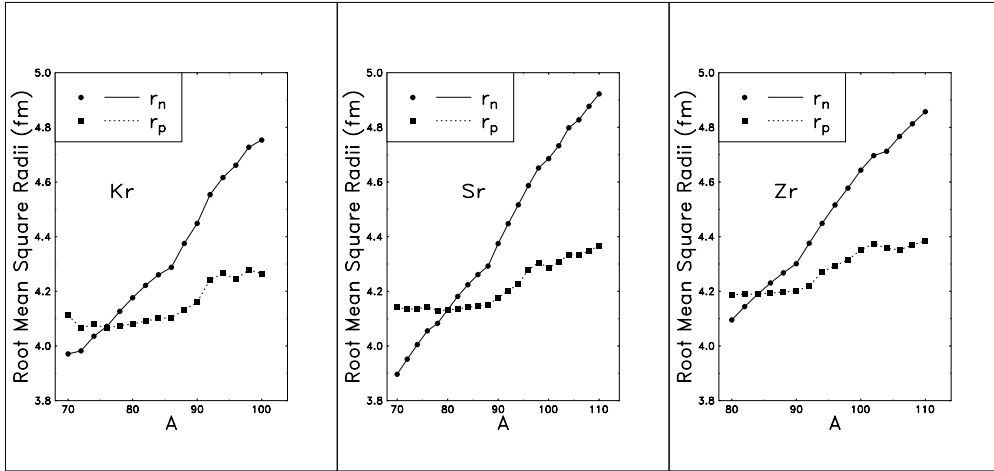
Figure 4.15: Nuclear skin thickness as a function of mass number for Sn isotopes obtained in the RMF theory using ChiM parameter set.

Figure 4.16: Calculated energy surface for ^{186}Pb, the lowest three energy states are in the form of oblate, spherical and prolate shape.

Figure 4.17: The rms proton and neutron radii for Kr, Sr and Zr isotopic chains obtained in the RMF theory using ChiM parameter set.

A	ChiM	FRDM	NLSH	expt.
70	-580.58	-578.33	-575.87	-577.80
72	-607.45	-607.00	-604.00	-607.11
74	-634.34	-631.99	-628.49	-631.28
76	-657.21	-654.82	-651.64	-654.23
78	-677.65	-675.56	-672.69	-675.55
80	-697.48	-695.05	-693.45	-695.44
82	-716.70	-714.57	-713.39	-714.27
84	-734.63	-732.69	-733.16	-732.26
86	-750.96	-748.97	-750.06	-749.23
88	-761.98	-761.22	-760.00	-761.80
90	-773.36	-771.95	-769.89	-733.21
92	-785.12	-782.35	-779.84	-783.22
94	-796.71	-791.89	-789.88	-791.76
96	-804.06	-800.85	-799.46	-799.95
98	-813.25	-808.87	-807.51	-
100	-821.68	-815.68	-814.02	-

Table 4.2: The binding energy (MeV) of Kr isotopes obtained from the parameter set ChiM in comparison with other parameter sets: FRDM [Möl95] and NL-SH [Lal95]. The empirical values [Aud03] are shown in the last column.
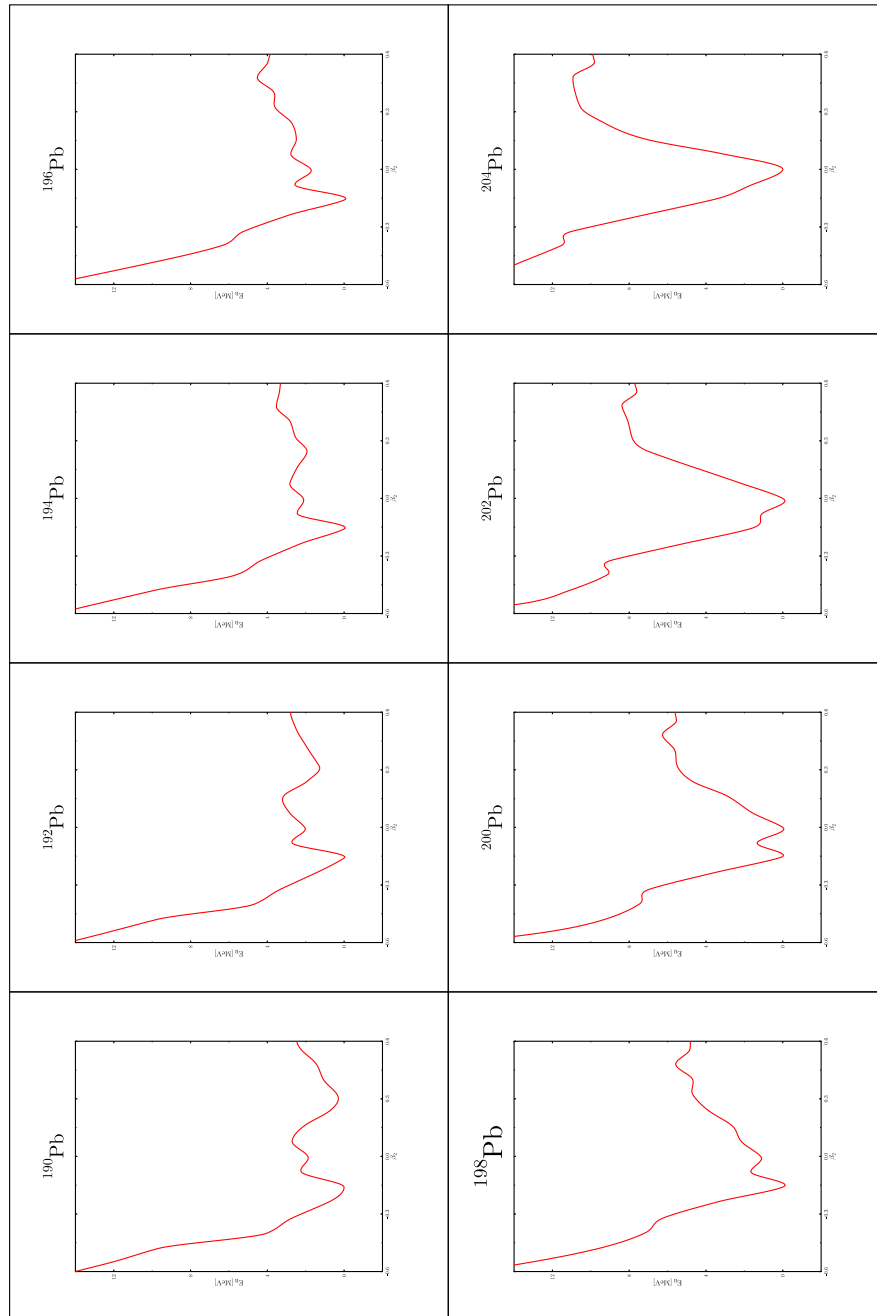
**Figure 4.18:** Superdeformed shapes of Pb isotopes.

–V–

Survey of Lambda Hypernuclei

Nuclei that are found in nature consist of nucleons (protons and neutrons), which themselves are made of u (up) and d (down) quarks. However, there also exist s (strange)quarks and even heavier flavours, called charm, bottom and top. Baryons that contain one or more strange quarks are called hyperons (Lambdas and others). A Lambda consists of one u, d and s quark each. If such a hyperon is bound in a nucleus, a hyper nucleus is created. Hypernuclei with one hyperon have been known for more than 30 years now and have been extensively studied experimentally [Pov76].

The Λ hyperon is a baryon, with mass 1115.684 ± 0.006 MeV/c^2, 20% greater than the mass of the nucleon, zero charge and isospin I = 0. It carries a new quantum number, not contained normally inside the nuclei, the strangeness S = -1. The Λ hyperon is unstable and decays with lifetime 263 ± 2 ps, typical of the weak interaction that doesn't conserve strangeness and makes a free Λ mainly disintegrate in a nucleon-pion system. Since strangeness, however, is conserved in strong interaction and the Λ particle is the lighter particle in the family of hyperons (baryon with strangeness), the Λ particle can associate with nucleons inside nuclei and form hypernuclei.

Lambda hypernuclei are excellent probes of the structure of the nucleus; the Lambda interacts strongly with the nucleus and is distinguishable from the nucleons. In hypernuclear experiments using electron beams, an electron strikes a proton with enough energy to transform it into two new particles: a kaon and a lambda hyperon. The original electron and the new kaon fly out of the nucleus, leaving the lambda hyperon behind. In this way, experimentalists have added an impurity to the nucleus - a lambda hyperon - that they can use to study the structure of the nucleus and the properties of the hypernucleus itself. The mere existence of hypernuclei is of great scientific interest, it gives indeed a new dimension to the traditional world of nuclei by revealing the existence of a new type of
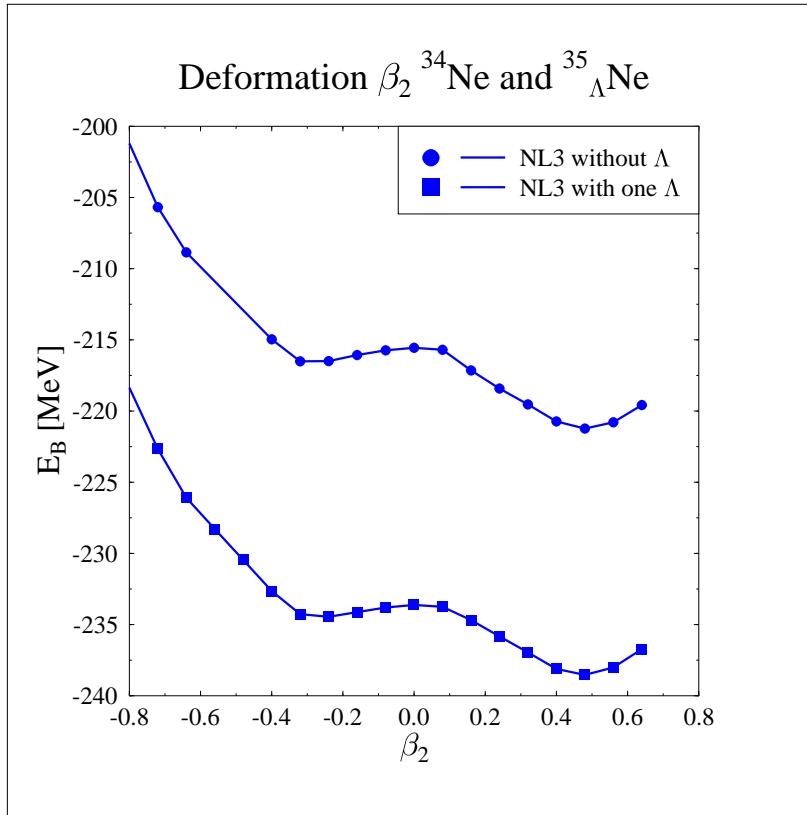
Figure 5.1: Deformation β_2 of ^{34}Ne and ^{35}Ne isotopes without Λ and with Λ (with parameter set NL3).

nuclear matter and generating new symmetries, new selection rules, etc. Hypernuclei represent the first kind of flavoured nuclei (with new quantum numbers), in direction of other exotic nuclear systems (charmed nuclei and so on).

Hypernuclei have been first observed by Danysz and Pniewski in 1953 [Dan53]. The life-time of hypernuclei is typically about 10^{-10} s, essentially given by the lifetime of the Lambda. Since the strangeness quantum number is conserved by the strong and electromagnetic interactions, at least hypernuclei containing the lightest hyperon, the Lambda, live long enough to have sharp nuclear energy levels. Therefore they offer opportunities for nuclear spectroscopy, as well as reaction mechanism and other studies (hypernuclear physics). Their physics is different from that of normal nuclei because a hyperon, having a different value of the strangeness quantum number, can share space and momentum coordinates
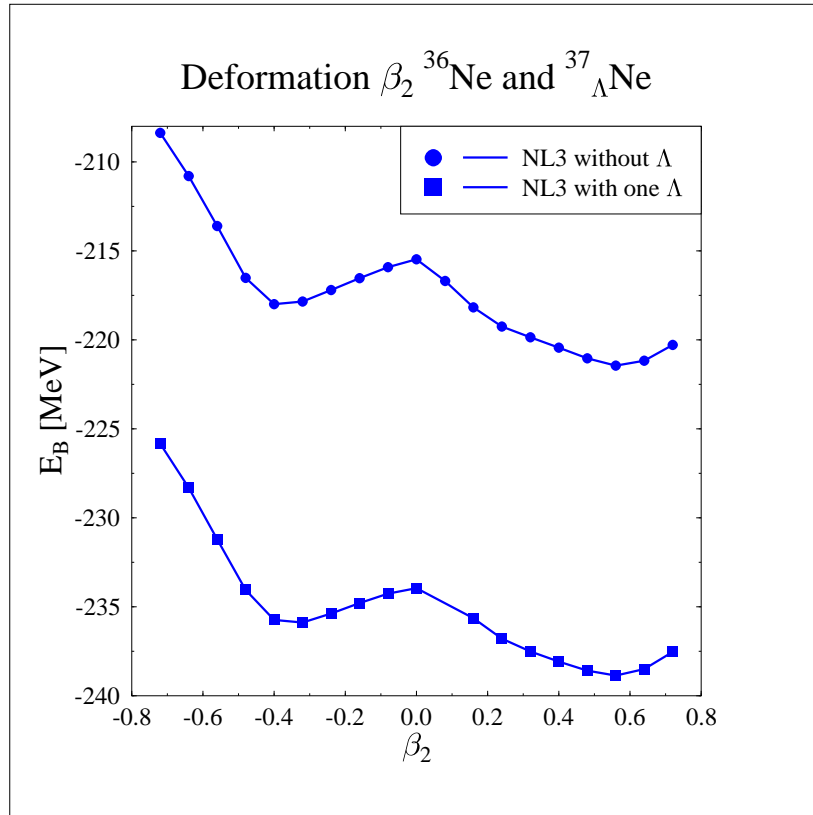
Figure 5.2: Deformation β_2 of ^{36}Ne and $^{37}_{\Lambda}Ne$ isotopes without Λ and with Λ (with parameter set NL3).

with the usual four nucleons that can differ from each other in spin and isospin. Already 30 years ago, hypernuclei with up to $A = 15$ have been produced [Can74] and some years later even heavier hypernuclei could be observed at CERN [Brü76, Brü78, Ber79, Ber80, Ber81] and AGS [Bon74, Chr79, May81, Chr88] where also excited states has been investigated. There are new experimental programs planned at the new heavy-ion facility FAIR@GSI to extend the knowledge of hypernuclei to higher neutron numbers, i.e. large isospin. Previous theoretical descriptions of hypernuclei have been done in Skyrme-Hartree-Fock models [Mil88, hyp96] and relativistic mean-field calculations [Mar89, Ruf88]. A very interesting and theoretically challenging project is to study the stability line of nuclei for large neutron excess (neutron dripline) and its change when additional hyperons are included in the nucleus, leading to the study of exotic hypernuclei.
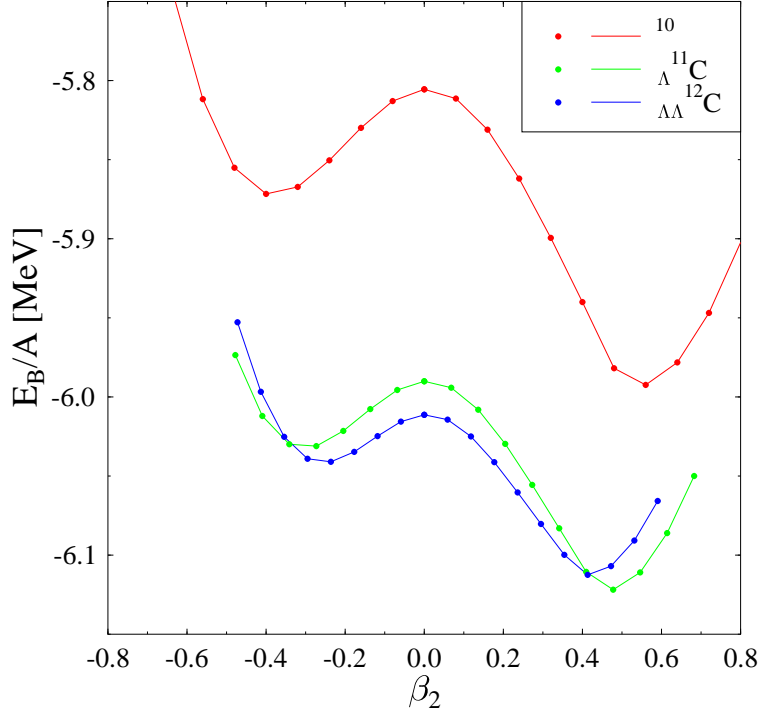
Figure 5.3: Potential energy surface of C isotopes without Λ, with Λ and with $\Lambda\Lambda$ (with parameter set ChiM).

5.1   Structure of Λ-hypernuclei

A Λ-hypernucleus represents as $^A_\Lambda Z$. In this Λ-hypernucleus, $^A_\Lambda Z$, a bound state of Z protons, (A-Z-1) neutrons and a Λ hyperon are contributed. The ground state of such a system consists of the (A-1) nucleons accommodated in the ground state of the nucleus $^{(A-1)}Z$ and the Λ hyperon in its lowest energy state. The Λ hyperon, consisting of the strangeness quantum number, is a distinguishable baryon and is not limited by the Pauli exclusion principle, thus it can occupy one of the quantum states already filled up with the nucleons. This characteristic feature gives the Λ hyperon, embedded in a hypernucleus, a distinctive role in exploring nuclear structure.

One of the bulk properties, the binding energy B_Λ of a Λ particle in the hyper-

nucleus $^A_\Lambda Z$ in its ground state is generally defined as:

$$B_\Lambda = M_{\mathrm{N}} + M_\Lambda - M_{\mathrm{hyp}} \qquad (5.1)$$

here,

M_{N} = the mass (in MeV/c^2) of the nucleus $^{(A-1)}Z$
M_Λ = the mass (in MeV/c^2) of the Λ particle
M_{hyp}= the mass of the hypernucleus $^A_\Lambda Z$ (experimentally measured)

In Fig. 5.1 and Fig 5.2 , with the effective interaction NL3, the axial deformation of Ne isotopes are compared without Λ and with Λ hyperon. According to these figures, one can observe that deformed nuclei could reduce, however not too pronounced, the strength of the deformation by inclusion of Λ hyperon. From Fig 5.3, the potential energy surface of the core ^{10}C isotope, $^{11}_\Lambda$C hypernucleus and $^{12}_{\Lambda\Lambda}$C hypernucleus by applying the RMF theory with ChiM parameter set are observed. The deformation of C isotope can effectively reduce by adding two Λ hyperons than one although the difference in energy levels is small. In the density profile of these nuclei, we can observe that the Λ hyperon density distribution for $^{12}_{\Lambda\Lambda}$C hypernucleus is neraly the same as the baryon density distribution while the the Λ hyperon density distribution for $^{12}_\Lambda$C is smaller than the matter density distribution. If we add more Λ hyperons, we can observe the halo in hypernuclei with the long tail of Λ hyperon density distribution.

5.2 Halos in Hypernuclei

The inclusion of the Λ hyperon does not produce an excessive change in bulk properties but shifts the neutron dripline to larger neutron numbers [Vre98] (see also in Fig. 6.1). The two-neutron separation energies S_{2n} for ordinary nuclei, single-Λ and double-Λ hyper nuclei of Be and Ca isotopes, respectively, at the proton and neutron driplines are shown in Fig. 5.5 and Fig. 5.6. Apart from the neutron halo, as the Λ hyperon is less bound than the corresponding nucleon in nuclei, it is worth to investigate the existence of corresponding hyperon halos. The hyperon carbon isotopes are presented in Fig. 5.7 by using the RMF theory with the parameter set ChiM. When two Λ hyperons are added to the core ^{12}C, the nucleon density distributions remain the same and the hyperon density distribution at the tail are comparable with those of nucleons. We can predict a hyperon halo for C isotope by adding three Λ hyperons to the the core ^{12}C with clear evidence of a long tail of the hyperon density which is extended far outside
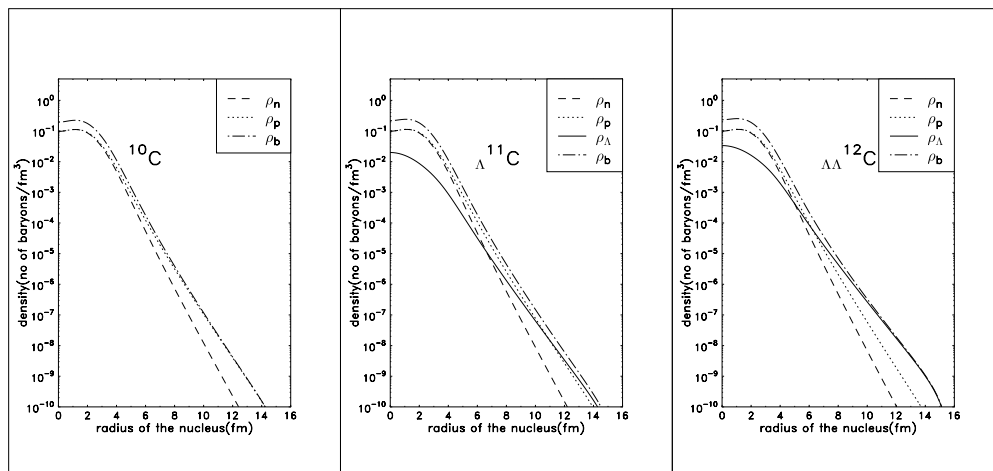
Figure 5.4: Proton, neutron, baryon and lambda density distributions of C isotopes.

of its core.
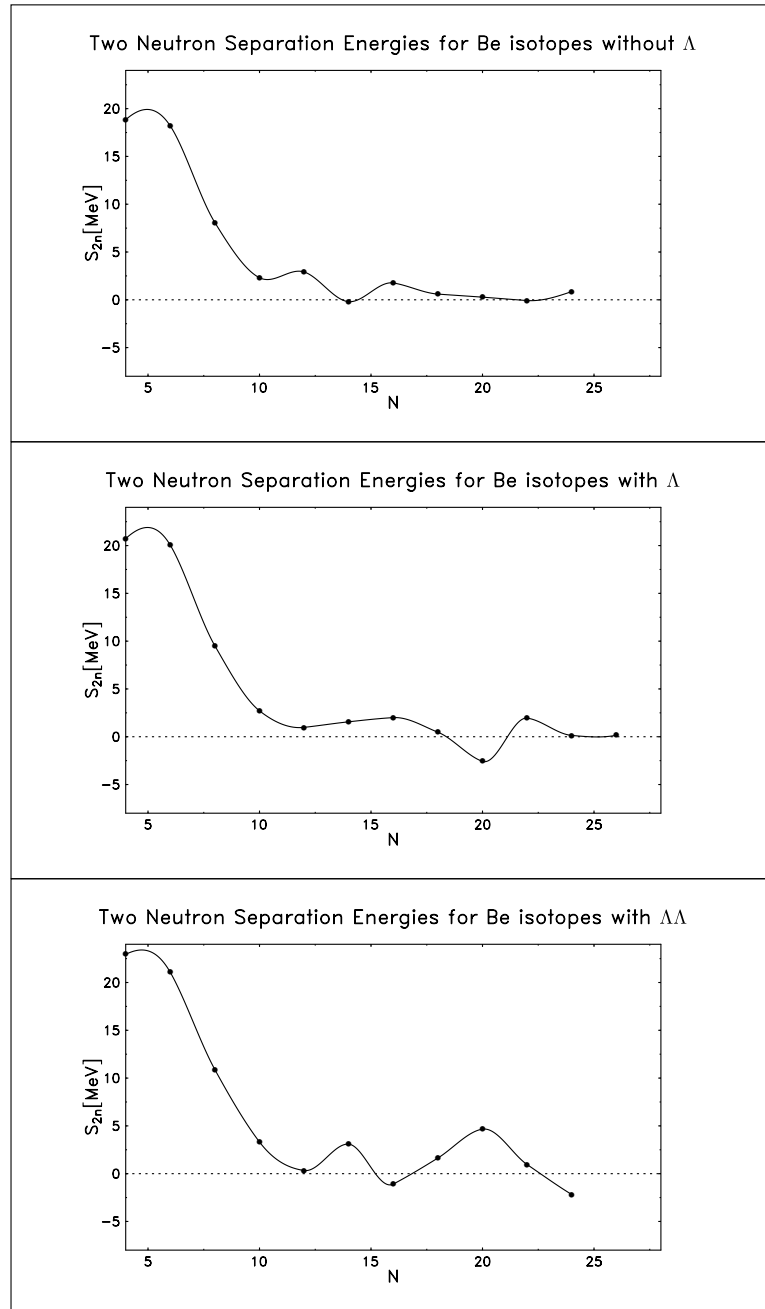
Figure 5.5: Two neutron separation energies of Be isotopes: without Λ , with Λ and with $\Lambda\Lambda$ (^{8}Be and ^{12}Be are last proton and neutron bound nuclei).
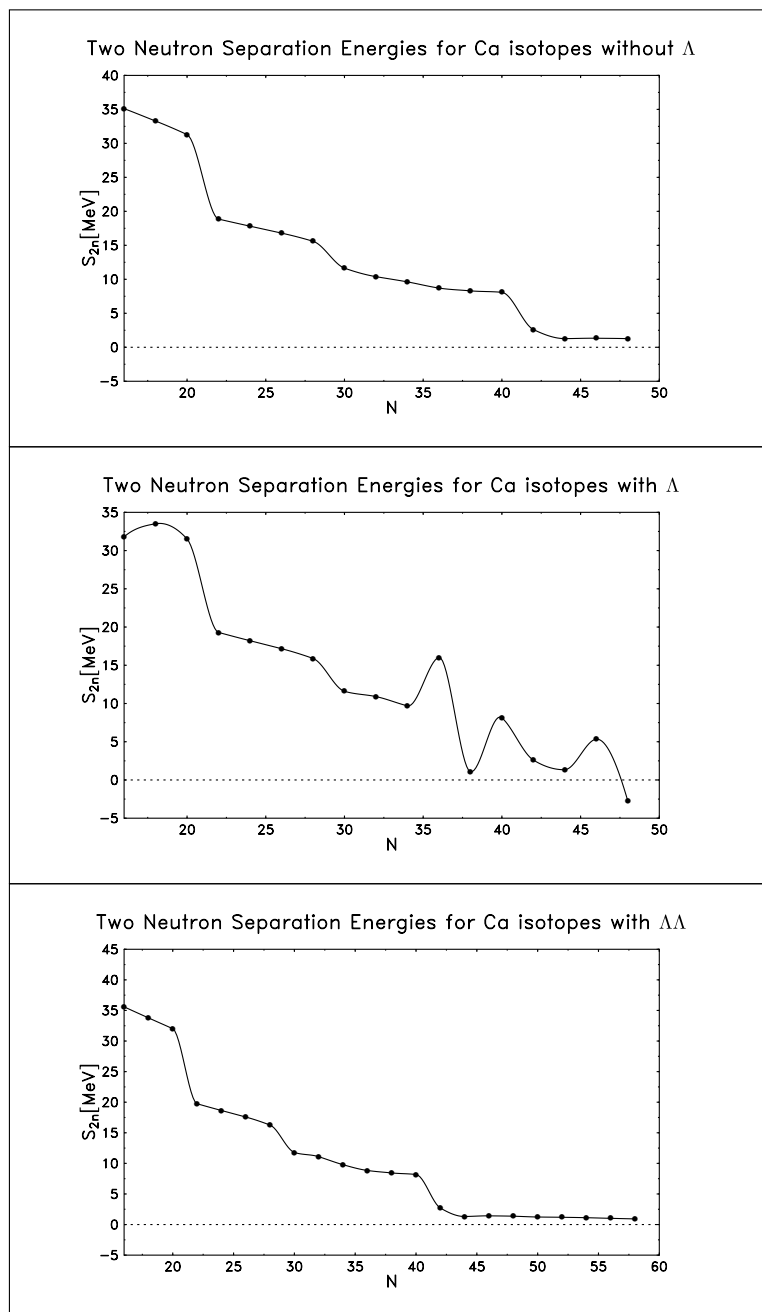
Figure 5.6: Two neutron separation energies of Ca isotopes: without Λ , with Λ (Λ: ^{40}Ca and ^{58}Ca are last proton and neutron bound nuclei).
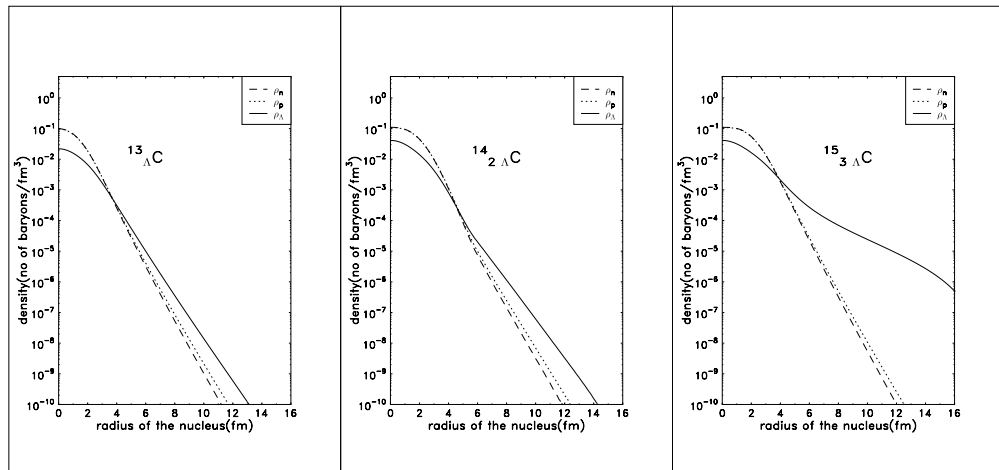
Figure 5.7: Density distributions for Λ (solid), neutron (long-dashed) and proton(dotted) in $^{13}_{\Lambda}$C, $^{14}_{2\Lambda}$C and $^{15}_{3\Lambda}$C in logarithmic scales.

–VI–

DRIPLINES

One of the driving forces of today's nuclear physics efforts is the journey to the extreme limits in several directions. For nuclear charge and mass this journey involves nuclei heavier than any that occur in nature or that have been produced in the laboratory, leading the research field of superheavy nuclei; for the neutron-to-proton ratio, it involves the driplines, the limits of nuclear stability along the axes of proton and neutron number. As more and more neutrons are added to a given nuclide, the neutron binding energy will become eventually negative, leading to the emission of neutrons. The boundary of the region of the (N-Z) plane where this occurs constitutes the "neutron dripline" and its counterpart on the proton rich side, the "proton dripline".

The locations of the drip lines on the chart of nuclei are still an open question. In particle accelerators, the existence of about 3,000 isotopes can be studied. [Aud03]. The exact location of the neutron drip line is of great interest in nuclear physics research [Lun03], but the short lifetimes of these exotic nuclei and the difficulty involved in making them results this a tremendous task. Nevertheless, some progress has been made. The location of the proton drip line is known for atoms with up to 90 protons, that is, up to thorium. The investigation of the proton drip line is easier compared to that of the neutron drip line, because electric repulsion between protons restricts the number that can be added to a nucleus with a given number of neutrons [Hee07]. The procedure is very different for neutron-rich nuclei, because there is no additional electric repulsion by adding neutrons. The neutron drip line is therefore relatively distant from the β stability line on the chart of nuclei, and is therefore much harder to reach experimentally. Furthermore, the number of neutrons that can theoretically be added to a nucleus increases as the number of protons increases.
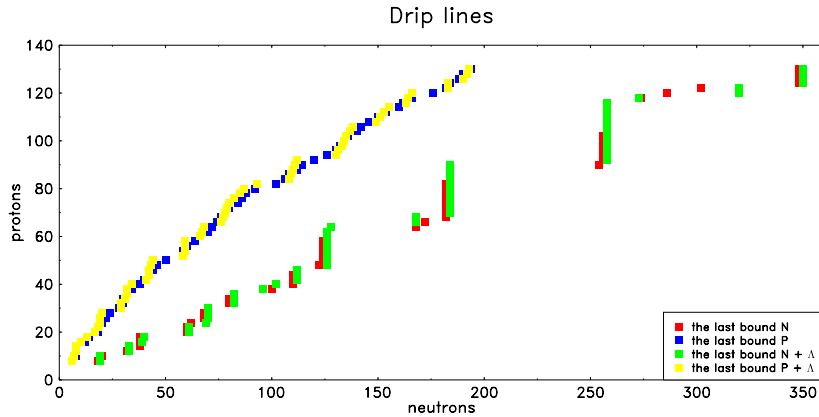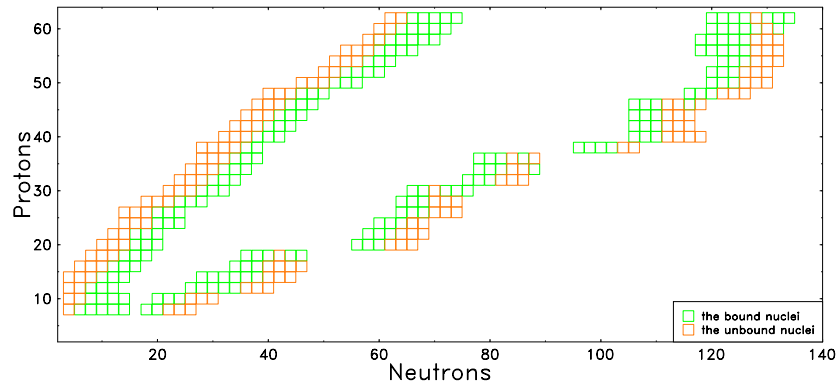
Figure 6.1: Neutron and Proton Driplines (within Z = 8 to Z =130) without Λ and with Λ (NL3)

6.1   Proton dripline

There are different definitions of the proton dripline from a theoretical point of view. One can define it as the location where the proton separation energy passes through zero ($S_p = 0$ MeV) [Han03]. According to this definition, many nuclei still exist beyond the drip line. An alternative definition of the drip line is described as the value of Z and N for which the last proton is no longer bound and the limitation of the typical nuclear timescale of $\sim 10^{-22}$s which is a reasonable timescale for the existence of a nucleus [Mue43]. The dripline and the existence of a nucleus could also be related to the limitation of radioactivity of $\sim 10^{-12}$s [Cer77]. The driplines are the limits of the nuclear landscape where additional protons and neutrons can no longer be kept inside the nucleus and they drip out literally [Jon04]. In our present work, we define the proton dripline as the boundary between the positive value and the negative value of the separation energy. Proton separation energy becomes negative when the additional protons are no longer bound in a nucleus and the Fermi energy is getting positive. A negative proton separation energy means that the nucleus can spontaneously decay by the emission of protons. Nuclei inside the dripline are stable with respect to the spontaneous emission of nucleons, whereas these outside the driplines can spontaneously decay by the emission of one and/or two nucleons.
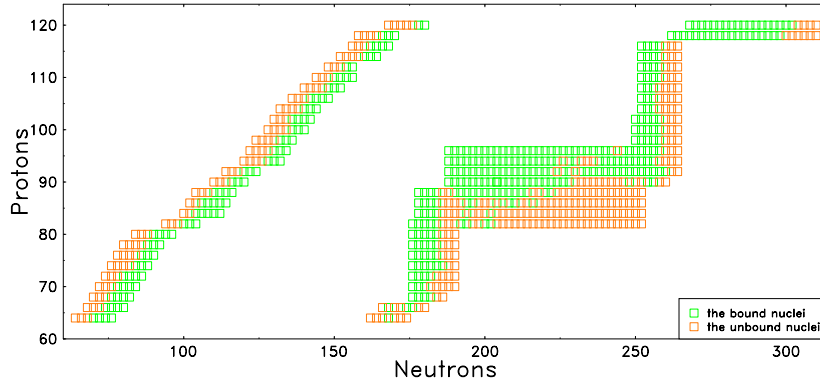
Figure 6.2: Neutron and Proton Driplines (within Z = 8 to Z =60) including deformation (with the parameter set NL3)

6.2 Neutron dripline

It is generally accepted that the neutron dripline has been reached for all elements up to oxygen, which has eight protons and can have a maximum of 16 neutrons [Tho04], although recent calculations suggest the existence of oxygen isotopes up to 32 neutrons [Gri05]. Beyond oxygen, the drip line has been tentatively assigned for elements up to sodium, which has 11 protons and a possible maximum of 26 neutrons. Baumann et al. now report the discovery of two more neutron-rich isotopes: a magnesium isotope (40Mg, which has 12 protons and 28 neutrons) and an aluminium isotope (42Al, which has 13 protons and 29 neutrons). Previous descriptions of nuclei close to the neutron dripline in the framework of RMF theory [Sha94] have been successfully attempted.

6.3 Mapping Neutron and Proton driplines

When neutrons are successively added to a nucleus on the nuclear stability line, the binding energy of the last neutron decreases steadily until it is no longer bound and the nucleus decays by neutron emission. At a certain line, the nucleus will no longer bind extra neutrons. This is called neutron drip line and its counterpart is called the proton drip line. In other words, an unstable atomic nucleus beyond the dripline will leak free neutrons and the neutron separation energy is zero at the neutron drip line. The proton and neutron drip lines define the limits of existence for finite nuclei. The theoretical knowledge of the properties of nuclei
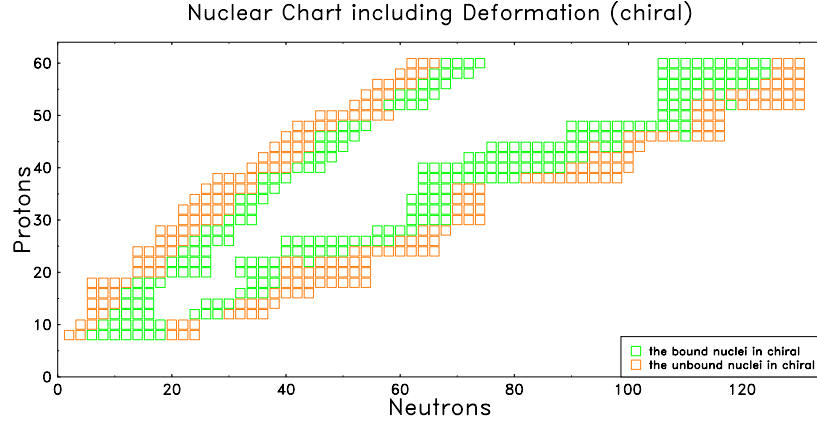
Figure 6.3: Neutron and Proton Driplines (within Z = 62 to Z =120) including deformation (with the parameter set NL3)

up to the neutron drip line will provide a better understanding of the stellar nucleosynthesis and neutron stars in nuclear astrophysics. The position of the drip lines is still uncertain and its experimental determination is a problem of foremost interest in the field. Baumann and et. al. reported a siginficant advance in the determination of the neutron dripline: the discovery of two neutron-rich isotopes - ^{40}Mg and ^{42}Al - that are predicted to be dripline nuclei [Bau07]. The discovery of ^{40}Mg as the neutron dripline nucleus and the most recently observed dripline nucleus ^{44}Si are in agreement with our prediction of neutron drip line by applying the RMF theory with the parameter set ChiM.

From Fig. 6.1, which shows the position of the driplines of nuclei and hypernuclei (obtained in spherical approximation with the parameter set NL3), we can read off the shell closure of nuclei and predict new magic numbers. The last bound protons (with blue and yellow square) show the normal proton dripline and the proton dripline with the inclusion of one Λ hypernucleon. For the last bound neutrons, observing the red and green squares in this Fig. 6.1, one can observe the normal neutron dripline and the neutron dripline with the inclusion of one Λ hypernucleon. These results are useful to understand the structure of the nucleus and more specifically, physics close to the drip lines.

Both proton and neutron driplines with the inclusion of Λ hypernuclei move towards the neutron rich sides from the driplines of nuclei without Λ. From this results, we can conclude that hypernuclei can accept more neutrons and are more strongly bound than normal nuclei. One can observe that prominent shell clousre in neutron driplines. Neutron dripline with the inculsion of Λ hypernuclei displays

Figure 6.4: Neutron and Proton Driplines (within Z = 8 to Z =60) including deformation (with the parameter set ChiM)

the shell clousure at the isotonic chains with neutron magic numbers (N = 82, 126, 184. Isotonic chains with neutron magic numbers could not preserve well on the normal neutron dripline. Shell closure shows on normal neutron dripline at the neutron numbers (N = 80, 124, 182). One can observe two new magic numbers (N = 258, 350) in the mapping of the neutron dripline with the inclusion of Λ hypernuclei and (N = 256, 348) for the normal neutron dripline.
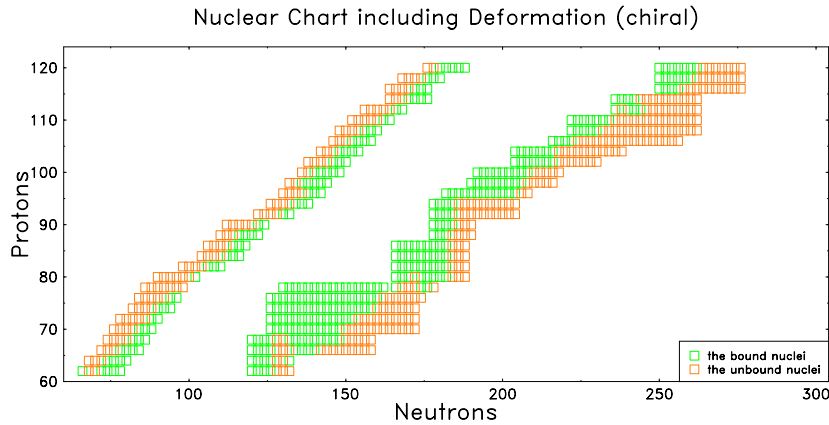
Figure 6.5: Neutron and Proton Driplines (within Z = 62 to Z = 120) including deformation (with the parameter set ChiM)

The drip lines including axial deformations are calculated (with the parameter

set NL3)and described in Fig 6.2 and Fig. 6.3 for the nuclei ($8 \leq Z \leq 60$) and nuclei ($60 \leq Z \leq 120$) respectively. Unlike in spherical calculations, isotonic chains with neutron magic numbers could preserve well on the neutron dripline including axially deformation. Shell closures appear on the neutron dripline at the neutron numbers (N = 82, 126, 184) while isotopic chains with proton magic numbers move away from the neutron magic numbers (except for the Z = 20). In the region of ($82 \leq Z \leq 96$), we can observe that some bound nuclei are located after the neutron dripline. The neutron dripline could display very well except this region.

A smiliar calculation was done for the drip lines including axial deformations (with the parameter set ChiM)and described in Fig. 6.4 for ($8 \leq Z \leq 60$) nuclei and Fig. 6.5 for ($60 \leq Z \leq 120$) nuclei . Isotopic chains with proton magic numbers move away from the neutron magic numbers (except for the Z = 20). It can be cleary seen in Fig. 6.4. This result agrees with the above calculation (in Fig. 6.2) with the parameter set NL3. For larger nuclei ($60 \leq Z \leq 120$) as shown in Fig. 6.5, the proton and neutron driplines are more distinct than in the calculation with NL3 parameter set. Isotonic chains with neutron magic numbers could preserve well (as in the calculation of parameter set NL3) on the neutron dripline including axially deformation. Shell closures are seen at the neutron dripline at the neutron numbers (N = 82, 126, 184) while isotopic chains with proton magic numbers move away from the neutron magic numbers (except for the Z = 20).

6.4 Survey of Axial deformation between driplines

The RMF theory with ChiM parameter set can reproduce the deformations of finite nuclei very well. In the present work, we performed a systematic study of 1661 nuclei to verfiy the axial deformation of even-even nuclei ($8 \leq Z \leq 100$) with different numbers of neutrons. This is the first time this study has been performed using RMF theory with parameter set ChiM. Studies of deformed nuclei in the range ($8 \leq Z \leq 100$) have already been done in RMF+BCS calculations with different parametrizations, and within the FRDM and HFB-2 framework. A comprehensive view of these calculation can be found in [Gen05]. The quadrupole deformation obtained here for all even-even nuclei with $8 \leq Z \leq 100$ between the proton and neutron driplines can be seen in Fig. 6.9. From the analysis of this calculation, we can conclude that:
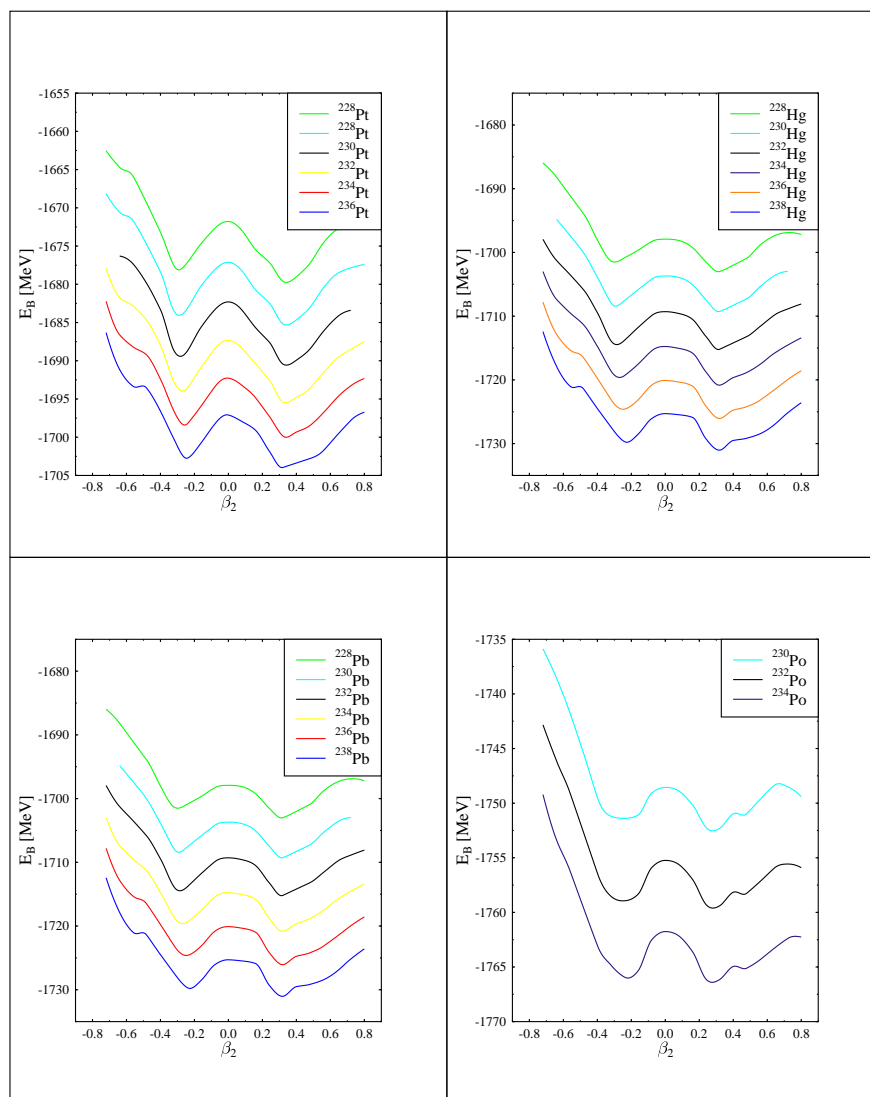
Figure 6.6: Deformation β_2 in prolate deformation (Z = 78 to 84) region.

1) Most of the spherical nuclei ($-0.05 \leq \beta_2 \leq 0.05$) are located at or near magic numbers.

2)While isotonic change with well-known neutron magic numbers (N =82, 126,
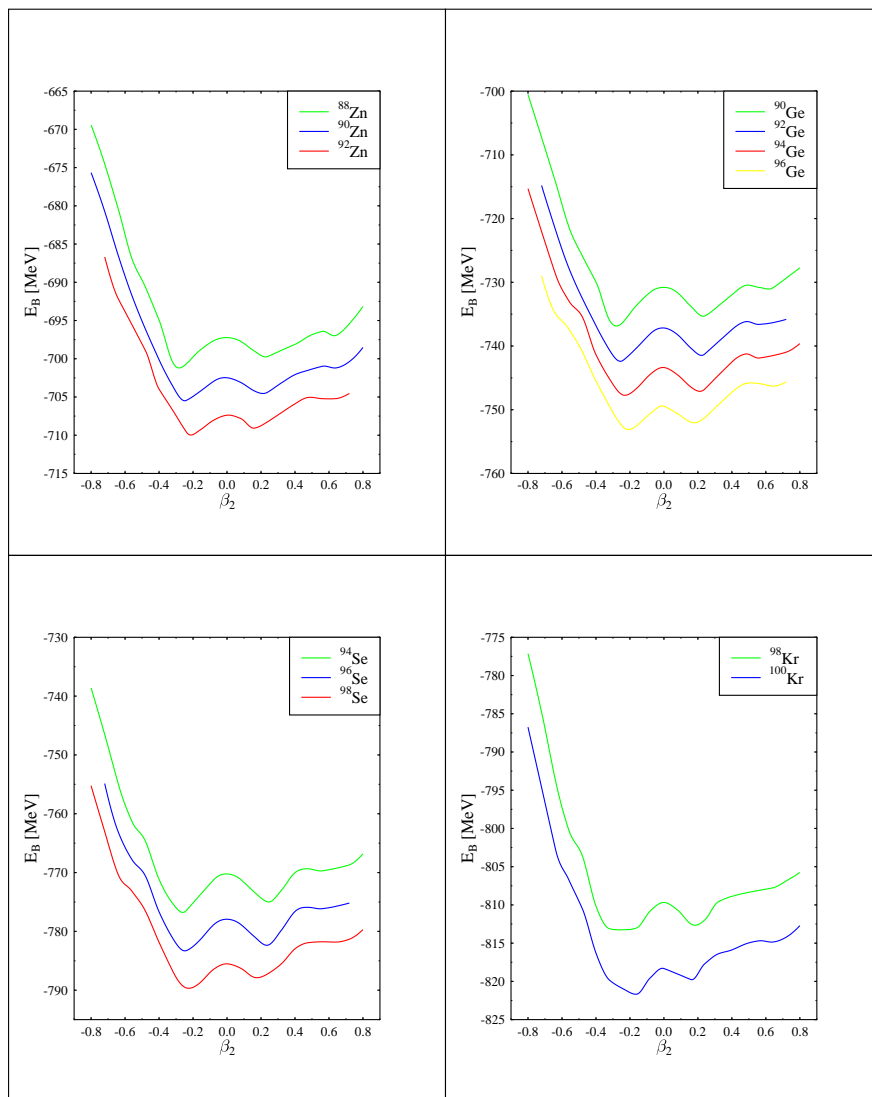
Figure 6.7: Deformation β_2 in oblate deformation ($Z = 30$ to 36) region.

184) preserve spherical shapes for the entire chain, isotopic chain with proton
magic numbers are usually deformed when one moves away from the neutron
magic numbers (except for the $Z = 8$ and 20 isotopic chain). Semi-magic
numbers ($Z = 40, 172, 182, 186$) can be observed from this axial deformation
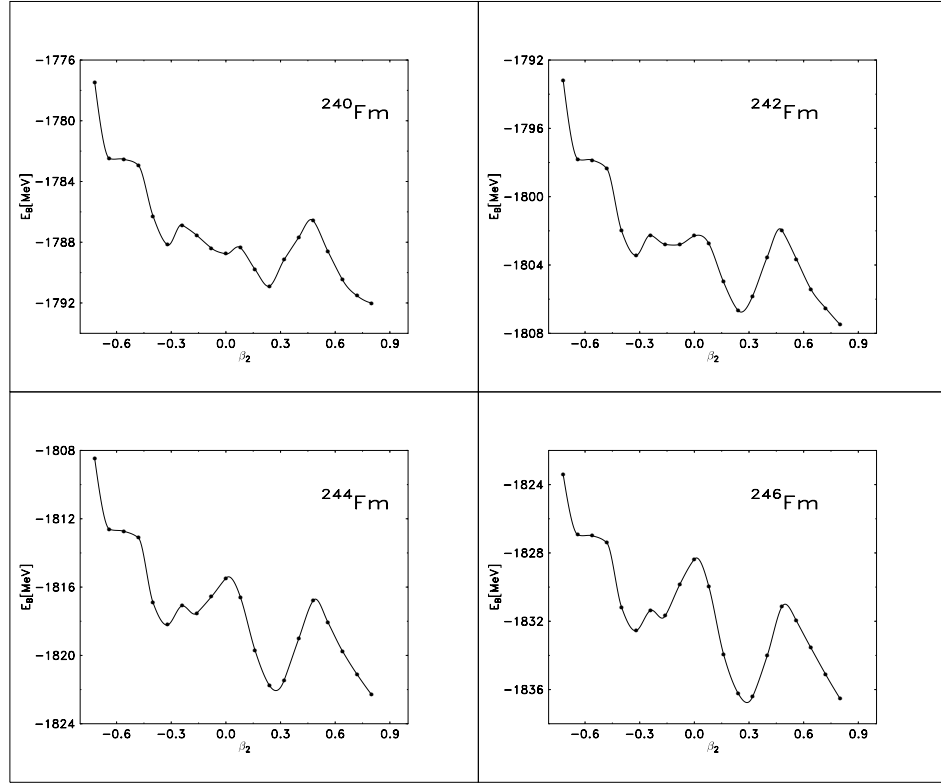
Figure 6.8: Potential energy surfaces for Fm isotopes close to the proton dripline

calculation ($8 \leq Z \leq 100$). Among these results, we can observe well-known doubly magic nuclei (^{16}O, ^{40}Ca, ^{48}Ca, ^{132}Sn, ^{208}Pb) except for the ($Z = 28$ isotopic chain). And another new two doubly magic numbers are observed in Pb isotopes, namely ^{262}Pb and ^{264}Pb (N = 180, 182).

3) Among Pb isotopes, oblate deformation nuclei ($\beta_2 \sim 0.2$) are located near proton dripline. Some neutron rich Pb isotopes are axially prolate deformed ($0.2 \leq \beta_2 \leq 0.3$). The rest of Pb isotopes are in spherical shape.

4) Most of prolate deformed nuclei are observed in the nuclei with a charge larger than Z =50 when moving away from the magic numbers either isotonically or isotopically.

5) There are also several regions where strongly prolate and oblate deformations coexist. Axially prolate deformed nuclei from one of regions with distinct prolate deformation is shown in Fig. 6.6. This prolate region ranges from Z = 78 (Pt isotope) to Z = 84 (Po isotope). These nuclei have a substantial prolately deformed nuclear ground state ($0.3 \leq \beta_2 \leq 0.4$) and excited oblately deformed states. From this calculation, one can see the coexistence of prolate and oblate shapes. Os and Pt isotopes (Z = 76 and 78) exhibit a large number of isotopes with axially prolate deformation except near the neutron shell closure (N = 126).

6) We found superdeformed nuclei near the proton and neutron driplines of Cf (Z = 98) isotopes and Fm (Z = 100) isotopes ($0.7 \leq \beta_2 \leq 0.8$). The superdeformation of Fm isotopes near proton and neutron driplines is shown in Fig. **??**. For Cm (Z = 96) isotopes, one can see superdeformed nuclei only near neutron dripline.
7) Oblately deformed nuclei are rare. There are some oblate regions in this axially deformation of even-even nuclear chart. Axially oblate deformation from one of the oblate deformed region is described in Fig. 6.7. This oblate region lies among the isotonic changes of Zn isotopes (Z = 30) to Kr isotopes (Z = 34). These nuclei are quite deformed nuclei ($0.2 \leq \beta_2 \leq 0.3$)

Axially deformed nuclei from the proton dripline to the neutron dripline for Magnesium which are calculated by using RMF theory with the ChiM parameter set, are shown in Fig. 6.13. These deformed nuclei, ^{20}Mg to ^{42}Mg cover three magic numbers: N= 8, 20 and 28 and include the strongly deformed nuclei ^{22}Mg, ^{24}Mg and ^{38}Mg. ^{22}Mg is the proton dripline nucleus and ^{40}Mg is the neutron dripline nucleus. We can see the existence of nuclear shell structure at magic numbers N =8 and 20 but the old magic number 28 disappear and shows relatively large deformation. This result agrees with the density dependent RMF theory. These results show the occurrence of oblate and prolate minima for various isotopes and are in general agreement with other relativistic and non relativistic mean field calculations [Lal98, Bür02a].
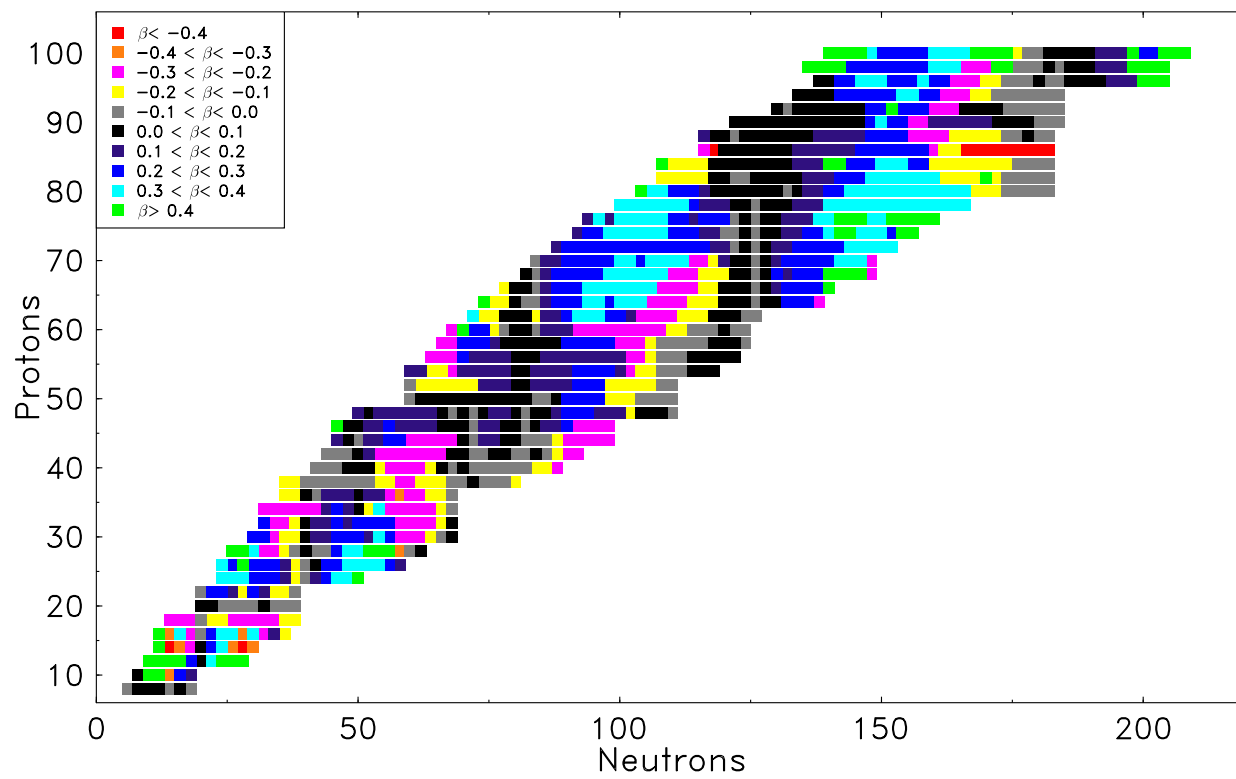
Figure 6.9: Axial deformation of even-even nuclei between driplines calculated by ChiM
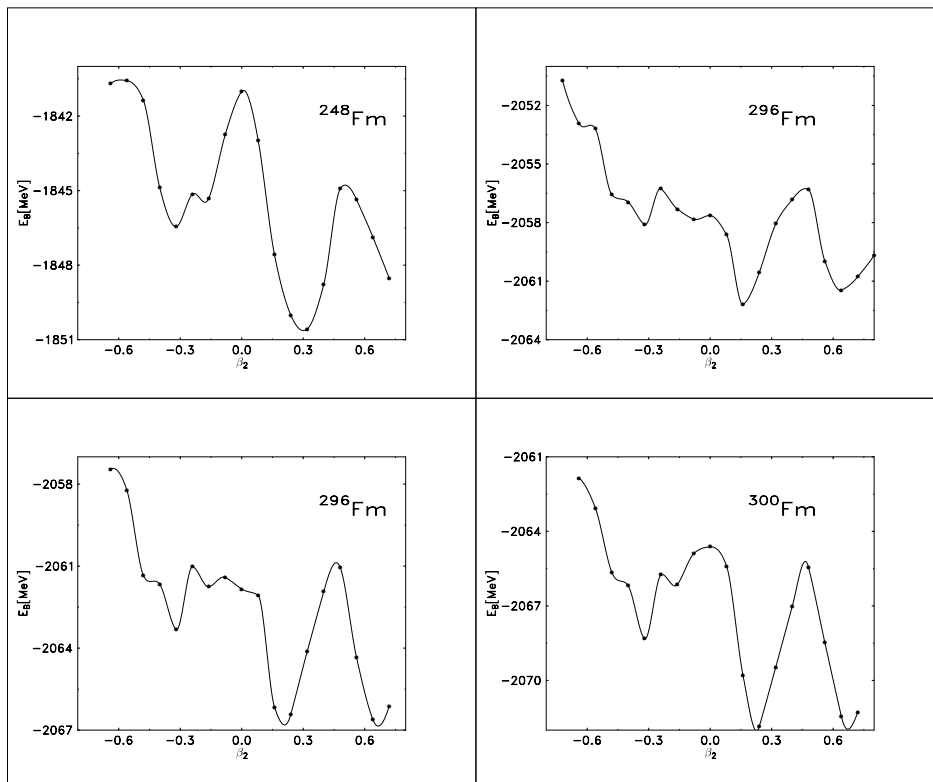
Figure 6.10: Potential energy surfaces for Fm isotopes: close to the neutron dripline.
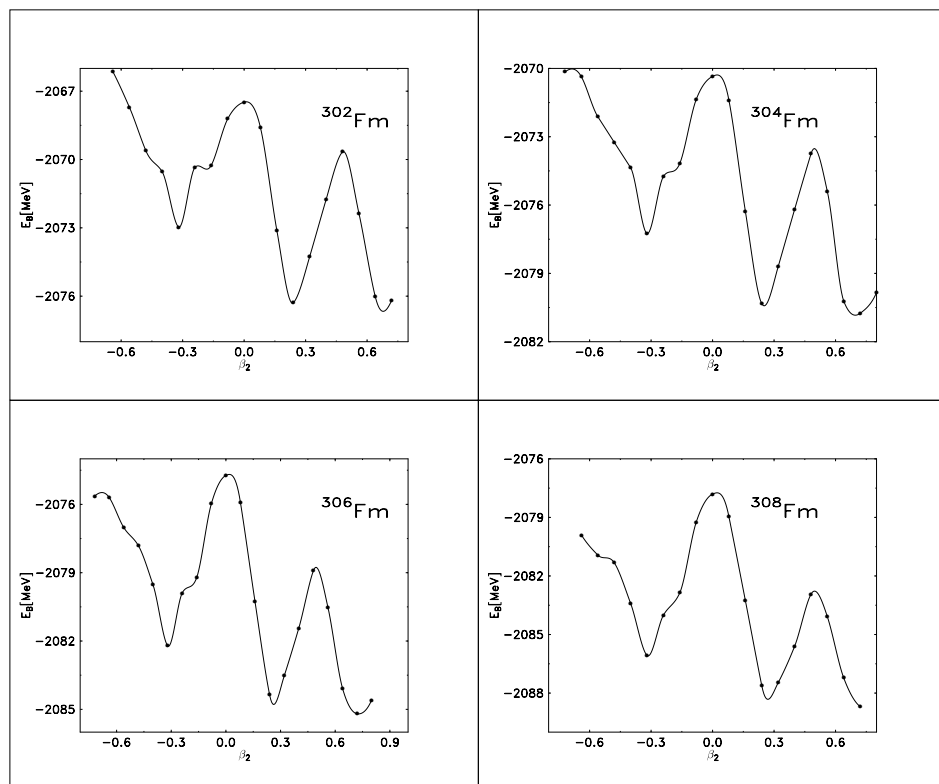
Figure 6.11: Potential energy surfaces for Fm isotopes: close to the neutron dripline.
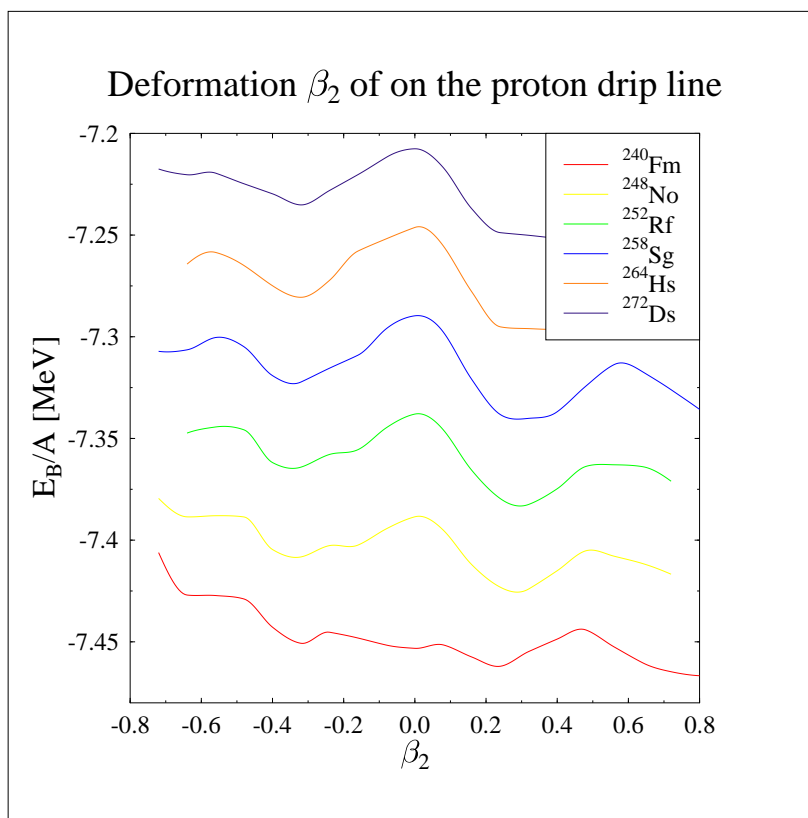
Figure 6.12: Deformation β_2 on the proton dripline (Z = 100 to 110)
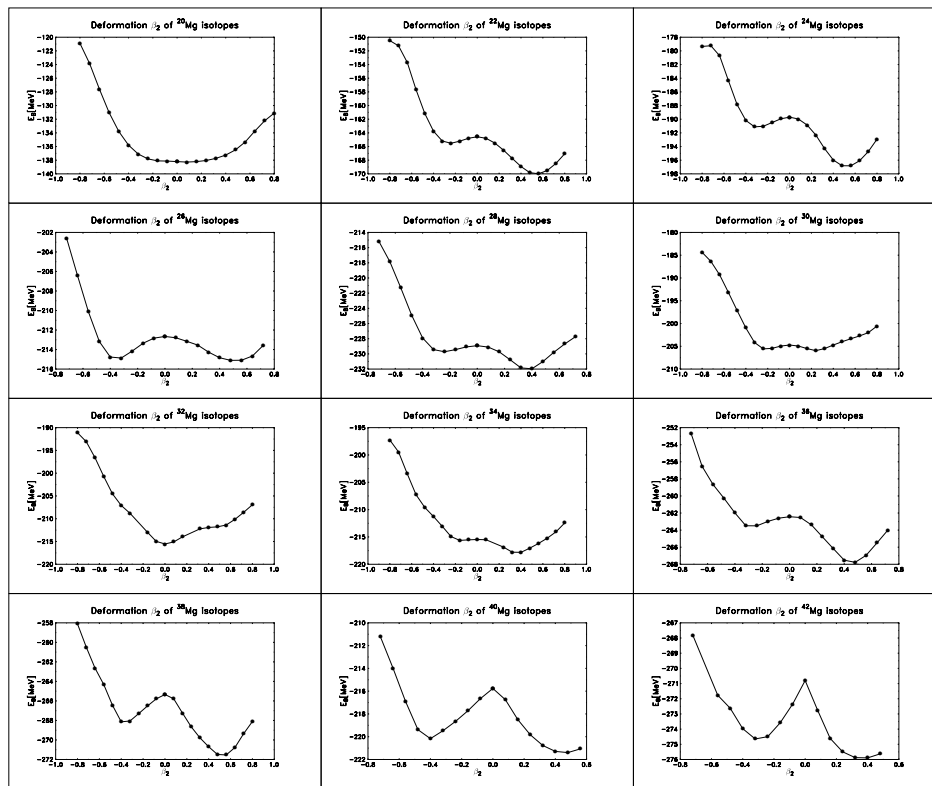
Figure 6.13: Deformation $\beta 2$ of Mg isotopes: from proton dripline to neutron dripline

$-$VII$-$

STRUCTURE OF SUPERHEAVY NUCLEI

The nuclei with charge number Z > 100 are known as superheavy elements (SHEs). To understand the properties of superheavy nuclei is important not only for testing the limits of nuclear structure, but might also be relevant in nuclear astrophysics and nucleosynthesis. The idea of superheavy elements emerged at the end of the sixties and the beginning of the seventies, the time when heavy-ion physics had its advent. The existence of superheavy elements was predicted about 30 years ago on the basis of the nuclear shell model, which was originally developed in 1949. The model explains why nuclei with certain magic numbers of neutrons and protons are especially stable. These nuclei have closed shells of either protons or neutrons. Magic nuclei are spherical in shape and characterised by exceptionally high nuclear binding energies. The stability of superheavy nuclei is mainly determined by shell effects. At the magic proton or neutron numbers, 2, 8, 20, 28, 50, 82, as well as N = 126 for neutrons, nuclei have higher stability and abundance compared with their neighbours. Particularly, the highest stability is observed in the case of the doubly magic nuclei. The most stable nuclei observed are doubly magic having closed shell of both protons and neutrons. The heaviest known doubly magic nucleus is ^{208}Pb, an isotope of lead consisting of Z = 82 protons and N = 126 neutrons. Predictions based on the shell model show that the next doubly magic nucleus in the sequence might contain either 114, 120 or 126 protons and a total of 172 or 184 neutrons (relativistic calculations seem to favour a magic number of Z=120). Typical predictions of their lifetimes vary between seconds and many thousands of years.

Moreover, other studies predict a whole superheavy *island of stability* around these proton and neutron numbers. Various predictions of the position of the island of relatively stable superheavy elements exist around Z = 114 or 120, N
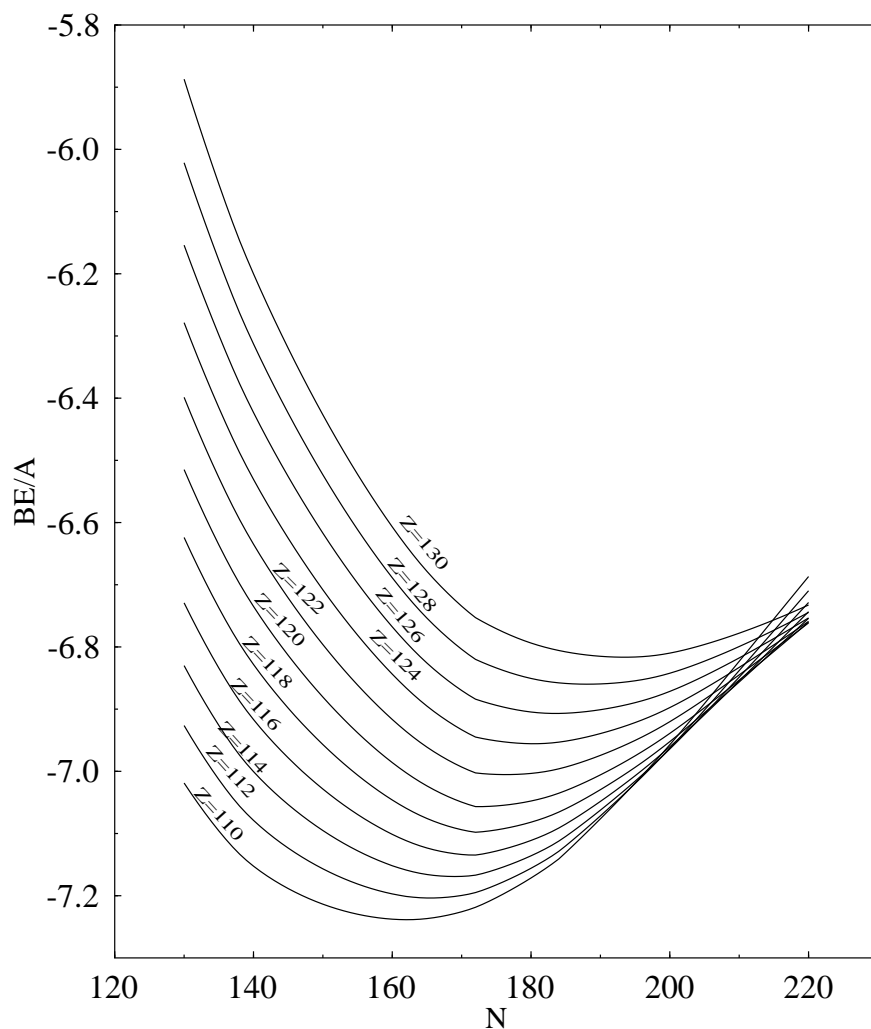
Figure 7.1: Binding energy/nucleon vs no of neutrons within Z= 110 and Z = 130 (NL3)

= 172, 184 and 196, respectively, and one around Z = 164, N = 318. The first superheavy elements are elements up to 112 which were discovered at GSI, Darmstadt [Hof95b, Hof95a, Hof96] and Berkeley [Ghi95a, Ghi95b, Oga95]. Physicists

from Russia and the US have identified two new superheavy elements 115 and 113 in experiments at the Joint Institute for Nuclear Research (JINR) in Dubna [Laz94, Laz95, Laz96]. Elements 115 and 113 were created in collisions between a beam of calcium-48 ions and an americium-243 target made at the Lawrence Livermore National Laboratory in California. The same collaboration discovered element 114 in 1998 and element 116 two years later. The evidence of element 118 and its α-decay chains have been observed at Berkeley [Nin99]. These developed and the current experimental facilities produce more new elements and isotopes and the expected magic Z =114 in progress. Element 118 has been indirectly discovered in experiments conducted at the Flerov Laboratory of Nuclear Reactions in Dubna, Russia by a collaboration of researchers from Russia's Joint Institute for Nuclear Research and the Lawrence Livermore National Laboratory in California.

The production of superheavy elements is not an easy task. The more protons and neutrons are packed into a nucleus, the less stable an atom becomes. Moreover, the increase in the charge of a nucleus makes it increasingly unstable against fission due to increased Coulomb repulsion. But the untiring research over decades have now reached the point where new SHEs has been synthesised at various laboratories in GSI, Darmstadt, Berkeley (USA) and Dubna (Russia). The only method that is being successfully used for such a synthesis is that of the complete fusion reaction. In complete fusion reactions, the two colliding nuclei merge to form a compound nucleus, giving at most a few atoms of the SHE in an experiment.

7.1 Two-nucleon enery gap

All the heaviest elements found are believed to be well deformed. However, spherical doubly magic superheavy elements are still expected to exist. A quantity , which is important for measuring magicity, is the two-nucleon energy gap. The two-proton and two-neutron gaps are defined as

$$
\begin{aligned}
\delta_{2p}(N,Z) &= E(Z+N,N) - 2E(Z,N) + E(Z-2,N) \\
\delta_{2n}(N,Z) &= E(Z,N+2) - 2E(Z,N) + E(Z,N-2)
\end{aligned}
\tag{7.1}
$$

They are directly related to the two-nucleon separation energies and can be used to investigate the magicity. At magic shells a pronounced peak can be shown in the two-nucleon gap [Bür98, Ben99]. So far, the two-nucleon shell gaps have been extensively used to be an indicator for the magic number and to analyze

Deformation β_2 of $^{292}120(\text{NL3})$
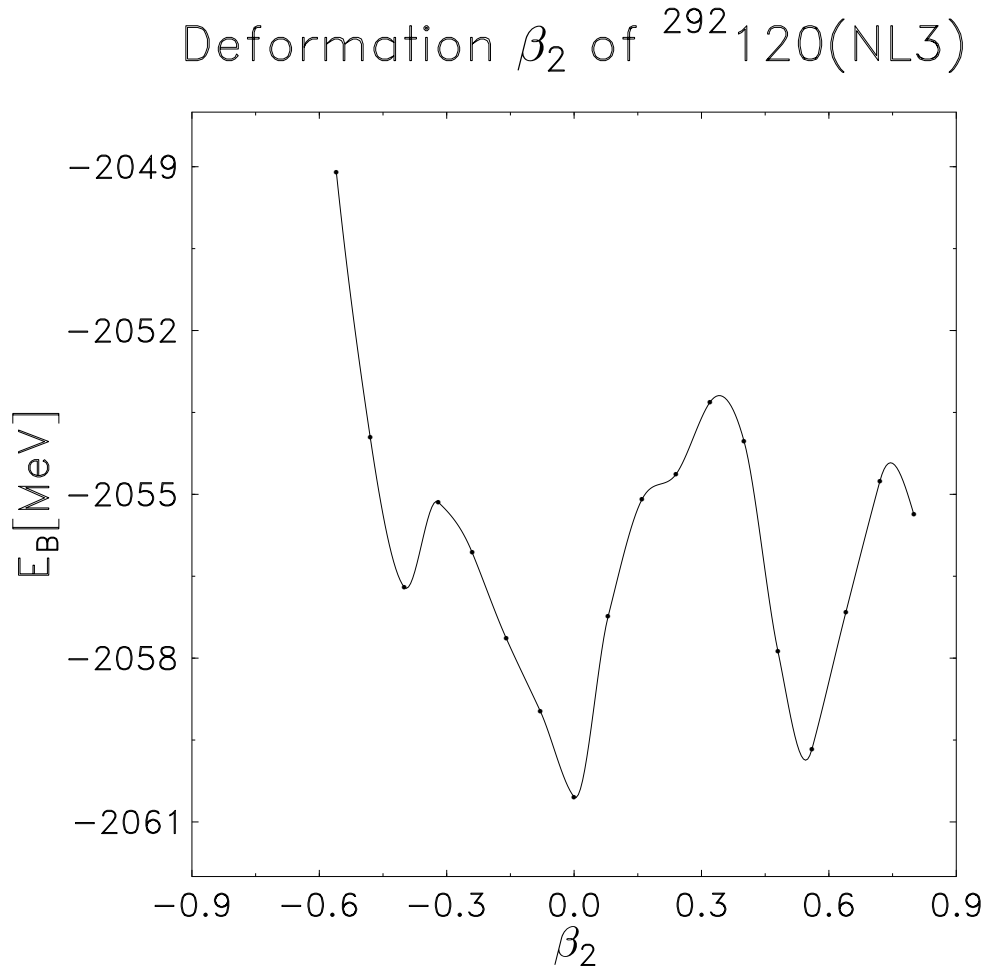
Figure 7.2: Deformation β_2 of $^{292}120$ (NL3).

the shell quenching phenomenon. By applying RMF theory with the parameter ChiM, two-nucleon gaps δ_{2N} are determined in both spherical and axially two-dimensional calculation [Sch02]. From this calculation, one can observe a weak signal for a shell closure at N = 172 and N = 184, which is in agreement with most relativistic calculations.
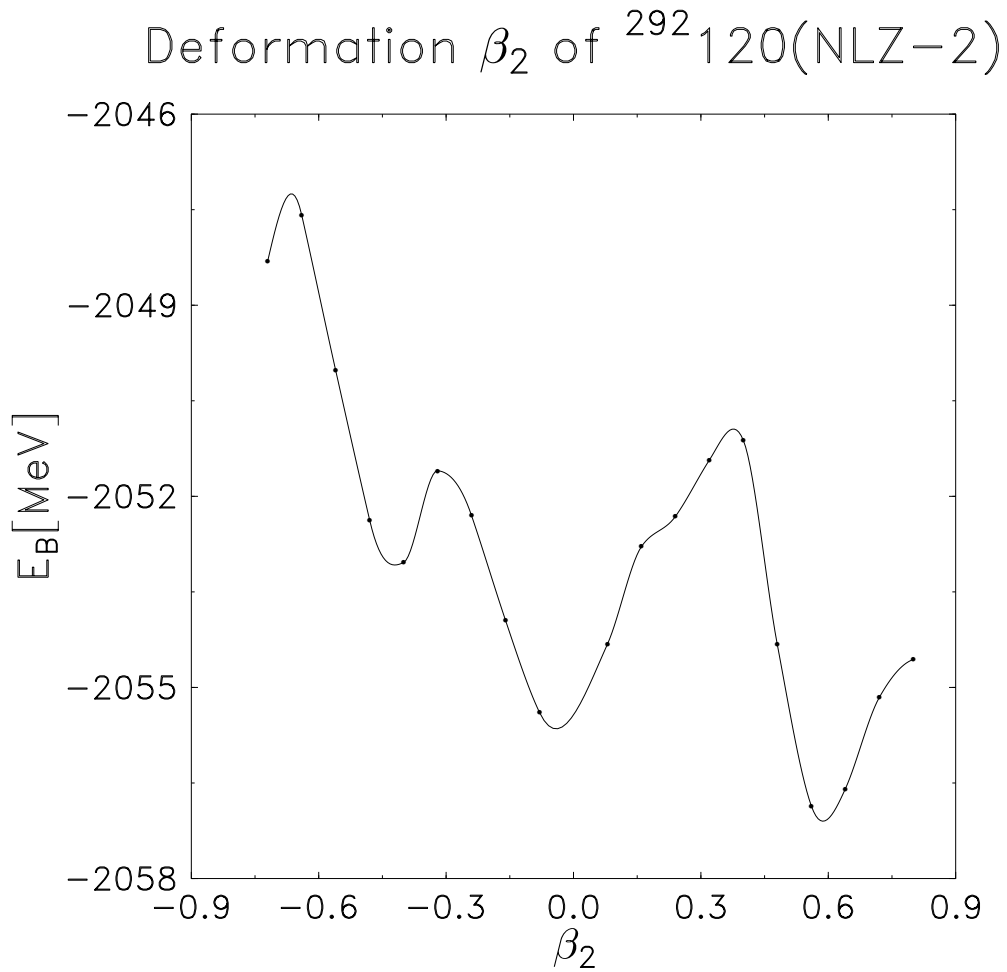
Figure 7.3: Deformation β_2 of ^{292}120 (NLZ-2).

7.2 Island of Stability

The island of stability is a technical term in the realm of superheavy nuclei that represents the possibility of elements with particularly stable "magic numbers" of protons and neutrons. The possible existence of islands of superheavy elements was introduced by Walter Greiner in one of the regular Saturday-meetings at GSI at the end of sixties. The island, a small region of longer-lived, superheavy nuclei projects out from a sea of short-lived nuclei and that reputedly live for anything

from milliseconds to days. Over the past few decades, many different experimental efforts to approach this range of nuclei and observe long-lived superheavy elements have been launched. The verification of the existence of an island of stability is one of the most challenging topics in world-wide heavy ion research facility. In various theoretical studies islands of superheavy elements around Z = 120, N = 172, 184 and 196, respectively, and the one around Z = 164, N = 318 were predicted.

Applying RMF theory with the effective interaction NL3, one expects the next doubly magic number is at Z = 120 and N = 172. The binding energies per nucleon for superheavy elements (from Z = 110 to Z =130) are shown in Fig.7.1. This calculation is carried out by using RMF theory with the effective interaction NL3. One can clearly observe that the minimum binding energy for this region of superheavy nuclei is at N= 172. This result is performed in spherical approximation. The new doubly magic number (Z = 120, N = 172) is still consistent in the axially symmetric two-dimensional calculation. The ground state of ^{292}120 is in spherical shape and another excited state is prolately deformed as shown in Fig. 7.2.

From the calculation of RMF theory with the parameter NLZ-2, the ground state displays prolate deformation and another excited state is spherical as in Fig. 7.3. From this (using the parameter NLZ-2) calculation, it is not quite clear whether the excited spherical shape might be the real minimum of the system and the deformed state might vanish as stable state in a more complete three-dimensional and reflection-asymmetric calculation. In RMF theory with the parameter NL3, the energy difference of the spherical ground state and prolate excited state are not so different. Deformation of the superheavy element (Z = 120 and N = 172) by applying the RMF theory with the parameter ChiM, can be observed in Fig. 7.4. ^{292}120 shows quite a complex structure with two oblate excited states, one prolate excited states and spherical excited state. The nuclear ground state of ^{292}120 is in a strongly prolate shape. For all these results more extended calculations beyond axial and reflection symmetry should be performed to investigate the stability of the strongly deformed states [Bür04].

In Fig. 7.5 and Fig. 7.6, the deformation properties of the superheavy element of (Z = 120 and N = 184) are investigated by applying RMF theory with parameters ChiM and NLZ-2. This doubly magic nucleus, which is predicted by the shell model, displays three different shapes (oblate, prolate and spherical) but shows a quite prolate deformation in the ground state. The energy difference between the ground state and excited state is relatively large in comparison with the above superheavy element (Z = 120 and N = 172). In both calculations of the RMF theory with the parameters ChiM and NLZ-2, the existence of a doubly

Deformation β_2 of ^{292}120(ChiM)
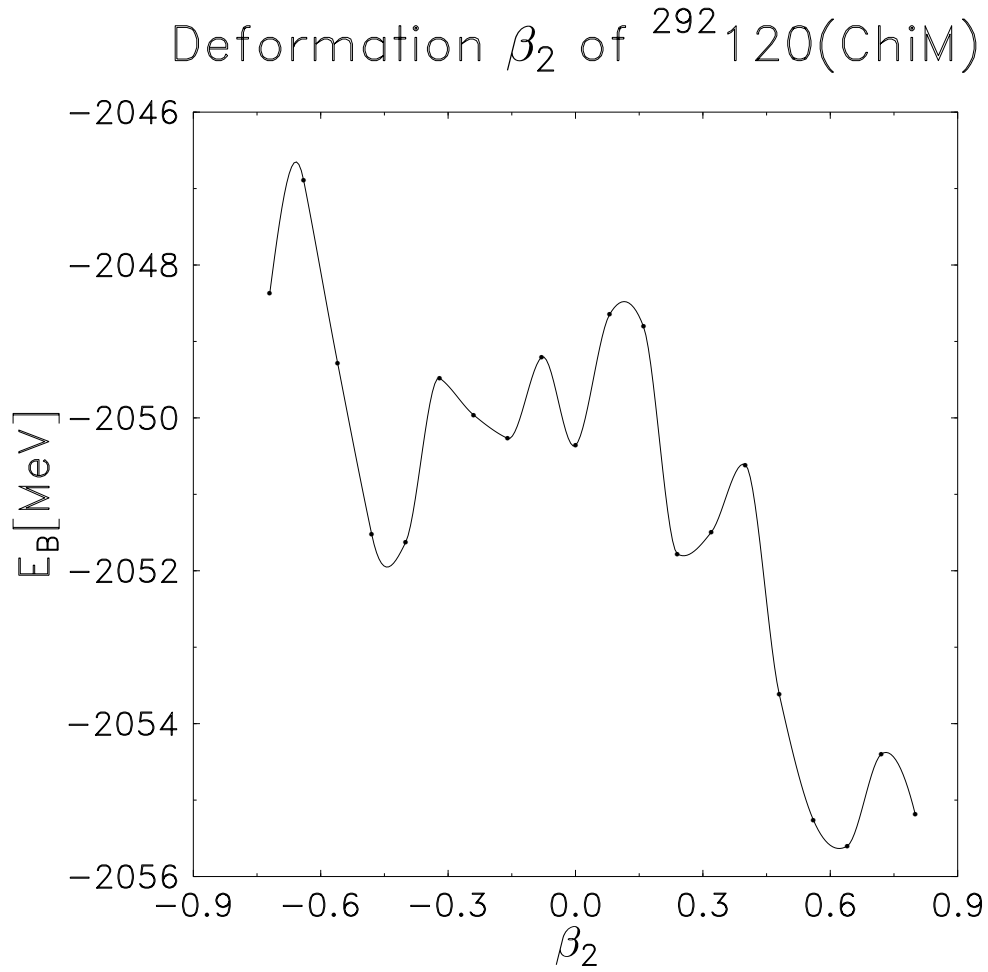
Figure 7.4: Deformation β_2 of ^{292}120 (ChiM).

magic nucleus is not clear in case of the superheavy element (Z = 120 and N = 184). For the NL-Z2 parameter, by adding reflection-asymmetric shape degree of freedom and triaxial degree of freedom, one can observe the minimum ground states for superheavy elements (Z = 120 and N = 172, 184) are in spherical shape [Bür04]. It is an interesting task to study these element more carefully in a three dimensional calculation for the various parameter sets in such a way that one can observe where the minimum ground state is located.

Deformation β_2 of $^{304}_{184}$120 isotopes
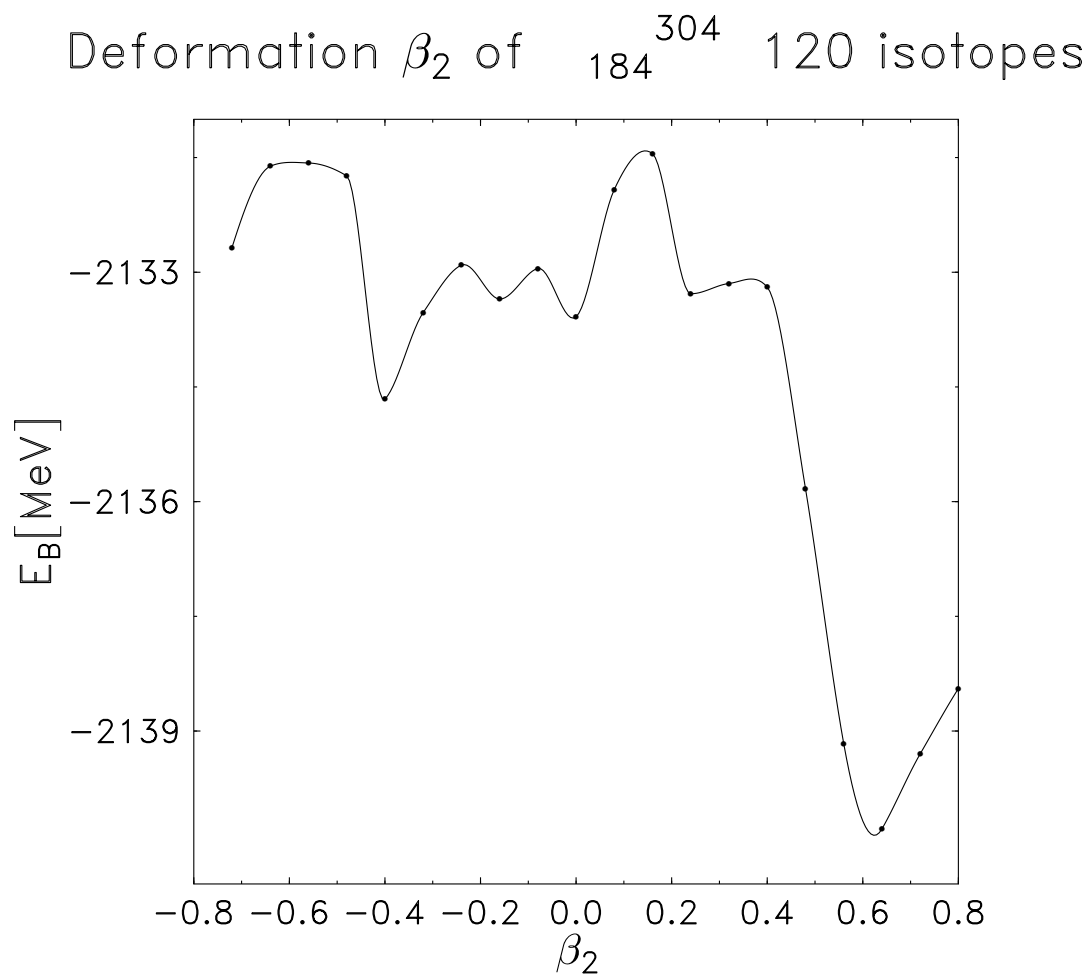
Figure 7.5: Deformation $\beta 2$ of ^{304}120 isotope(with ChiM)
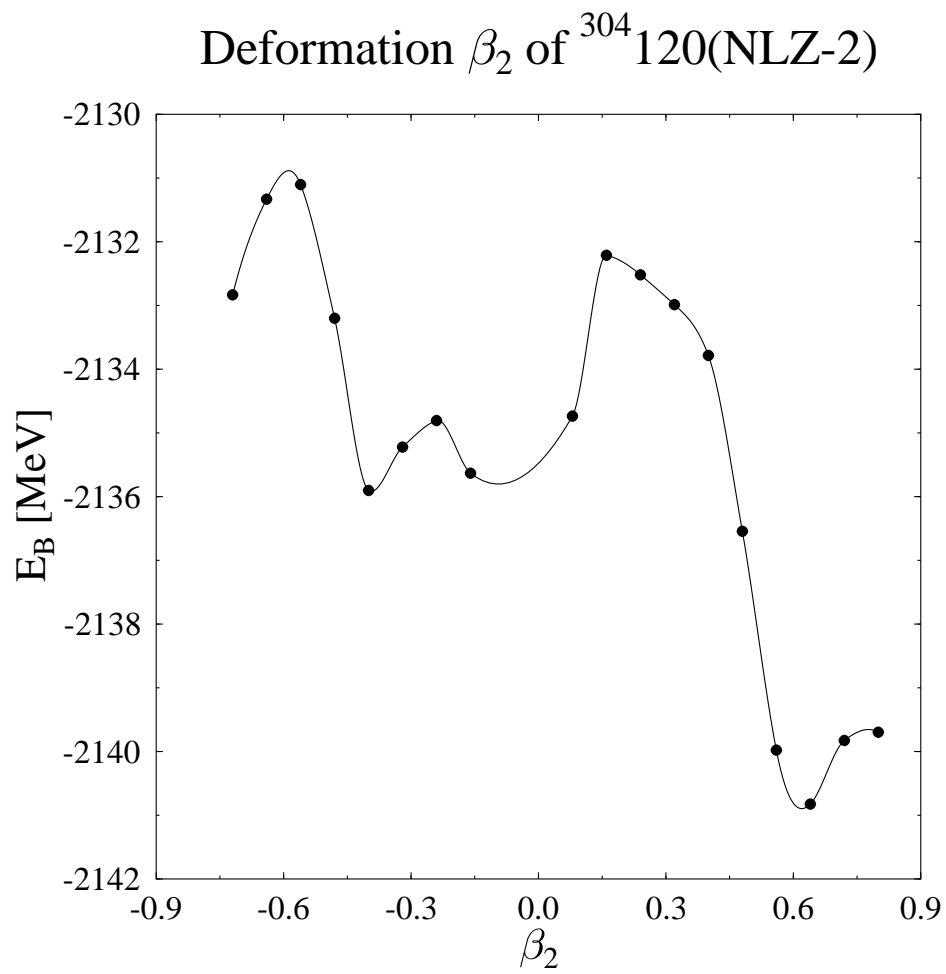
Figure 7.6: Deformation $\beta 2$ of ^{304}120 isotope (with NLZ-2).

–VIII–

Summary and Outlook

In this work the nuclear structure of exotic nuclei and superheavy nuclei is studied in a relativistic framework. In our approach, the relativistic meson field theory plays a central role of the study. In the relativistic mean-field (RMF) approximation, the nucleons interact with each other through the exchange of various effective mesons (scalar, vector, isovector-vector). This model approximates the exact density functional of the strongly interacting system by restricting the mesonic fields to their mean field values. In most of the RMF calculations, the no-sea approximation is applied. Therefore the anti-nucleon degree of freedom are not taken into account. Overall, it was shown that the relativistic mean field model is as flexible and powerful as the non-relativistic models with the additional bonus that some relativistic effects, as the spin-orbit force, come out naturally in the relativistic model and it allows an explanation of the nuclear saturation. [Due56, Mil72, Wal74]. Adopting a numerical code on the basis of the RMF model, the self-consistent Dirac (for the nucleons and the Lambda) and the Klein-Gordon equations (for the mesons) were solved numerically in spherical and axially deformed approximation. It was shown before [Sch02] that this model successfully describes finite nuclei and nuclear matter saturation properties.

The elements with even charge number Z (from 8 to 120) and their properties over the whole range of possible even neutron numbers are investigated and calculated by using three parameter sets ChiM [Sch02], NLZ-2[Bür02b] and NL3 [Lal97]. The RMF model descriptions (NL3 and NL-Z2) are quite successful in describing the properties of nuclear properties over a wide range of mass numbers. The prominent feature of NL-Z2 is its low incompressibility. The chiral model (ChiM), using a chiral symmetry has been developed for a good description of nuclear saturation and a reasonable description of nuclei and hypernuclei with a single model and a single set of parameters. The nuclear asymmetry energy in ChiM parameter is quite close to the empirical value. In a test case for the

properties of deformed nuclei the chiral model (ChiM) shows fair agreement with the experimental result [Fis00] in the prediction of ^{68}Se for the nuclear ground states with substantial oblate ($\beta_2 \sim$ -0.3) deformation.

By applying the RMF theory with different three parameter sets, we have determined the properties of exotic nuclei and a number of superheavy nuclei in a calculation of their nuclear structure. Extensive studies in the investigation of drip lines have been performed in this work. When neutrons are successively added to a nucleus on the nuclear stability line, the binding energy of the last neutron decreases steadily until it is no longer bound and the nucleus decays by neutron emission. At certain values of neutron numbers (for given charges), the nuclei will no longer bind extra neutrons. These values define the neutron drip line and its counterpart is called the proton drip line. In other words, an unstable atomic nucleus beyond the drip line will leak free neutrons and the neutron separation energy is zero at the neutron drip line. The proton and neutron drip lines define the limits of existence for finite nuclei. The understanding of nuclei up to the neutron drip line provide a better understanding of the stellar nucleosynthesis and neutron stars in nuclear astrophysics. The position of the drip lines is still uncertain and its experimental and theoretical determination is a problem of great interest in the field. The drip lines including axial deformations (with the parameter ChiM) are described for ($8 \leq Z \leq 120$) nuclei. Isotopic chains with proton magic numbers move away from the neutron magic numbers (except for the case Z = 20). This result agrees with the above calculation with the parameter NL3. For larger nuclei, the proton and neutron drip lines are more clearly observed than in the calculation with NL3 parameter. Isotonic chains with neutron magic numbers stay pronounced (as in the calculation of parameter NL3) up to the neutron drip line including axially deformation. Shell closure along the neutron drip line can be seen at the neutron numbers (N = 82, 126, 184) while isotopic chains with proton magic numbers move away from the neutron magic numbers (except for Z = 20).

This work puts special emphasis on studying the proton rich and neutron rich elements up to the proton drip line and neutron drip line respectively. We performed a systematic study of 1661 nuclei to verify the axial deformation of even-even nuclei ($8 \leq Z \leq 100$) with different numbers of neutrons. This is the first time this has been done by using RMF theory with a chiral parameter set (ChiM). Proton quadrupole deformation parameters β_{2p} for nuclei ($8 \leq Z \leq 100$) have already been studied with RMF+BCS calculations, the FRDM mass and the HFB-2 models. As resultt of the systematic study of our calculation, we can conclude that

1) Most of spherical nuclei (-0.05 $\leq \beta_2 \leq$ 0.05)are located at or near magic numbers.

2)While isotonic change with well-known neutron magic numbers (N =82, 126, 184) preserve spherical shapes for the entire chain, isotopic chain with proton magic numbers are usually deformed when one moves away from the neutron magic numbers (except for the Z = 8 and 20 isotopic chain). Semi-magic numbers (Z = 40, 172, 182, 186) can be observed from this axial deformation calculation ($8 \leq Z \leq 100$). Among these different numbers of axial deformation, we can observe well-known doubly magic nuclei (^{16}O, ^{40}Ca, ^{48}Ca, ^{132}Sn, ^{208}Pb) (except for the Z = 28 isotopic chain).

3) Among Pb isotopes, oblately deformed nuclei ($\beta_2 \sim 0.2$) are located near the proton drip line. Some neutron rich Pb isotopes are prolately deformed (0.2 $\leq \beta_2 \leq$ 0.3). The rest of the Pb isotopes are in spherical shape.

4) Most of prolately deformed nuclei are observed for nuclei with a charge larger than Z =50 when moving away from the magic numbers either isotonically or isotopically.

5)There are several regions where strongly prolate and oblate deformations co-exist. In one of the prolate region, one can clearly observe the shape coexistence of prolate and oblate shapes. Os and Pt isotopes (Z = 76 and 78) exhibit a large number of prolate deformation except near (N = 126).

6) We found superdeformed nuclei near the proton and neutron drip lines of Cf (Z = 98) isotopes and Fm (Z = 100) isotopes ($0.7 \leq \beta_2 \leq 0.8$). The superdeformation of Fm isotopes near proton and proton drip lines is discussed. For Cm (Z = 96) isotopes, one can see superdeformed nuclei only near the neutron drip line.

7) Oblately deformed ground-state nuclei are rare. There are some oblate regions in the chart of deformation of even-even nuclei. Axially symmetric oblate deformation from one of the oblate deformed region is described. This oblate region lies among the isotonic chains of Zn isotopes (Z = 30) to Kr isotopes (Z = 34). These nuclei are quite deformed nuclei ($0.2 \leq \beta_2 \leq 0.3$)

Axially deformed nuclei from the proton drip line to neutron drip line for Magnesium which are calculated by using RMF theory with ChiM parameter are discussed. From these calculation, it is found that the occurrence of oblate and prolate minima for various isotopes are in general agreement with other relativis-

tic and non relativistic mean field calculations [Lal98, Bür02a].

Knowledge about nuclei far away from the line of exotic nuclei may improve our present insight, not only into the origin of the element abundance on the Earth, but also into the processes leading to the formation of matter in the universe. The study of exotic nuclei has attracted world-wide attention due to their large isospin and interesting properties such halos and skins. The RMF theory with the parameter set ChiM can predict the neutron halo in Ne isotope, the neutron skin thickness in istopes near Z =40 isotopic chain, Sn and Pb isotopes. The neutron halo and the neutron skin thickness are predicted from the calculation of density distributions and the difference between the rms neutron and proton radii. The nuclear groundstate properties such as the binding energy per nucleons and two neutron separation energy of these exotic nuclei are in good agreement with the experimental value [Aud03] and non-relativistic, FRDM [Möl95] calculations.

It is interesting to investigate the deformation of Pb isotopes. We observe that the lowest three states in the energy spectrum of the neutron deficient nucleus ^{186}Pb are spherical, oblate and prolate as shown in Fig. 4.16. Our calculation is in agreement with other three-dimensional calculation [And00]. Potential energy curves for $^{190-204}$Pb exhibit a considerably high excitation energy relative to the ground state superdeformation (SD) bands and shallow wells in the superdeformation minimum in comparison with its neighbouring nucleus ^{192}Pb signifies that it is difficult to form the stable SD state. The SD states can still be observed in these nuclei and there is reasonable agreement with the RMF theory (with the parameter set NL3, PK1, TM1 and NLSH) [Guo06] and experimental observations. The calculated deformation in the SD minima of $^{190-204}$Pb lies between 0.6 and 0.7.

The RMF theory with the parameter set ChiM can be employed not only for normal nuclei but also hypernuclei. The same calculation as in the case of exotic nuclei was repeated by adding Λ hyperons. A Λ consists of one u, d and s quark each. If such a hyperon is bound in a nucleus, a hypernucleus is created. Hypernuclei with one hyperon have been known for more than 30 years and have been extensively studied experimentally [Pov76]. Lambda hypernuclei are excellent probes of the structure of the nucleus; the Lambda interacts strongly with the nucleus and is distinguishable from the nucleons. The axial deformation of Ne isotopes are compared without Λ and with Λ hyperon. According to these calculation, one can observe that deformed nuclei could reduce, however not too pronounced, the strength of the deformation by inclusion of a Λ hyperon. On the other hand, the inclusion of the Λ hyperon does not produce excessive change in bulk properties but shifts the neutron drip line outward. The hyperon carbon isotopes were calculated in this work by using the RMF theory with the parameter

set ChiM. When two Λ hyperons are added to the core ^{12}C, the nucleon density distribution remains largely the same and hyperon density distributions at the tail are comparable with those of the nucleons. We could predict a hyperon halo for C isotopes by adding three Λ hyperons to the core ^{12}C with the evidence of the long tail of the hyperon density which is extended far outside of its core.

Mapping the proton and neutron drip lines is extensively discussed. The same calculation was repeated by adding one *Lambda* hyperon in the nuclei. The Lambda hyperon is an excellent probe of the structure of the nucleus, because it is located in the centre of the nucleus. By determining the position of the drip lines using the RMF model one can observe the difference between the drip lines of ordinary nuclei and those of hypernuclei with one lambda, which could be very interesting for the planned experiments at FAIR/GSI in the region of very neutron-rich hypernuclei. The drip line inclusion of one Lambda hyperon can display shell closure at the magic numbers: 82, 126, 184 in such a way that the hypernuclei can accept more neutrons and are more strongly bound than the normal nuclei.

This work is concluded with the study of superheavy nuclei. The RMF theory with the three different parameter sets (ChiM, NL3, NL-Z2) are reviewed. Based on the detail analysis of the two-nucleon separation energies S_{2n} and S_{2p} and two-nucleon shell gaps δ_{2p} and δ_{2n}, the proton and the neutron shell closures have been predicted by applying the RMF theory with the effective interactions ChiM, NL3 and NL-Z2. Proton numbers Z =114, 120 and neutron numbers N = 172, 184, 258 are supported by all effective interactions to be magic. According to the calculation of potential energy surfaces of superheavy nuclei with different parameter sets, their ground states varies with the parameter sets. For these particular nuclei, it would be very interesting to extend our calculation assuming axially symmetric deformation to an investigation within a full three dimensional calculation so that one can reliably determine where the true ground state is located.

−Appendix A−

Nuclear Deformation

The sequence of nuclear shape used to compute the deformation energy is given via the spherical multipole moments $Q_{\lambda 0}$ respectively by the deformations β_λ:

$$\beta_\lambda = \frac{4\pi}{3AR_0^\lambda} Q_{\lambda 0}, \tag{A.1}$$

where A is the total number of nucleons, $R_0 = 1.2\ A^{1/3}$. However these parameters do not coincide with the collective parameters used in the parameterization of the nuclear surface

$$R(\theta) = \frac{R_0}{c(\beta)} \Big(1 + \sum_\lambda \beta_\lambda Y_{\lambda 0}(\theta, 0) \Big), \tag{A.2}$$

where $c(\beta)$ is a quantity related to the volume conservation. In the present work, we consider only quadrupole and hexadecupole deformations. For small deviations from spherical minimum the deformed density can be expressed as a Talayor series in the collective parameters:

$$\rho(r, \theta) = \rho(r) + \sum_{n=1}^{\infty} \frac{(-1)^n}{n!} \left(\frac{R_0}{c(\beta)} (\beta_2 Y_{20}(\theta, 0) + \beta_4 Y_{20}(\theta, 0)) \right)^n \left(\frac{\mathrm{d}^n \rho(r)}{\mathrm{d}r^n} \right) \tag{A.3}$$

For ρ (r) we use the spherical density computed microscopically within the RMF approach:

$$\rho(r) = \sum_\alpha v_\alpha^2 \bar{\psi}_\alpha(r) \gamma_0 \psi_\alpha(r), \tag{A.4}$$

where the $\psi_\alpha(r)$ are the single-particle wavefunctions and v_α^2 their corresponding occupation probabilities. Substituting the above expression in equation (2) and truncating the sum at n = 7 we obtain a set of two non-linear equations relating

119

the quadrupole and hexadecupole moments (Q$_2$, Q$_4$) to the collective parameters (β_2, β_4).

References

[And00]   A. N. Andreyev und et al., Nature **405** (2000), 430.

[ANL07]   *Anl,argonne national laboratory*, http://www.anl.gov, 2007.

[Aud03]   G. Audi, A. H. Wapstra und C. Thibault, Nucl. Phys. A. **729** (2003), 337–676.

[Bau07]   T. Baumann und et al., Nature **449** (2007), 1022.

[Bec02]   C. Beckmann, P. Papazoglou, D. Zschiesche, S. Schramm, H. Stöcker und W. Greiner, Phys. Rev. C. **65** (2002), 024301.

[Bei75]   M. Beiner, H. Flocard, N. V. Giai und P. Quentin, Nucl. Phys. A. **238** (1975), 29.

[Ben99]   M. Bender, K. Rutz, P. G. Reinhard und W. Maruhn, J. A. Greiner, Phys. Rev. C. **60** (1999), 034304.

[Ben03]   M. Bender, P. H. Heenen und P. G. Reinhard, Reviews of Modern Physics **75** (2003), 121.

[Ber79]   R. Bertini und et al., Phys. Lett. B. **83** (1979), 306.

[Ber80]   R. Bertini und et al., Phys. Lett. B. **90** (1980), 375.

[Ber81]   R. Bertini und et al., Nucl. Phys. A. **360** (1981), 315.

[Bla76]   J. P. Blaizot, D. Gogny und B. Grammaticos, Nucl. Phys. A. **265** (1976), 315.

[Bla80]   J. P. Blaizot, Phys. Rep. **64** (1980), 171.

[Blu94]   V. Blum, J. A. Maruhn, P. G. Reinhard und W. Greiner, Phys. Lett. B. **323** (1994), 262.

[Bog77]   J. Boguta und A. Bodmer, Nucl. Phys. A. **292** (1977), 413.

[Bon74]   G. c. Bonnazzola, T. Bressani, R. Cester und E. Chiavassa, Phys. Lett. B. **53** (1974), 297.

[Bro75]   G. E. Brown und W. Weise, Phys. Rep. **22** (1975), 279.

[Brü76]   W. Brückner und et al., Phys. Lett. B. **62** (1976), 481.

[Brü78]   W. Brückner und et al., Phys. Lett. B. **79** (1978), 157.

[Bür98]   T. Bürvenich, K. Rutz, M. Bender, P. G. Reinhard, J. A. Maruhn und W. Greiner, Euro. Phys. J. **A3** (1998), 139.

[Bür02a] T. Bürvenich, *Untersuchung und weiterentwicklung eines relativistischen punktkopplungsmodells zur anwendung in der kernstrukturphysik*, Dissertation, J. W. Goethe Universität Frankfurt am Main, 2002.

[Bür02b] T. Bürvenich, D. G. Madland, J. A. Maruhn und P. G. Reinhard, Phys. Rev. C. **65** (2002), 044308.

[Bür04]   T. Bürvenich, M. Bender, J. A. Maruhn und P. G. Reinhard, Phys. Rev. C. **69** (2004), 014307.

[Can74]   T. Cantwell und et al., Nucl. Phys. A. **236** (1974), 445.

[Cer77]   J. Cerny und J. Hardy, Ann. Rev. Nucl. Part. Sci. **27** (1977), 333.

[Cha97]   E. Chabanat, P. Bonche, P. Haensel, J. Meyer und R. Schaeffer, Nucl. Phys. A **627** (1997), 710.

[Chi74]   S. A. Chin und J. D. Walecka, Phys. Lett. B **52** (1974), 24.

[Chr79]   R. E. Chrien und et al., Phys. Lett. B. **89** (1979), 31.

[Chr88]   R. E. Chrien und et al., Nucl. Phys. A. **478** (1988), 705c.

[con03]   *The contemporary physics education project*, http://www.cpepweb.org, 2003.

[Cow91]   J. J. Cowan, F.-K. Thieleman und J. W. Truran, Phys. Rep. **208** (1991), 267.

[Dan53]   M. Danysz und J. Pniewski, Philos. Mag. **44** (1953), 348.

[Due56]   H. Duerr, Phys. Rev. **103** (1956), 469.

[Fee49]   E. Feenberg, Phys. Rev. **75** (1949), 320.

[Fis72]   E. O. Fiset und J. R. Nix, Nucl. Phys. A. **193** (1972), 647.

[Fis00]   S. M. Fischer und et al., Phys. Rev. Lett. **84** (2000), 4064.

[Fuk93]   N. Fukunishi, T. Otsuka und I. Tanihata, Phys. Rev. C. **48** (1993), 1648.

[Fur97]   R. J. Furnstahl, B. D. Serot und H. B. Tang, Nucl. Phys. A. **615** (1997), 441.

[Fur98]   R. J. Furnstahl, J. J. Rusnak und B. D. Serot, Nucl. Phys. A. **632** (1998), 607.

[Gam90]   Y. Gambhir, P. Ring und A. Thimet, Ann. Phys. (N.Y.) **198** (1990), 132.

[Gen05]   L. Geng, H. Toki und J. Meng, Prog. Theo. Phys **113** (2005), 785.

[Ghi95a]   A. Ghiorso und et al., Phys. Rev. C. **51** (1995), R2293.

[Ghi95b]   A. Ghiorso und et al., Nucl. Phys. A. **583** (1995), 861c.

[Gre96]   W. Greiner und J. A. Maruhn, *Nuclear models*, Springer, New York, 1996.

[Gri05]   K. A. Gridnev, D. K. Gridnev1, V. G. Kartavenko, V. E. Mitroshin, V. N. Tarasov, D. V. Tarasov und W. Greiner, Eur. Phys. J. A. **25** (2005), 353.

[Gru69]   J. Grumann, U. Mosel, B. Fink und W. Greiner, Z. Phys. **228** (1969), 371.

[Gui94]   *The rapid proton capture process*, http://csep10.phys.utk.edu/guidry/RIB-7-94html/rp-root.html, 1994.

[Guo06]   J.-Y. Guo, Z.-Q. Sheng, Fang und Xiang-Zheng.

[Han87]   P. G. Hansen und B. Jonson, Eur. Pys. Lett. **4** (1987), 409.

[Han95]   P. G. Hansen und A. S. Jensen, Ann. Rev. Nucl. Part. Sci. **45** (1995), 591.

[Han03]   P. G. Hansen und J. A. Tostevin, Ann. Rev. Nucl. Part. Sci. **53** (2003), 219.

[Hax99] O. Haxel, J. H. D. Jensen und H. E. Suess, Phys. Rev. **75** (19499), 1766.

[Hee07] P.-H. Heenen, Nature **449** (2007), 992.

[Hin04] D. Hinde und M. Dasgupta, Nature **431** (2004), 748.

[Hoc94] T. Hoch, D. G. Madland, P. Manakos, T. Mannel, B. A. Nikolaus und D. Strottman, Phys. Rep. **242** (1994), 253.

[Hod00] P. E. Hodgson, E. Gadioli und E. Gadioli Erba, *Introductory nuclear physics*, Oxford University Press, New York, 2000.

[Hof56] R. Hofstandter, Reviews of Modern Physics **28** (1956), 214–254.

[Hof95a] S. Hofmann und et al., Z. Phys. A. **350** (1995), 281.

[Hof95b] S. Hofmann und et al., Z. Phys. A. **350** (1995), 277.

[Hof96] S. Hofmann und et al., Z. Phys. A. **354** (1996), 229.

[Hor81] C. J. Horowitz und B. D. Serot, Nucl. Phys. A. **368** (1981), 503.

[Hor84] C. J. Horowitz und B. D. Serot, Phys. Lett. B **140** (1984), 181.

[hyp96] A. density-dependent relativistic Hartree approach for hypernuclei, J. Phys. G. **22** (1996), 1421.

[Jon04] B. Jonson, Phys. Rep. **389** (2004), 1.

[Kra91] A. Krasznahorkay und et al., Phys. Rev. Lett. **66** (1991), 1287.

[Lal95] G. A. Lalazissis und M. M. Sharma, Nucl. Phys. A. **586** (1995), 201–218.

[Lal97] G. A. Lalazissis, J. Knig und P. Ring, Phys. Rev. C. **55** (1997), 540.

[Lal98] G. A. Lalazissis, A. R. Farhan und M. M. Sharma, Nucl. Phys. A. **628** (1998), 221.

[Laz94] Y. A. Lazarev und et al., Phys. Rev. Lett. **73** (1994), 624.

[Laz95] Y. A. Lazarev und et al., Phys. Rev. Lett. **75** (1995), 1903.

[Laz96] Y. A. Lazarev und et al., Phys. Rev. C. **54** (1996), 620.

[Lee86]   S.-J. Lee, J. Fink, A. B. Balantekin, M. R. Strayer, A. S. Umar, P. G. Reinhard, J. A. Maruhn und W. Greiner, Phys. Rev. Lett. **57** (1986), 2916.

[Lon04]   W. H. Long, J. Meng, N. V. Giai und S. G. Zhou, Phys. Rev. C. **69** (2004), 034319.

[Lun03]   D. Lunney, J. M. Pearson und C. Thibault, Rev. Mod. Phys. **75** (2003), 1021.

[Mar89]   J. Mares und J. Zofka, Z. Phys. A. **333** (1989), 209.

[May48]   M. G. Mayer, Phys. Rev. **74** (1948), 235.

[May49]   M. G. Mayer, Phys. Rev. **75** (1949), 1969.

[May50]   M. G. Mayer, Phys. Rev. **78** (1950), 22.

[May81]   M. May und et al., Phy. Rev. Lett. **47** (1981), 1106.

[Men06]   J. Meng, H. Toki, S. G. Zhou, S. Q. Zhang, W. H. Long und L. S. Geng, Prog. Part. Nucl. Phys. **57** (2006), 470.

[Mil72]   L. D. Miller und A. E. S. Green, Phys. Rev. C **5** (1972), 241.

[Mil88]   D. J. Millener, C. B. Dover und A. Gal, Phys. Rev. C. **38** (1988), 2700.

[Möl95]   P. Möller, J. R. Nix, W. D. Myers und W. J. Swiatecki, At. Data and Nucl. Data Tables **59** (1995), 185–381.

[Mue99a]   A. C. Mueller, Nucl. Phys. A. **654** (1999), 215c.

[Mue99b]   A. C. Mueller, Nucl. Phys. A. **654** (1999), 215c–234c.

[Mue43]   A. C. Mueller und B. M. Sherrill, Ann. Rev. Nucl. Part. Sci. **1993** (43), 529.

[Mye66]   W. D. Myers und W. J. Swiatecki, Nucl. Phys. **81** (1966), 1.

[Mye69]   W. D. Myers und W. J. Swiatecki, Ann. Phys. **55** (1969), 395.

[Mye70]   W. D. Myers, Nucl. Phys. A. **145** (1970), 387.

[Mye85]   W. D. Myers, W. J. Swiatecki und C. S. Wang, Nucl. Phys. A. **436** (1985), 185.

[Nik92]   B. A. Nikolaus, T. Hoch und D. G. Madland, Phys. Rev. C. **46** (1992), 1757.

[Nil69]   S. G. Nilsson, C. F. Tsang, A. Sobiczewski, Z. Szymanski, S. Wycech, C. Gustafson, I. L. Lamm, P. Möller und B. Nilsson, Nucl. Phys. A. **131** (1969), 1.

[Nin99]   V. Ninov und et al., Phys. Rev. Lett. **83** (1999), 1104.

[Oga95]   Y. T. Oganessian, Nucl. Phys. A. **583** (1995), 823.

[Pov76]   B. Povh, Rep. Prog. Phys. **39** (1976), 823.

[Qia03]   Y.-Z. Qian, Prog. Part. Nucl. Phys. **50** (2003), 153.

[Ran74]   J. Randrup, S. E. Larsson, P. Möller, A. Sobiczewski und A. Lukasiak, Phys. Scr. **10A** (1974), 60.

[Rei88]   P. G. Reinhard, Z. Phys. A. **329** (1988), 257.

[Rei89]   P. G. Reinhard, Rept. Prog. Phys. **52** (1989), 439.

[Rei95]   P. G. Reinhard und H. Flocard, Nucl. Phys. A. **584** (1995), 467.

[Rin80]   P. Ring und P. Schuck, *The nuclear many-body problem*, Springer, New York, 1980.

[Rin96]   P. Ring, Prog. Part. and Nucl. Phys. **37** (1996), 193.

[Ruf88]   M. Rufa, P. G. Reinhard, J. A. Maruhn, W. Greiner und M. R. Strayer, Phys. Rev. C. **38** (1988), 390.

[Rut99]   K. Rutz, *Struktur von atomkernen im relativistic-mean-field-modell*, Dissertation, J. W. Goethe Universität Frankfurt am Main, 1999.

[Sch02]   S. Schramm, Phys. Rev. **C66** (2002), 064310.

[Ser79]   B. D. Serot und J. D. Walecka, Phys. Lett. B. **87** (1979), 172.

[Ser86]   B. D. Serot und J. D. Walecka, Adv. Nucl. Phys. **16** (1986).

[Ser92]   B. D. Serot, Rept. Prog. Phys. **55** (1992), 1855.

[Sha93]   M. M. Sharma, M. A. Nagarajan und P. Ring, Phys. Lett. B. **312** (1993), 377.

[Sha94]   M. M. Sharma, G. A. Lalazissis, W. Hillebrandt und P. Ring, Phys. Rev. Lett. **72** (1994), 1431.

[Sug94]   Y. Sugahara, H. Toki und P. Ring, Theor. Phys. **92** (1994), 803.

[Suz95]   T. Suzuki und et al., Phys. Rev. Lett. **75** (1995), 3241.

[Tan85a]   I. Tanihata und et al., Phys. Rev. Lett. **55** (1985), 2676.

[Tan85b]   I. Tanihata und et al., Phys. Rev. Lett. **55** (1985), 2676.

[Tan92]   I. Tanihata, D. Hirata, T. Kobayashi, S. Shimoura, K. Sugimoto und H. Toki, Phys. Lett. B. **289** (1992), 261.

[Tan96]   I. Tanihata, J. Phys. G: Nucl. Part. Phys. **22** (1996), 157.

[Tan99]   I. Tanihata, Nucl. Phys. A. **654** (1999), 235c.

[Tho04]   M. Thoennessen, Rep. Prog. Phys. **67** (2004), 1187.

[Tre81]   J. Treiner, H. Krivine und O. Bohigas, Nucl. Phys. A. **371** (1981), 253.

[Vau72]   D. Vautherin und D. M. Brink, Phys. Rev. C. **5** (1972), 626.

[Vre98]   D. Vretenar, W. Pschl, G. A. Lalazissis und P. Ring, Phys. Rev. C. **57** (1998), R1060.

[Vre05]   D. Vretenar, A. V. Afanasjev, G. A. Lalazissis und P. Ring, Phys. Rep. **409** (2005), 101.

[Wal74]   J. D. Walecka, Ann. Phys. (N.Y.) **83** (1974), 491.

[Wal04]   J. D. Walecka, *Theoretical nuclear and subnuclear physics*, Imperial College Press and World Scientific Publishing Co. Pte. Ltd., London, 2004.

[Was88]   D. A. Wasson, Phys. Lett. B **210** (1988), 41.

[Woo54]   R. D. Woods und D. S. Saxon, Phys. Rev. **95** (1954), 577.

[Zhu91]   Z. Y. Zhu, H. J. Mang und P. Ring, Phys. Lett. B **254** (1991), 325.

Acknowledgements

Many people helped and supported me so as to accomplish this dissertation, and I owe my warmest gratitude to all of them.

First and foremost I would like to extend my great deal of gratitude to my supervisor, Prof. Stefan Schramm, for his instruction, guidance, advice and stimulating discussion as well as for numerous opportunities to learn and to attend conferences and workshops. His patience and continuous supervision rescued me from despair on countless occasions. I am deeply indebted to his kindness, his confidence in me, and his inexhaustible efforts as a mentor. My sincere appreciation to Prof. Walter Greiner for his invaluable teaching, kind support and an opportunity to accomplish my work.

I wish to express my gratitude to Dr. Thomas J. Bürvenich for offering his expertise, useful suggestions and discussions on many topics of my work. I am also grateful to Prof. Igor Mishustin and Prof. Jürgen Schaffner-Bielich for their invaluable suggestions and guidance on my work.

I would like to gratefully acknowledge the support of Frankfurt Institute for Advanced Studies (FIAS), Center for Scientific Computing (CSC) and all members of Nuclear Astrophysics. Many thanks also go to all of my friends, especially Sophie Nahrwold, Stephanie Lo and Tri Hendro Atmoko Utomo for their encouragement, friendship and help.

Special recognition is extended to my former teachers, my aunts and all my brothers and sisters for all of their kind support and well understanding, without which none of this work would have been possible.

Last but absolutely not least, my deepest gratitude go to my parents for supporting, comforting and encouraging me throughout my life. I am forever grateful to them for enlightening the insight and essence of education.

Lebenslauf

Name : Khin Nyan Linn
Geburtstag: 23.04.73
Geburtsort: Mandalay, MYANMAR

Bildungsweg:

- 1978-1983
  Besuch des Grundschule an der No (14) Grundstufe Schule, Mandalay (MYANMAR)

- 1984-1990
  Besuch des Gymnasium an der No (22) Oberstufe Schule, Mandalay (MYANMAR)

- March 1990
  Abitur

- Feb.1993
  Beginn des Physikstudiums an der Mandalay Universität, Mandalay (MYANMAR)

- Juni.1996
  Bachelor in Physik

- Juni.2001
  Master in Kernphysik

- Seit Jan 2002
  Wissentschaftlicher Mitarbeiter am Institut für Physik der Yadanbon-Universität, Mandalay (MYANMAR)

- Juni 2005
  Beginn des Promotionsstudiums am Institut für Theoretische Physik. Thema der Dissertation: Structure of Exotic Nuclei and Superheavy Elements in Meson Field Theory.

Akademische Lehrer

PD. Dr. Elena Bratkovskaya

Dr. Thomas J. Bürvenich

Prof. Dr. Carsten Greiner

Prof. Dr. Dr. h. c. mult. Walter Greiner

Prof. Dr. Joachim A Maruhn

Prof. Dr. Igor Mishustin

Prof. Dr. Dirk-Hermann Rischke

HD. PD.Dr. Jrgen Schaffner-Bielich

Prof. Dr. Stefan Schramm

Prof. Dr. Steven Soff

Prof. Dr. Horst Stöcker